ADSORPTION OF IONS ON HEMATITE (α-Fe_2O_3)

A COLLOID-CHEMICAL STUDY

A. BREEUWSMA

553.312:541.183.24

A. BREEUWSMA

ADSORPTION OF IONS ON HEMATITE (α-Fe_2O_3)

A COLLOID-CHEMICAL STUDY

PROEFSCHRIFT

TER VERKRIJGING VAN DE GRAAD
VAN DOCTOR IN DE LANDBOUWWETENSCHAPPEN,
OP GEZAG VAN DE RECTOR MAGNIFICUS,
PROF. DR. IR. H. A. LENIGER,
HOOGLERAAR IN DE TECHNOLOGIE,
IN HET OPENBAAR TE VERDEDIGEN OP WOENSDAG 18 APRIL 1973
DES NAMIDDAGS TE VIER UUR IN DE AULA VAN DE
LANDBOUWHOGESCHOOL TE WAGENINGEN

H. VEENMAN & ZONEN B.V. – WAGENINGEN – 1973

STELLINGEN

I

Bij de interpretatie van de adsorptie van ionen door oxiden dient rekening te worden gehouden met de porositeit van het oppervlak.

II

De sterke adsorptie van Li^+ en Mg^{2+} ionen aan hematiet, in vergelijking met de overige alkali- respectievelijk aardalkali-ionen, hangt waarschijnlijk samen met het feit dat eerstgenoemde ionen in de hematietstructuur passen.

III

Bij specifieke adsorptie in het ladingsnulpunt verschuiven het ladingsnulpunt en het iso-elektrisch punt in tegengestelde richting.

IV

Het door HINGSTON et al. beschreven mechanisme van de fosfaatadsorptie door oxiden is in strijd met elementaire fysisch-chemische wetmatigheden.

F. J. HINGSTON, A. M. POSNER and J. P. QUIRK, J. Soil Sci. **23** 177 (1972)

V

Toepassing van de STERN-theorie in haar oorspronkelijke vorm geeft geen bevredigend model van de structuur van de elektrische dubbellaag op oxiden.

B. VAN RAY and M. PEECH, Soil Sci. Soc. Amer. Proc. **36**, 587 (1972)

VI

De door CARLSON en OVERSTREET verrichte metingen van de adsorptie van aardalkali-ionen aan montmorilloniet bij hoge pH, vormen geen afdoend bewijs voor het optreden van een versterkte hydrolyse van de geadsorbeerde ionen.

R. M. CARLSON and R. OVERSTREET, Soil Sci. **103**, 213 (1967)

VII

De door WARSHAW en ROY gebruikte differentiërende kenmerken voor de identificatie van 2:1 phyllosilicaten geven geen voldoende inzicht in de variatie in samenstelling en eigenschappen welke binnen deze groep van mineralen optreedt.

G. M. WARSHAW and R. ROY, Geol. Soc. Amer. Bull. **72**, 1455 (1961)

VIII

Het verdient aanbeveling om bij de classificatie van 2:1 phyllosilicaten gebruik te maken van driehoeksdiagrammen waarin per (halve) eenheidscel de totale lading, en respectievelijk de lading per tetraëder- en per octaëderplaat zijn uitgezet.

IX

Bij de verwijdering van fosfaten uit afvalwater wordt ten onrechte geen aandacht geschonken aan de mogelijkheden die bepaalde gronden in dit opzicht kunnen bieden.

X

Een heffing voor het zuiveringsschap die niet afhankelijk is van bijvoorbeeld het aantal gezinsleden of van het waterverbruik, vormt een aanslag op het beginsel dat de vervuiler betaalt.

Wet Verontreiniging Oppervlaktewateren (1970)

XI

Wegens het feit dat woeste terreinen bij de jeugd duidelijk in een behoefte voorzien, is het van belang de aanleg en/of reservering van dergelijke terreinen in bestemmings- en saneringsplannen op te nemen.

A. Breeuwsma
18 april 1973

VOORWOORD

Bij de voltooiing van dit proefschrift wil ik allereerst mijn ouders bedanken voor de gelegenheid die zij mij hebben gegeven om te studeren en 'student te zijn'. Hoewel zij liever één boerenzoon op het land zagen dan tien langs de kant (in Wageningen), hebben zij mij steeds loyaal gesteund.

Waarde promotor, de vorige promovendus aarzelde tussen Hooggeleerde Lyklema en beste Hans. Ik onderken deze aarzeling, maar wil eveneens de tweede aanspreekwijze beklemtonen. Deze weerspiegelt de plezierige en vriendschappelijke sfeer die er onder jouw leiding bij de afdeling Fysische en Kolloïdchemie is gegroeid. Aan je grote interesse in mijn werk en de verhelderende discussies heb ik veel gehad. Slechts één ding heb je me niet duidelijk kunnen maken: hoe je temidden van je bijzonder drukke werkzaamheden altijd tijd had om gedeelten van dit proefschrift te lezen en op je gemak te bespreken.

Wat de overige, al dan niet wetenschappelijke, werkers van de afdeling betreft: tegenwerkers heb ik niet gekend, medewerkers des te meer. Ik meen in de geest van allen te handelen als ik slechts enkelen met name noem.

Ab van der Linde, voor de kritische en nauwgezette manier waarop jij het grootste deel van de experimenten hebt uitgevoerd ben ik je zeer erkentelijk. Ook de namen van De Jager, Hoeks, Stoop en Troelstra wil ik hier vermelden omdat in dit proefschrift gebruik is gemaakt van werk dat zij tijdens hun ingenieursstudie hebben verricht.

De onverdroten ijver en de opgewektheid waarmee het manuscript werd getypt door Willy van der Made-Kleijne, die de laatste dagen spontaan werd bijgestaan door Maria Hendriks, houden een belofte in voor de toekomst van het Betuwse landschap. Gerard Fleer, jouw kritische en volhardende medewerking bij de voorbereiding van het manuscript voor de drukker heb ik zeer gewaardeerd.

De figuren werden bewonderenswaardig gemaakt door de heer Moritz van de Stichting voor Bodemkartering. Voor deze dienstverlening én voor de gelegenheid die ik heb gekregen om ook in diensttijd aan het proefschrift te werken, ben ik aan de Directie van de Stichting voor Bodemkartering veel dank verschuldigd.

Brian Vincent, ik ben blij dat we steeds jouw opmerkingen hebben kunnen ontcijferen. Nogmaals hartelijk dank voor de snelle en grondige wijze waarop jij de Engelse tekst hebt 'bekommatarieerd' en gecorrigeerd.

CONTENTS

1. INTRODUCTION

1.1. General introduction

Iron oxides are found widespread in nature, for example in the soil and in natural waters. They are also important in industry and engineering. In addition to the mining and metallurgy of iron ores, they are used in paints, ion-exchangers and magnetic tapes and they are well-known as corrosion products. Their role is often connected with their ability to adsorb ionic and non-ionic compounds such as plant nutrient anions or polymers and with their colloid-chemical properties, notably in the soil and in natural waters.

By way of illustration a short account will be given in the following sections of the functions of iron oxides in the soil, a subject which induced us to undertake the present study.

In this chapter the notion 'iron oxide' is taken quite generally to include all oxides with the composition $Fe_2O_3.nH_2O$ where $0 \leqslant n < 3$. The following chapters are more specifically devoted to hematite (α-Fe_2O_3).

1.2. Iron oxides in soils

1.2.1. *Introduction*

From a colloid-chemical point of view the most important soil constituents are the clay minerals, the humus compounds, the Al- and Fe-(hydr)oxides and the polynuclear hydrolyzed species of Al. The clay minerals usually consist of platy silicates ('layer silicates'). The unit layers are composed of combinations of tetrahedral silica sheets and octahedral hydroxyl sheets containing Al, Fe or Mg in the octahedral positions. The planar surfaces of the clay particles often carry a 'permanent' negative charge, due to isomorphous substitution of cations in the tetrahedral or octahedral layers. In addition, positive charges may be present at the edges owing to proton association on octahedral and tetrahedral hydroxyl groups. The net surface charge, however, remains negative under most conditions. Humus compounds are also negatively charged in the pH range normally found in soils (pH 4–8), due to dissociation of carboxyl groups and hydroxyl groups.

Fe- and Al-(hydr)oxides and the polynuclear Al-complexes, on the other hand, may be positively charged over this pH range. As a result, the (hydr) oxides and hydrolyzed species achieve two important functions in soils. In the first place, they contribute greatly to the anion retention capacity of the soil, important plant nutrients (e.g. phosphate, sulphate, molybdate) being strongly

TABLE 1-1. Forms and occurrence of highly-crystalline iron oxides in soils.

Group	Form	Name	Symmetry class	Lattice parameters (Å)	Habit[1]	Colour[1]	Occurrence[2] in soils
anhydrous oxides	α-Fe_2O_3	hematite	hexagonal	a = 5.028 c = 13.74	granular	red	++ (tropics) — to + (temperate climate)
	γ-Fe_2O_3	maghemite	tetragonal	a = 8.34 c = 25.02		light-brown	—
	Fe_3O_4	magnetite	cubic	a = 8.40		black	—
oxyhydroxides (monohydrates)	α-FeOOH	goethite	orthorhombic	a = 4.60 b = 10.00 c = 3.03	needles	yellow	++ (temperate climate) + (tropics)
	γ-FeOOH	lepidocrocite	orthorhombic	a = 3.06 b = 12.51 c = 3.87	needles	orange	— (well-drained soil) + (poorly-drained soil)

[1] habit and colour when fine-grained
[2] ++: abundant +: common —: rare

adsorbed by them. Secondly, the charge contrast between these soil constituents and, especially, the clay minerals leads to important interaction phenomena such as the reduction of the cation exchange capacity of the clay minerals and the promotion of soil aggregation.

It is evident that the quantitative significance of these processes strongly depends upon the composition of the soil, i.e. the relative amounts and natures of the soil constituents. With respect to iron oxides, many soils contain not more than a few per cent of iron oxides, expressed as grams of Fe_2O_3 per gram of dry soil. In these soils anion adsorption by iron oxides is nevertheless important, whereas interaction phenomena seem to be negligible. In soils where a (relative) accumulation of iron oxides has taken place, iron oxide contents may be considerably higher. In temperate humid climates such soils are present, for example, in lowland areas where iron has been supplied by the ground water. However, the most extensive areas of soils rich in iron oxide are found in tropical and subtropical regions. Here, the relative accumulation of iron (and aluminium) oxides is due to the intensive weathering of the primary soil minerals and the extensive washing-out of the released silica. These soils, therefore,

have a low content of weatherable primary minerals. The predominant clay mineral is kaolinite, a 1:1 layer silicate (one tetrahedral sheet attached to one octahedral sheet). In contrast, 2:1 layer silicates (two tetrahedral sheets and one octahedral sheet) such as illite, montmorillonite and vermiculite prevail in the iron oxide enriched soils of the temperate climates. There is a large variety of tropical and subtropical soils, the classification of which is still developing (BURINGH 1970, Soil Taxonomy 1970). For the sake of brevity and convenience we shall refer to them simply as weathered soils. It is not surprising that, especially in these soils, anion adsorption by iron oxides and the interaction of iron oxides with clay minerals are of the utmost importance. A more detailed survey of these processes is given in the following sections.

1.2.2. *Forms and occurrence*

In discussing the forms of iron oxides in soils, it is convenient to distinguish between highly-crystalline and poorly- or micro-crystalline iron oxides. Mineralogical data on highly-crystalline iron oxides have been discussed by ROOKSBY (1961) and compiled in table 1–1. In addition, the distribution of these minerals in soils, as reported by SCHWERTMANN (1959), is given in the last column of this table.

It is apparent from this table that hematite (α-Fe_2O_3) and goethite (α-FeOOH) are the most frequently occurring highly-crystalline iron oxides in soils. Hematite is the dominant iron oxide mineral in (red) tropical soils but it is less common in soils of the humid-temperate climate. Goethite is found both in tropical and temperate regions. In the latter areas especially, the most recent formations of goethite consist of finely divided, poorly-crystalline minerals. They are, therefore, distinguished from the highly-crystalline forms and nowadays called limonite (ROOKSBY 1961). Furthermore, in recent deposits of iron oxides, 'amorphous' iron oxides are found with the general chemical composition $Fe_2O_3.nH_2O$, $1 < n < 3$. The notion 'amorphous' means that no structure can be detected with the X-ray and electron diffraction techniques which are normally used. However, it has been recently shown (VAN DER GIESSEN 1966) that 'amorphous' oxides may in fact be micro-crystalline. One may conclude that little is known about the detailed structure of the finely divided iron oxides in the soil, although, due to their high surface area, they are the most active forms of iron oxides in adsorption and interaction phenomena.

1.2.3. *Anion adsorption*

The adsorption of anions by the inorganic part of the soil is very specific to the nature of the soil constituent as well as to the type and concentration of the anion.

Anions like chloride and nitrate are not strongly adsorbed at the positive

edges of the clay minerals. In fact, their negative adsorption at the negative faces normally exceeds any positive adsorption at the edges. A notable exception is the positive adsorption of chloride which occurs with kaolinite at low pH (DE HAAN 1965, SUMNER and REEVE 1966). Consequently, adsorption of these anions is predominantly governed by the oxides. Sulphate is more strongly adsorbed at the clay mineral edges, leading in some cases (CHAO et al. 1962) to a slight positive overall adsorption. The adsorption by iron (and aluminium) oxides, however, is much higher. Removal of a few per cent of these materials leads to a substantial decrease in adsorption of sulphate by the soil (CHAO et al. 1962).

Phosphate is particularly strongly adsorbed by clay minerals. The overall adsorption is always positive and, in dilute solutions, is of the order of μmol's per gram of dry clay. Nevertheless, the adsorption of phosphate by the oxides tends to be at least an order of magnitude higher (BACHE 1964, MULJADI et al. 1966, HINGSTON et al. 1967 and 1968). Hence iron (and aluminium) oxides play a significant role in the adsorption of phosphate by soils, even when the oxide content is not more than a few per cent. The affinity of phosphate for oxides is so high that, at high concentrations, it reacts with the bulk of the oxides. Decomposition occurs and is followed by precipitation of iron or aluminium phosphates (HASEMAN et al. 1950, KITTRICK and JACKSON 1955, TAYLOR et al. 1964, TAMINI et al. 1964 and 1968). This situation may be present in the neighbourhood of dissolving phosphate fertilizer particles in the soil and it is in many soils (KITTRICK and JACKSON 1955, TAMINI et al. 1964) the basis of the so-called phosphate fixation process.

Other important plant nutrients such as molybdate and borate are also strongly adsorbed by iron oxides (REISENAUER et al. 1962, REYES and JURINAK 1967, SIMS and BINGHAM 1968).

Little study has been made of the anion adsorption mechanism. It is generally assumed that anions like chloride and nitrate are physically adsorbed, i.e. attracted by the (positive) surface through electrostatic forces (DE HAAN 1965). Anions such as sulphate (AYLMORE et al. 1967), phosphate (BACHE 1964, MULJADI et al. 1966, HINGSTON et al. 1967 and 1968), molybdate (REISENAUER et al. 1962) and borate (SIMS and BINGHAM 1968) on the other hand, are thought to be chemisorbed, i.e. they exchange with surface hydroxyl groups, and thus find themselves in the first co-ordination shell of the underlying metal ion. This reaction is sometimes referred to as anion penetration (JURINAK 1966) or specific adsorption (HINGSTON et al. 1967 and 1968). It is probable that some knowledge of the mechanism of the adsorption process would be helpful in understanding the nature of the desorption process. There is evidence that this problem is also of some interest in agricultural practice, at least for phosphate. In addition to (dissolved) inorganic and organic phosphates, adsorbed phosphate may be an

important source for plants (MURMANN and PEECH 1969). Very little is known so far about the reversibility of the adsorption of phosphate on different soil constituents. There are indications that the reversibility is better for clays than for oxides (MULJADI et al. 1966). However, more detailed studies are needed, especially in very dilute solutions because the concentration of phosphate in the soil solution is generally not more than a few ppm (SCHEFFER and SCHACHTSCHABEL 1966).

1.2.4. *Interaction with clay minerals*

Iron oxides are commonly reported as having an iso-electric point above pH 6.5 (PARKS 1965). Probably, they do not contribute directly to the cation exchange capacity (CEC) of soils, except perhaps in some weathered soils at high pH. However, there is a definite indirect effect. At low pH, iron oxides are able to compensate part of the negative charge of the clay minerals in soils. This leads to another feature which is important in soil fertilitity, viz. the reduction of the CEC. The relative significance of this effect depends upon factors such as the relative amounts, sizes, charges and crystal structures of the soil constituents, the concentration and composition of the soil solution, etc.

Experimentally, a significant reduction of the CEC of clays has been found with fresh, partly neutralized solutions of ferric chloride (COLEMAN et al. 1964, CARSTEA 1968), but ageing for some weeks at room temperature seems markedly to suppress the reduction (CLARK and NICHOL 1968). Ageing results in the formation of comparatively large particles of iron oxide which, apparently, are less effective. It is probably for this reason that this type of CEC reduction is of minor importance in soils with a low or moderate content of iron oxide (RICH 1968). In most of these soils the highly active, positive, hydrolyzed species of Al account for the greater part of the reduction (RICH 1960, COLEMAN et al. 1964). However, in some of the weathered tropical soils iron oxides cause a definite reduction of the CEC (SUMNER 1963).

For the same reasons which give rise to the CEC reduction, iron oxide particles exert a direct influence on soil aggregation and, therefore, on soil structure and permeability. In addition, factors affecting the reversibility of the mutual coagulation (attraction between oppositely charged lyophobic particles) may be equally important. Synthetic mixtures of soil material and iron oxides have revealed that 'amorphous' oxides are highly effective in aggregation, in contrast to highly-crystalline oxides, indicating a significant influence of the particle size (SCHAHABI and SCHWERTMANN 1970). As expected, aggregation increases with decreasing pH (SCHAHABI and SCHWERTMANN 1970). In soils, aggregate stability has been shown to be related to the iron oxide content (CHESTERS et al. 1957, AREA and WEED 1966). Furthermore, an intimate association of iron oxides and kaolinite is said to be responsible for the very poor disper-

sibility of a well-known type of weathered soil, namely the latosols (KOENIGS 1961, Soil Taxonomy 1970).

1.3. THE ELECTRICAL DOUBLE LAYER ON IRON OXIDES

The foregoing brief summary has shown that the adsorption of ions on iron oxides is very important for the understanding of some fundamental processes in the soil. However, on closer inspection it appears that very little is known about the nature of the adsorption mechanisms. The same holds for the colloidal interaction between iron oxides and clay minerals.

It is well-known from electro- and colloid-chemical studies of, for example, the mercury and silver iodide/solution interfaces that detailed information can be obtained about the nature of adsorption and colloidal interaction phenomena. (DELAHAY 1965, OVERBEEK 1952). When the present investigation was initiated, little study had been made of the iron oxide/solution interface, however. These considerations induced us to carry out a detailed study of the electrical double layer on one of the forms of iron oxide, namely hematite (α-Fe_2O_3).

Silver iodide is an important model for electrical double layer studies because stable sols of it can be prepared, allowing double layer parameters to be related to the results of stability and electrophoresis measurements. This is also possible with insoluble oxides. Other analogies between the AgI/solution and oxide/solution interfaces are that both are reversible and that the analytical techniques to obtain the surface charge are very similar. Fundamental data about the double layer on silver iodide have been obtained from potentiometric titrations of silver iodide suspensions. These suspensions are titrated with an electrolyte solution containing one of the potential-determining ions, Ag^+ and I^-. The surface charge, originating from the adsorption of the potential-determining ions, can be derived from these titrations. It is a function of the surface potential and the nature and concentration of the supporting electrolyte (OVERBEEK 1952, LYKLEMA 1961, LYKLEMA and OVERBEEK 1961, LYKLEMA 1963, BIJSTERBOSCH and LYKLEMA 1965, LYKLEMA 1966a and 1966b). Additional information on ion binding and double layer structure is gained from stability measurements (KLOMPÉ 1941, TROELSTRA 1941, REERINK and OVERBEEK 1954, LYKLEMA 1966a and 1966b) and from electrokinetics (BIJSTERBOSCH 1965).

With respect to the iron oxides, stability measurements (FREUNDLICH 1903) and electrokinetic measurements (HAZEL and AYRES 1931, JOHANSEN and BUCHANAN 1957a and 1957b, VAN SCHUYLENBORGH and SÄNGER 1949, VAN SCHUYLENBORGH et al. 1950) previously prevailed in colloid-chemical studies (cf. the review by PARKS 1965). The potentiometric titration technique was first systematically applied to the iron oxide system by PARKS and DE BRUYN

(1962). They measured the adsorption of the potential-determining H^+ and OH^- ions on hematite as a function of pH in solutions of potassium nitrate. JOY and WATSON (1964) extended this method in their study of the adsorption of collector ions on hematite. Whilst the present study was in progress, more work was published in which potentiometric titrations were used. DE BRUYN and his coworkers (ONODA and DE BRUYN 1966, BÉRUBÉ et al. 1967) have paid special attention to the adsorption kinetics and the role of surface hydration. At the same time, ATKINSON et al. (1967) proposed an adsorption equation for the potential-determining ions. Finally, AHMED and MAKSIMOV (1968) have also measured the adsorption of these ions in (1–1) electrolytes, but by a different technique.

In addition, a number of interesting studies have been performed on other oxide/solution interfaces such as silica (TADROS and LYKLEMA 1968 and 1969a), glass (TADROS and LYKLEMA 1969b), quartz (LI and DE BRUYN 1966), rutile (BÉRUBÉ and DE BRUYN 1968) and zinc oxide (BLOK 1968, BLOK and DE BRUYN 1970).

The results and interpretation of these studies will be discussed along with our own results.

1.4. OUTLINE OF THE PRESENT STUDY

From the various forms of iron oxides hematite was chosen as a model on account of its low solubility and well-defined bulk structure. Moreover, hematite sols are easier to handle than, for example, goethite sols, the latter tending to form voluminous gels upon coagulation.

Hematite sols were prepared synthetically and characterized by various techniques, with special emphasis on the surface properties. Because of its important role in ion adsorption on other oxidic materials (TADROS and LYKLEMA 1968, 1969a and 1969b) particular attention was paid to the possible occurrence of surface porosity (Chapter 2.). Potentiometric titrations with acid or base were performed on hematite sols yielding the surface charge as a function of pH. On this basis, the adsorption on hematite was studied for several anions (Cl^-, NO_3^-, SO_4^{2-} and $H_xPO_4^{x-3}$) and cations (Li^+, K^+, Cs^+, Mg^{2+}, Ca^{2+}, Sr^{2+}, Ba^{2+}). In some cases additional direct measurements of counterion and co-ion adsorption were made. The experimental set-up for the titrations and counter charge measurements is described in Chapter 3. The results and discussion are presented in Chapter 4. for all ions except phosphate. To complement the picture of the double layer structure on hematite, stability measurements were carried out with the same electrolytes as used in the potentiometric titrations (Chapter 5.). The (ad)sorption of phosphate on hematite follows a pattern different from that of the other ions. This topic is therefore separately treated in Chapter 6.

2. PREPARATION, CHARACTERIZATION AND SURFACE CHEMISTRY OF THE SAMPLES

2.1. MATERIALS

All chemicals used in the present work were analytical reagent grade. All solutions were prepared with water that was purified by distilling it once and then percolating it over a goethite column to remove any adsorbable impurities. Subsequently, CO_2 was removed by boiling for 20 minutes and the water either used directly or stored in a glass vessel with a soda lime-tube and siphon.

2.2. PREPARATION OF SAMPLES

2.2.1. *Introduction*

One of the well-known methods of preparing hematite, also used in this study, is by hydrolysis of a ferric salt (WEISER 1935, SMITH and KIDD 1949). This hydrolysis reaction and ageing of the precipitate should be carried out in neutral or acid solutions because in basic solutions only goethite is formed (WEISER 1935, SCHWERTMANN 1965). Anions which form complexes with the ferric ion retard the crystallization (MACKENZIE 1957, SCHWERTMANN et al. 1968). Therefore, salts containing anions such as nitrate and perchlorate are more suited than those containing, for example, sulphate and phosphate. Furthermore, the rate of crystallization increases if the electrolyte is removed after the formation of the precipitate (WEISER 1935, FRIPIAT and PENNEQUIN 1965, HSU 1964).

The hydrolysis reaction may be forced to completion by raising the temperature or by the addition of base. The former method was applied by DE BRUYN and his coworkers (PARKS and DE BRUYN 1962, ONODA and DE BRUYN 1966, BÉRUBÉ et al. 1967) and by ATKINSON et al. (1967). However, it has not been checked whether in this case the hydrolysis reaction was indeed completed before the heat treatment was finished. If the hydrolysis which occurred at a pH < 1 is not complete before the excess salt is removed by washing, precipitation of amorphous iron oxides on the hematite particles might occur. Of course, subsequent ageing would meet this objection but has not been applied in these investigations. The hematite sample thus prepared was reported to contain at least five to ten per cent of goethite and amorphous oxides (PARKS 1960).

A more rapid method of preparation consists of neutralization of a ferric salt solution by the addition of base. At ambient temperatures a brown amorphous precipitate is formed. After ageing of this precipitate at ambient tem-

peratures, a mixture of hematite, goethite and amorphous iron oxides is found (SCHWERTMANN 1965). However, ageing at temperatures in the range 100 to 150 °C has been reported to yield a pure hematite sample (WEISER and MILLIGAN 1935, TROELSTRA 1941).

2.2.2. *Experimental*

It was decided, on the basis of the discussion in the foregoing section, to prepare hematite samples by the addition of a roughly equivalent amount of base to a boiling solution of ferric nitrate. After that, autoclave treatment was applied to promote complete crystallization. Preliminary investigations were carried out in order to establish the experimental conditions needed to minimize the contents of other iron oxides, i.c. goethite and amorphous oxides. The preparations were investigated by X-ray diffraction and differential thermal analysis[1].

The following procedure was finally adopted. Two litres of a solution containing 320 grams $Fe(NO_3)_3.9H_2O$ (Merck) were made to boil under reflux conditions and stirring. Then a concentrated solution of KOH (ca. 12 N) was added dropwise (25 drops per minute) until a pH of 7 was achieved. This process takes about 8 hours. The precipitate was washed with water by decantation as far as possible (attained electrolyte concentration ca. 0.05 M, pH ca. 7). Thereafter, the peptized samples were aged in an autoclave for another 8 hours at 140–150 °C. The final washing step was performed by decantation at pH 9, where the samples coagulated readily. The washing was stopped when the conductivity of the supernatant was equal to that of the conductivity water ($3 \times 10^{-6}\ \Omega^{-1}cm^{-1}$).

Three samples were prepared in the course of this study by mixing ten to fifteen batches each, before the autoclave treatment. The samples (A, B, C and D) were stored in conductivity water. A part of sample A, called A_d, was dried at 105 °C after the preparation and, after grinding, stored as a powder.

2.3. MINERALOGICAL AND CHEMICAL CHARACTERIZATION

2.3.1. *Mineralogical analysis*

2.3.1.1. Experimental

A mineralogical analysis of the samples A, B and C was carried out by means of X-ray, infrared and thermal analysis[2].

[1] Thanks for their co-operation are due to Dr. L. VAN DER PLAS and Mr. R. SCHOORL of the Department of Soil Science, Agricultural University, Wageningen.

[2] We are indebted to Dr. Ir. H. W. VAN DER MAREL of the Netherlands Soil Survey Institute for his assistance in the measurements and interpretation.

X-ray diffraction patterns were obtained with a Philips diffractometer using Co-Kα radiation.

Infrared analyses were performed with a Perkin Elmer Model N 13 spectrophotometer. KBr pellets were prepared containing 0.4 mg of hematite in 300 mg of KBr. Depending upon the wavelength required the following prisms were used: CaF_2 (2.5–3.6 μm), NaCl (3.6–14 μm) and KBr (14–25 μm).

In the thermal analysis with a Metrimpex Derivatograph (Hungary) three traces have been registered simultaneously, i.e. thermogravimetric (TG), differential thermogravimetric (DTG) and differential thermal analysis (DTA) traces. After drying at 110°C, 800 mg of the samples have been mixed with 400 mg of the inert material, α-Al_2O_3. Heating, in air, was performed at a rate of 10°C per minute.

2.3.1.2. Results and discussion

None of the X-ray diagrams contained peaks which could be attributed to forms of iron oxide other than hematite or goethite. The diagrams of sample A and C contained a small diffraction peak at 4.18 Å, indicating the presence of approximately five per cent or less goethite. Sample B did not give this peak and thus it would seem that goethite is not present in this sample.

The infrared spectra of samples A and C, in contrast to that of B, showed small absorption bands at 800 and 895 cm^{-1}. These bands have been observed in the spectrum of goethite but not in that of hematite (VAN DER MAREL 1966). Therefore, these results confirm the presence of small amounts of goethite in samples A and C.

The various thermal analysis curves obtained are given in figure 2–1 for samples B and C. The curves for sample A closely resemble those for sample C. The DTG traces show a dip around 100°C corresponding to the loss of primarily physically adsorbed water. Infrared spectroscopy revealed that the 1630 cm^{-1} peak of physically adsorbed water disappeared after heating of the pellet to 170°C. Furthermore, sample C shows a slight increase in loss of weight around 290°C, in contrast to sample B. This loss of weight is presumably to be ascribed to the convertion of traces of goethite into hematite. Finely divided or poorly-crystallized goethite has been found to be converted into hematite below 300°C (MACKENZIE 1957). The concomitant endothermic DTA peak is not revealed in the present case. One might argue that this could be caused by overlap of the endothermic peak by an exothermic one due to crystallization of amorphous iron oxides (MACKENZIE 1957), if present. However, this is unlikely if one considers the TG data. In the temperature range of 240–340°C the weight of sample C decreased by approximately 0.75%. If 5% of goethite were present 0.50% of the loss of weight would be already accounted for by goethite water. The remaining loss of 0.25% has to be attributed to chemisorbed water and

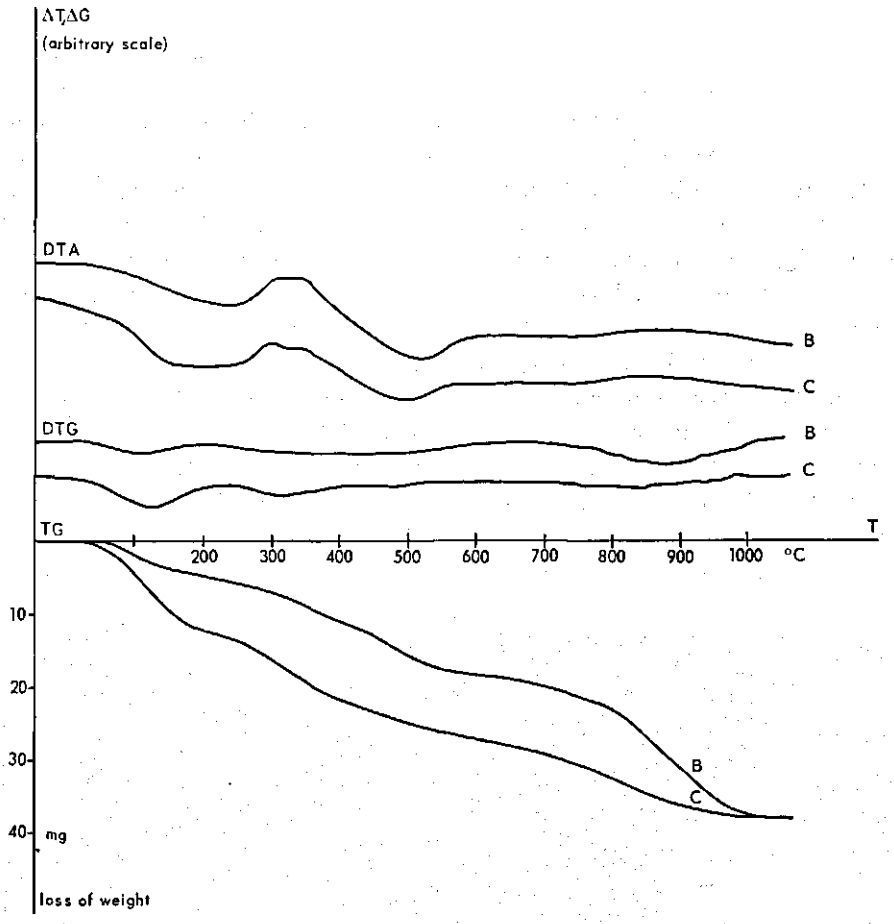

FIG. 2-1 DTA, DTG and TG curves for hematite (samples B and C). Heating rate: 10°C/minute. Sample weight: 800 mg.

amorphous oxide water, if any. Since amorphous iron oxides have at least 10% of structural water, it does not seem very likely that sample C contains more than, say, 2% of amorphous material. The same holds for the other samples.

Summarizing, it can be concluded that the hematite samples have less than 2% of amorphous material, if any. In addition, samples A and C have not more than approximately 5% of goethite. The DTA traces of acid hydrolysis preparations of hematite as reported by PARKS (1960) have a pronounced dip at about 350°C, suggesting a higher contamination with goethite than our samples A and C. In addition, the water content of these acid hydrolysis preparations is higher than that of the present samples by about 1.5% at 600°C.

2.3.2. *Chemical analysis*

The Fe_2O_3 content of the samples was measured after dissolution of the samples according to the citrate-dithionite method (MEHRA and JACKSON 1960). The Fe concentration in the extracts was determined by atomic absorption with air-acetylene using a Techtron AA-4 atomic absorption spectrophotometer equipped with the amplifier read out unit and the burner-nebulizer assembly of the AA-5. The Fe_2O_3 percentages of samples A, B and C were 95.0, 96.0 and 95.5%, respectively. If these percentages and the water percentages to match, measured as the loss on ignition at 950°C, are added up, the following percentages are found for samples A, B and C, respectively: 99.9, 100.7 and 100.2%. Therefore the recovery is complete within experimental error.

Important traces of impurities, however, are not excluded. Actually, during the negative adsorption measurements (section 2.5.4.2.) it was found that the samples released Ca^{2+} and Mg^{2+} ions, the concentration of the former interfering with the measurement of the negative adsorption. This was somewhat unexpected and therefore it was verified whether this could be due to the presence of traces of these elements in the ferric nitrate reagent. To that end the

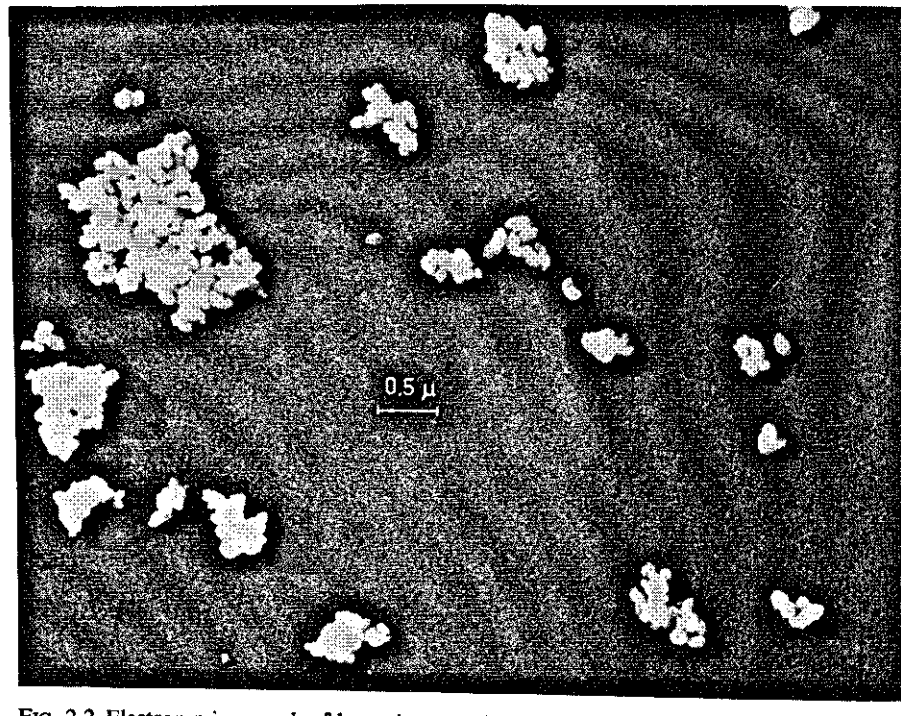

FIG. 2-2 Electron micrograph of hematite, sample A_d. Shadowed specimen. Total magnification: 15,000×. By courtesy of the Technical and Physical Engineering Research Service, Wageningen.

ferric nitrate reagent and the samples were analysed by atomic absorption. The samples were dissolved with citrate-dithionite. The addition method was used, adding approximately a one, two or three-fold excess of the cation of the solution to be analysed and extrapolating to zero absorbance. The ferric nitrate reagent was in this way found indeed to contain Ca^{2+} (0.03%) and Mg^{2+} (0.003%). If these ions were to be completely retained by the hematite samples one would expect a (maximum) impurity level of about 0.15% for Ca^{2+} and 0.015% for Mg^{2+}. The actual average values for the samples under study were found to be 0.04 and 0.01%, respectively. This clearly illustrates that the traces of Ca^{2+} and Mg^{2+} in the reagents are strongly retained by the samples, especially in the case of Mg^{2+}. As will be shown in Chapter 4. these results are confirmed by the study of the adsorption of these ions on hematite.

2.4. Electron micrographs

Additional information about the nature of the hematite samples was obtained from electron micrographs made by Dr. J. P. C. Holst, Unilever Research Laboratory, Vlaardingen, and Messrs. S. Henstra and H. G. Elerie, Technical and Physical Engineering Research Service, Wageningen. An appropriate quantity of sample A_d was dispersed by shaking after adjustment of the pH to 3 to promote dispersion. A small aliquot of this suspension was pipetted onto the grids and dried. One of the samples prepared in this way was shadowed.

Despite the peptization treatment the samples show considerable aggregation. The particles have rounded edges, perhaps due to melting in the electron beam. The shadowed sample (fig. 2–2) shows more or less globular particles. At a higher magnification (fig. 2–3) the projected images of the particles as seen on the micrograph resemble parallellograms with an included angle of about 60° and sides commonly between 400 and 700 Å. A rough estimate of the surface area, S_{EM}, of this sample was made by counting 40 particles and using the expression (Heywood 1970, Gregg and Sing 1967):

$$S_{EM} = \frac{K\sum n_i d_i^2}{\rho\sum n_i d_i^3} \qquad (2-1)$$

where K is a shape factor, ρ the solid density and n_i the number of particles with a mean projected diameter d_i, i.e. the diameter of a circle having the same area as the projected image of the particle. This image was calculated by use of the equation for a parallellogram with an included angle of 60°. The shape factor was taken as 8.5 (Heywood 1970), i.e. the value for rounded particles, and the density as 5.24 (Mellor 1934). By doing so, S_{EM} was found to be 26

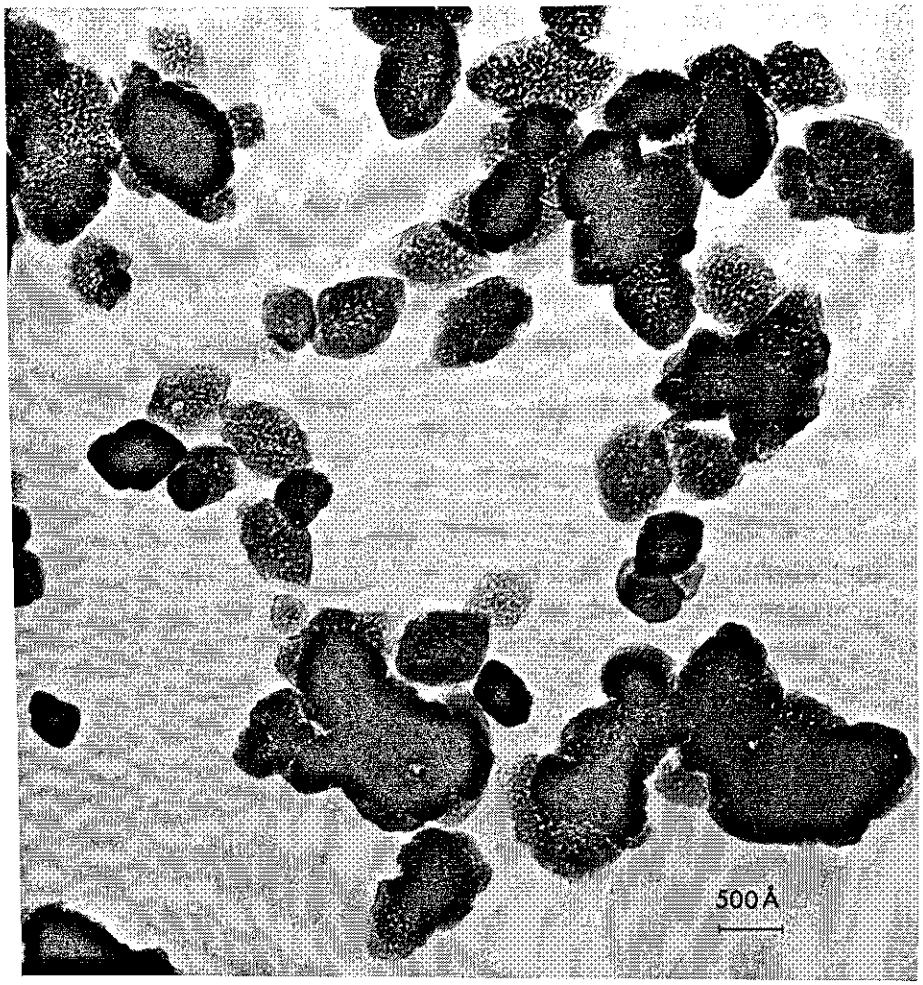

FIG. 2-3 Electron micrograph of hematite, sample A_d. Total magnification: 128,000×. By courtesy of Unilever Research Laboratory, Vlaardingen.

m^2g^{-1} for sample A_d. The error in S_{EM} is probably large (say 10 to 30%) owing to the limited number of particles counted and, especially, due to the uncertainty in the shape factor.

2.5. SURFACE AREA AND POROSITY

2.5.1. *Introduction*

In order to enable a comparison of adsorption on various substrates or on different batches of the same material, the surface area has to be known. Ad-

sorption methods are commonly used in surface area determinations. Very often the positive adsorption of an adsorbate from the gas (vapour) or liquid phase is used. The surface area is then calculated from the number of adsorbate molecules needed to cover the surface with a monolayer and the average area occupied by one molecule, that is the molecular area. The determination of both the monolayer point and the molecular area, is *not* (always) unambiguous. However, these problems appear to be largely solved for the gas adsorption method if nitrogen is employed as adsorbate (GREGG and SING 1967) (see below). It is the most widely used method in the measurement of the surface area of solids, irrespective of whether the solids are subsequently used as dry powder or as dispersed materials. It has been recently reported for silver iodide (VAN DEN HUL and LYKLEMA 1968) that the surface area of a dispersed solid may alter upon drying prior to the gas adsorption measurements. It is then necessary to measure the surface area of the dispersed solid *in situ*. In the case of silver iodide the negative adsorption method has been used. This method is based upon the the repulsion (negative adsorption) by a charged surface of ions with the same sign as the surface charge (co-ions) and the ensuing increase in salt concentration outside the range of the repulsion forces. The negative adsorption is proportional to the surface area and has the advantage of being independent of a molecular area, in contrast to positive adsorption. On the other hand, it yields the total surface area only if the surface is smooth and non-porous.

In addition to the specific surface area of a solid, its porosity is an important characteristic as it affects the positive as well as the negative adsorption. The porosity is also commonly studied by gas adsorption (GREGG and SING 1967). Thus information is obtained about the pores accessible to, for example, N_2 molecules. However, in the present study of the ionic adsorption on hematite it is the porosity of the surface with respect to ions which really counts. Whilst this work was in progress it became clear that materials such as precipitated SiO_2 (TADROS and LYKLEMA 1968 and 1969a) and glass (TADROS and LYKLEMA 1969b) are more porous with respect to (hydrated) cations than with respect to N_2 molecules. In this case both types of porosity occur together suggesting that they may be related. Moreover, as said before, the presence of nitrogen porosity is reflected in the negative adsorption. It is reduced when the double layers at opposite pore walls overlap each other. Therefore, a comparison of the negative and gas adsorption area also provides information about surface porosity (and smoothness).

The above considerations prompted us to study the surface area and porosity of the hematite samples by gas adsorption (nitrogen) as well as by negative adsorption (Ca^{2+}).

2.5.2. *BET areas*

2.5.2.1. Evaluation of the method

Gas adsorption areas were obtained with nitrogen and the monolayer point was determined according to the BET method. For a comprehensive evaluation of these and other gas adsorption methods the reader is referred to, for example, GREGG and SING (1967). Suffice it to state here that BRUNAUER, EMMETT and TELLER (1938) arrived at a well-known equation from which the monolayer volume can be derived. In a linearized form this equation reads:

$$\frac{p/p_0}{v(1-p/p_0)} = \frac{(c-1)\,p/p_0}{v_m c} + \frac{1}{v_m c} \qquad (2-2)$$

where p/p_0 is the relative vapour pressure of the adsorbate, v the volume of gas adsorbed, v_m the volume of gas adsorbed in a monolayer and c is a constant related to the (difference in) heats of adsorption in the first and subsequent layers.

The basic assumptions underlying the BET theory are:

1. the surface is homogeneous, i.e. the adsorption energy is independent of the site on the surface
2. lateral adsorbate-adsorbate interaction is absent
3. the heat of adsorption in the second and higher layers is uniform and equal to the heat of condensation
4. the number of adsorbed layers becomes infinite when the vapour pressure reaches saturation.

In practice, BET plots according to equation (2–2) are linear over a limited range of relative pressures: $0.05 < p/p_0 < 0.35$.

Especially assumptions 1 and 4 are responsible for the lower and upper limitation of the applicability range, respectively.

It is obvious that the assumption of an unlimited number of adsorbed layers becomes invalid for solids which contain pores that can accomodate only a finite number of adsorbed molecules (the so-called micropores, cf. section 2.5.3.). Introduction of a limited number of adsorbed layers (BRUNAUER et al. 1940) as a third parameter in the BET theory leads for microporous solids to areas which are lower than the BET areas (JOYNER et al. 1945). Other complications with microporous solids are the facts that in narrow pores the heat of adsorption (GREGG and SING 1967) and the molecular area (DE BOER et al. 1965) may be higher than at the non-porous surface. These points illustrate that it is always advisable to perform a (micro) porosity analysis not only for the assessment of porosity itself but also for a proper evaluation of the BET area.

The molecular area of nitrogen used in this study is 16.2 Å. This value, pro-

posed by EMMETT and BRUNAUER (1937), was calculated assuming normal liquid packing of nitrogen molecules in the complete monolayer. Efforts to determine this area experimentally from nitrogen adsorption measurements on adsorbents of known area (e.g. known from electron microscopy) have resulted in the range of values varying between 13.8 (VOET 1969) and 20.0 Å (PIERCE and EWING 1964). It appears from these studies that the nitrogen BET area calculated with 16.2 $Å^2$ as the molecular area does not diverge from the true area by more than about 20%. For other adsorbates the uncertainty is in general higher.

Finally, one important limitation of the nitrogen adsorption method may be mentioned, viz. its role in measuring the area of swelling materials such as certain clay minerals. The apolar nitrogen molecules are not able to penetrate between the clay platelets, in contrast to polar molecules such as water and ethylene glycol. Hence, the external area is measured in stead of the total area.

2.5.2.2. Experimental

The adsorption of nitrogen was measured by a continuous flow method using a Perkin Elmer-Shell sorptometer, model 212 C. The apparatus was designed by NELSON and EGGERTSEN (1958) and described in its present form by ETTRE et al. (1962).

A mixture of nitrogen and an inert carrier gas (helium) is passed over the sample in a tube, the effluent being monitored by thermal conductivity measurements which are registered with a recorder. The partial pressure of nitrogen is calculated from the flow rates of the carrier gas and the mixture as determined with a soap bubble flow meter at the exit of the system. This partial pressure is converted into a relative (vapour) pressure knowing the barometric pressure and the saturation pressure at the adsorption temperature (ca. –196°C). The adsorption of nitrogen by the sample which occurs upon immersion of the sample tube in a liquid nitrogen bath is indicated by a peak on the recorder. Similarly, the desorption is measured after removal of the nitrogen bath. The adsorption and desorption peaks are subsequently calibrated against the peak obtained by the injection of a known volume of nitrogen into the gas stream.

Following the above procedure, five measurements were made in the relative pressure range $0.10 < p/p_0 < 0.35$. The samples were outgassed prior to the measurements by heating the sample at 100°C overnight in a small helium flow. Following common practice the adsorption is expressed in cm^3 nitrogen at standard temperature and pressure (STP) per gram of solid. The area in cm^2 covered by one cm^3 of gas (STP) equals $6.02 \times 10^7\ a_m/22414$, where a_m is the molecular area in $Å^2$. For $a_m = 16.2\ Å^2$ the area covered by one cm^3 (STP) of nitrogen is thus calculated as 4.35 m^2. The data were plotted according to equation (2–2) and the monolayer volume, v_m, was determined from the slope

and intercept. The surface area in m^2g^{-1}, S_{BET}, follows then from $S_{BET} = 4.35\ v_m$.

2.5.2.3. Results and discussion

The areas of the adsorption and desorption peaks were in general only slightly different, yielding divergencies in surface area of 2% or less. The data reported here are average values. Preliminary investigations, carried out to establish the most appropiate conditions for outgassing showed that outgassing at 100°C for extended periods was not necessary, whilst outgassing at higher temperatures resulted in a considerable loss of surface area above a temperature of 200°C. It may be recalled that the DTG and infrared analyses indicated that drying at 100°C is not sufficient to remove all the physically adsorbed water. However, this does not seem to affect the nitrogen adsorption as the same BET area was found whether or not the sample was similarly outgassed at 170°C or *in vacuo* at 80°C.

Taking rounded values, the surface areas (table 2–1) of the samples A, B, C and D are 31, 18, 35 and 21 m^2g^{-1}, respectively. The standard deviation for a single measurement was calculated (NEN 1967) as 2.4 m^2g^{-1}. The coefficients of variation for the values of S_{BET} reported above amount to about 5% for the samples A and C to 5–10 % for B and D. The results of six replicate measurements of the surface of sample A_d carried out within two weeks of each other (not reported in table 2–1) yielded a coefficient of variation of 3.1 %.

In view of the experimental error the continuous decrease in surface area with time for sample A_d is significant. The reason for this phenomenon is not clear. The 'wet' samples, on the other hand, do not exhibit ageing phenomena. This is one of the reasons that wet, rather than dry samples have been used in the adsorption studies.

TABLE 2-1. Nitrogen BET areas of the hematite samples (m^2g^{-1})

Sample / Date of measurement	A_d	A	B	C	D
February 1968	34.0				
May 1968	28.5	29.5			
July 1968			18.1		
November 1968	24.5	27.8			
April 1969	23.5	32.5			
May 1969			18.0	34.0	
December 1969		33.8		36.0	
March 1971					21.0
March 1972					19.0 23.0
average area		31	18	35	21

A comparison of $S_{BET} = 24$ m^{2}g^{-1} and $S_{EM} = 26$ m^{2}g^{-1} for sample A_d, both measured in the same month, i.c. January 1969, reveals a fair agreement between these values. On the basis of the results to be described in the next section, S_{EM} would be expected to be somewhat smaller than S_{BET} (instead of larger).

From the BET area in table 2–1 an equivalent particle radius can be calculated for the 'globular' particles using $S = 3/\rho a$, where a is the particle radius. The values thus obtained vary from 164 Å for sample C to 318 Å for sample B.

Finally, it is noted that the reason for the low areas of the samples B and D as compared to the samples A and C is obscure since a clear indication for any variation in the preparation procedure seems to be absent.

2.5.3. *Surface porosity*

2.5.3.1. Principles and methods

The porosity of the samples was also investigated by nitrogen adsorption. In discussing this matter it is convenient to use the DUBININ classification of pores (DUBININ 1960). He distinguishes micropores (width $<$ 20 Å), transitional or intermediate pores (width between 20 and 200 Å) and macropores (width $>$ 200 Å). Depending upon the kind of porosity the normal monolayer-multilayer adsorption process is accompanied by closure of micropores (micropore-filling) or capillary condensation in transitional or macropores. The latter type of porosity is easily recognized from the adsorption and desorption isotherms by the occurrence of a hysteresis loop. Microporosity can be found by comparing the adsorption data with those for a non-porous reference solid.

An elegant way for performing this analysis was introduced by LIPPENS and DE BOER (1965). They plot the volume of gas adsorbed at a given relative pressure against the average thickness, t, of the adsorbed layer on the non-porous reference solid at the same relative pressure. For nitrogen on a non-porous sample the average thickness is calculated from $t = 3.54\ v/v_m$ where v is expressed in cm^3(STP)g^{-1}. When the sample which is being studied is non-porous and chemically related to the reference solid a straight t-plot is obtained, the slope of which gives the surface area, S_t, in m^{2}g^{-1} through $S_t = 15.5\ v/t$. Microporosity is easily observed as a downward deviation of the t-plot, whereas capillary condensation results in an upward deviation. A quantitative determination of the extent of porosity is also readily obtained by comparing the slope of the linear upper part of the t-plot with the slope of the first part. The former slope yields the external area, i.e. the area outside the pores plus the cross-sectional area of the pores. All the micropores and transitional pores have then been filled on reaching the linear position of the t-plot at higher relative pressures.

A somewhat modified procedure was recently proposed by SING (1968 and 1970a). He avoids the use of t as it may be that t is derived from an erroneous BET monolayer capacity, v_m. Instead of v_m he uses as a reference point the volume of gas adsorbed at a given value of the relative pressure, viz. $p/p_0 = 0.4$. At this relative pressure micropore-filling is usually completed whereas irreversible capillary condensation (causing hysteresis) commonly starts above this pressure. In this way t values are replaced by a_s values defined by $a_s = v/v_{0.4}$ and the surface area, S_a, is calculated for nitrogen adsorption in m^2g^{-1} from $S_a = 2.87\ v/a_s$ (v in cm^3 (STP)g^{-1}) where the factor 2.87 has been obtained by calibration against the BET area of the reference solid (Degussa Aluminium-oxide C).

The most serious problem in the assessment of porosity is in obtaining reliable reference data. One has to be sure that deviations from the t- or a_s-plot are not due to factors other than the porosity of the sample under investigation. It has, therefore, to be ascertained whether the reference solid is indeed entirely non-porous. That this is not always true is shown by the fact that the master curve, that is the adsorption isotherm for the reference solid, put forward by LIPPENS and DE BOER (1965) has been discredited for this very reason (PAYNE and SING 1969).

Furthermore, the difference in the heat of adsorption (c value) on the unknown and reference solid should not be too large. Although the master curves for nitrogen adsorption on widely different solids are in fairly close agreement (PIERCE 1968) it remains questionable whether a universal t-curve can be used for a precise interpretation of, for example, a nitrogen isotherm. It seems likely that, for this purpose, standard data are needed on a reference solid with an identical surface structure as the sample under investigation (SING 1970b).

2.5.3.2. Experimental

A static, volumetric method was used to study the porosity because the continuous flow method cannot be employed to measure a desorption isotherm. Moreover, the adsorption can be studied with the static method more accurately and over a wider relative pressure range. The adsorption measurements were performed by Ir. Th. J. OSINGA, Unilever Research Laboratory, Vlaardingen. The samples were degassed *in vacuo* at 80°C. A combined adsorption-desorption run was made with 65 mg of sample A_d. For a more accurate analysis the adsorption run was repeated using 490 mg. The adsorption data obtained with the latter quantity (table 2–2) have been used in the calculation of t- and a_s-plots.

2.5.3.3. Results and discussion

The nitrogen isotherm (fig. 2–4) clearly exhibits a hysteresis loop closing at

TABLE 2-2. Nitrogen adsorption as a function of relative pressure for sample A_d. S_{BET} = 28.8 m^2g^{-1}.

p/p_o	V (cm^3(STP)g^{-1})	p/p_o	V (cm^3(STP)g^{-1})
0.071	6.11	0.567	12.8
0.122	6.79	0.579	13.0
0.161	7.31	0.602	13.3
0.206	7.88	0.624	13.7
0.219	8.05	0.635	13.9
0.232	8.21	0.662	14.4
0.278	8.82	0.691	14.9
0.314	9.32	0.715	15.4
0.347	9.76	0.744	16.1
0.389	10.3	0.766	16.7
0.423	10.8	0.800	17.8
0.456	11.2	0.820	18.6
0.485	11.6	0.851	20.0
0.514	12.0	0.871	21.6
0.542	12.4	0.885	22.6

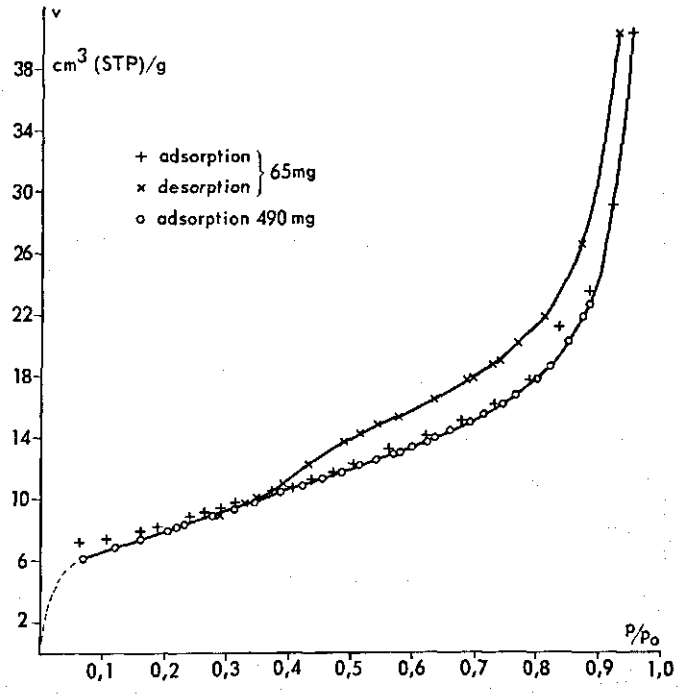

FIG. 2-4 Nitrogen adsorption isotherm for sample A_d.

$p/p_0 = 0.37$. The isotherm may be characterized as a type IV isotherm in the BDDT classification (BRUNAUER, DEMING, DEMING and TELLER 1940), indicating the presence of transitional pores. Due to the lack of standard nitrogen adsorption data on non-porous hematite, t- and a_s-plots have been calculated on the basis of standard data for silica (CARRUTHERS et al. 1968), alumina (LIPPENS and DE BOER 1965, PAYNE and SING 1969) and composite data from different solids (PIERCE 1968). The average layer thickness is based on an effective monolayer thickness of 3.54 Å.

As can be seen in fig. 2–5 only the LIPPENS and DE BOER (LB) t-plot extrapolates through the origin. The other t-plots give a negative intercept with the ordinate. The surface area, S_t, calculated from the first part of the LB-plot is 27.6 m^2g^{-1} which compares well with $S_{BET} = 28.8$ m^2g^{-1}. No *downward* deviation indicative of micropores is observed. On the contrary, at $t \simeq 4.5$ (or $p/p_0 \simeq 0.25$) a small and gradual *upward* deviation starts, confirming the presence of transitional pores. The onset of capillary condensation occurs at a lower relative pressure than revealed by the closure of the hysteresis loop, which may be due to reversible capillary condensation in the smallest pores (SING 1970a, BYE and SING 1967). Above $t = 4.5$ the t-curves definitely diverge, reflecting the variation in standard data. Especially the LIPPENS and DE BOER-

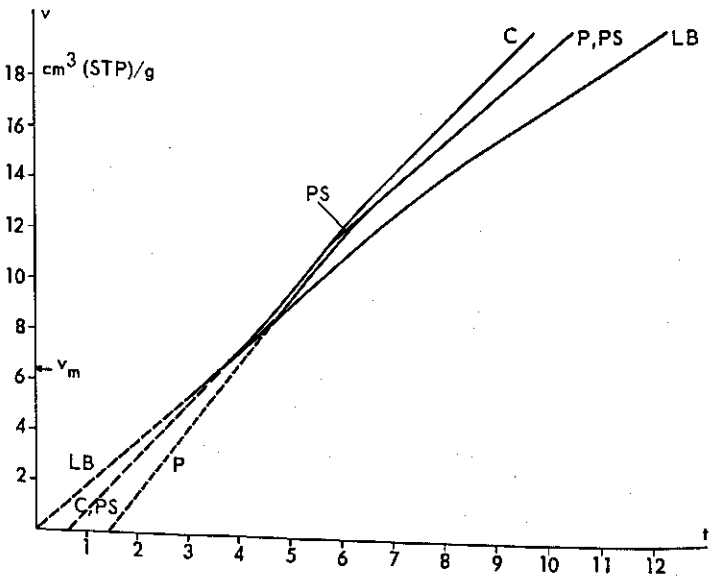

FIG. 2-5 t-plots for sample A_d using the adsorption data of table 2-2 and the standard nitrogen adsorption data of LIPPENS and DE BOER (LB), CARRUTHERS et al. (C), PIERCE (P) and PAYNE and SING (PS).

plot deviates. The other plots become linear again at $t \simeq 6.5$ (or $p/p_0 = 0.60$), indicating that the pores have been filled at this point. The use of inappropriate standard data is probably also responsible for the fact that the slope of the linear upper part of the t-plot is equal or (for silica) even somewhat higher than the slope of the first part. This would imply that the external surface area equals or exceeds the total area. The deviating t-plot of LIPPENS and DE BOER, on the other hand, yields an external area of 20.6 m^2g^{-1}, which seems a more reasonable result. As said before, the standard data of these investigators have been questioned by others (PAYNE and SING 1969, PIERCE 1968).

The a_s-plots calculated with the standard data for silica and alumina follow the same trends as the corresponding t-plots and, hence, do not provide extra information.

In conclusion, it may be stated that this particular hematite sample, and probably also the non-studied samples, show definite evidence for nitrogen porosity but a precise determination of the extent of porosity seems impossible because of the low degree of porosity and the lack of appropriate standard (nitrogen) adsorption data for non-porous hematite. It also follows that the equivalent particle radius is somewhat higher than was estimated in section 2.5.2.3. This radius probably varies between, say, 200 and 400 Å.

2.5.4. *Negative adsorption areas*

2.5.4.1. Theory

The negative adsorption (NA) area essentially follows from a comparison of the measured total amount of negatively adsorbed co-ions with the theoretical value per unit area as calculated from the diffuse double layer theory. The latter quantity has been derived using either the charge or the potential as the primary variable. The first method was introduced by SCHOFIELD (1947) who applied it to the calculation of the negative adsorption for an isolated (i.e. non-overlapping) flat double layer. This method has been especially employed in the determination of the NA area of clays (BOLT and WARKENTIN 1958, DE HAAN and BOLT 1963, DE HAAN 1964 and 1965). The second approach was followed by VAN DEN HUL et al. (1967) and LYKLEMA et al. (1970). They also introduced a method for the calculation of the NA area for spherical particles using the data tabulated by LOEB et al. (1961) for spherical double layers. According to these data the (negatively) adsorbed amounts for isolated spherical and flat double layers start to diverge at $\varkappa a < 20$, where $\varkappa$ is the reciprocal double layer thickness (see also eqn. (4–3), page 51) and a the particle radius.

Since $\varkappa a \simeq 1$ in the experiments to be described in the next section, the equations for an isolated spherical double layer as derived by VAN DEN HUL and

LYKLEMA were used in this study. The negative adsorption area, S_{NA}, is for aqueous solutions at 20 °C given by:

$$S_{NA} = \frac{1.64}{m} \times 10^3 \sqrt{z_{co}}\, V\left(\frac{\Delta c}{c}\right) \sqrt{c}\, I_+^{-1} \qquad (2-3)$$

where S_{NA} is expressed in m^2g^{-1}, m is the amount of adsorbent, z_{co} the valency of the co-ion (sign not included), V the liquid volume in 1, c the concentration of the electrolyte in moles l^{-1} and Δc the difference in electrolyte concentration before and after the introduction of the solid. I_+ is a parameter tabulated by LOEB et al. (1961). In the notation of these authors the subscript $_+$ refers to the negative adsorption. I_+ is a function of the valencies of the co-ions and counterions, of the reduced potential, y_d, and of the reduced radius, q_0. The latter dimensionless quantities are defined as $y_d = e\psi_d/kT$ and $q_0 = \varkappa a/\lambda$, where e is the elementary charge, ψ_d the diffuse double layer potential, k the BOLTZMANN constant, T the absolute temperature and $\lambda = (z_{co} + z_{ct})/2z_{ct}$, with z_{ct} as the valency of the counterion.

After substituting the specific surface area of a sphere as given by $S = 3/\rho a$ and after introducing $q_0 = \varkappa a/\lambda$ eqn. (2–3) can be rearranged (again for aqueous solutions at 20 °C) to:

$$V\left(\frac{\Delta c}{c}\right)\frac{\rho}{m} = 5.98\, I_+ \frac{z_{ct}}{q_0} \qquad (2-4)$$

The NA area can now be obtained by measuring $V(\Delta c/c)$ and by assigning some value to ψ_d and, hence, to y_d. In this study I_+/q_0 was calculated from eqn. (2–4) and q_0 and, hence, a was determined from a semi-logarithmic plot of I_+/q_0 against q_0 at given y_d. The accuracy of S_{NA} thus depends, amongst other things, on the error in ψ_d. As the negative adsorption becomes independent of ψ_d at high potential (above, say, 150 mV), it is recommended to measure the negative adsorption well below or above the point of zero charge.

2.5.4.2. Experiments and results

In the determination of the NA area for the hematite samples many problems were encountered. Unfortunately, not all of these could be satisfactorily solved in the course of this study. To point out the major difficulties relevant experiments and preliminary results will be discussed below.

The NA areas have been established with ca. 10^{-4} M solutions of $Ca(NO_3)_2$ at pH 4 where hematite carries a positive charge. An aliquot containing ca. 10 g of hematite was added to 50 ml polyethylene bottles. About 40 ml of electrolyte solution were then added and the pH adjusted with HNO_3. Subsequently, a dialysis bag containing 10 ml of water was placed in the bottles. Before use, the bags made of cellulose tubing (Arthur Thomas Co.; wall thickness 0.001

inch) were knotted and then rinsed with conductivity water until constant conductivity was obtained. A blank experiment, without hematite but with the same amount of electrolyte solution and water at the same pH, was run concurrently to determine the initial electrolyte concentration. All additions were made up by weight. Equilibrium was obtained after one week of end-over-end rotation of the adsorption bottles, as was checked before. The Ca^{2+} concentration of the solution inside the bag was determined using an Eppendorff flame photometer. The pH of the suspension was measured and the suspension was then evaporated and the solid dried to constant weight to determine the precise amount of hematite.

The experiment incurred three major practical problems. Firstly, the bags in the hematite dispersion often exhibited leaks after one week of rotation in contrast to those in the blank solutions. Sometimes as many as two out of three bags were damaged. Secondly, the blanks sometimes yielded a Ca^{2+} recovery of 100–130%, indicating some interference in the Ca^{2+} analysis which is somehow connected with the dialysis bags. Last but not least, the samples were found to release Ca^{2+}. This was observed when sample A was found to exhibit very high values for $100\,\Delta c/c$, of the order of 300%. This could be attributed to the release of Ca^{2+} ions by the sample as was found in blanks to which no (indifferent) electrolyte and dialysis bags had been added. In this case the equilibrium liquid was obtained by centrifugation. Similar blanks carried out with the other samples also demonstrated a variable Ca^{2+} release. It was impossible to correct the negative adsorption for this Ca^{2+} release, because of the wide variation obtained. Moreover, it is also expected to diverge from the release under the conditions of the negative adsorption experiment from a theoretical point of view. As the negative adsorption depends upon the electrolyte concentration it will change upon addition of salt to the system. Furthermore, extensive washing of the samples before use (at pH 4 with e.g. 1 M NaCl or K_2SO_4) was not sufficient to reduce the Ca^{2+} contamination to an acceptable level.

Finally, in order to avoid the difficulty of the Ca^{2+} release and to increase the accuracy of the measurements, an experiment was carried out with sample C using Ca^{45} labelled solutions of $Ca(NO_3)_2$[3]. As the sample does not release Ca^{45}, the initial radiochemical activity per unit volume equals that measured in the blank. Furthermore, the distribution of Ca^{45} over the system is the same as that of the non-radioactive Ca^{2+} ions. The equilibrium concentration, c, that is still needed for the calculation of $\varkappa$, was determined as before in a duplicate experiment in which no Ca^{45} was added. The uncertainty in the Ca^{45} determination by flame photometry is less critical now since the Ca^{2+} concen-

[3] The author gratefully acknowledges the assistance of Dr. Ir. M. G. M. BRUGGENWERT, Laboratory of Soils and Fertilizers, Agricultural University, Wageningen.

TABLE 2-3. Negative adsorption data for sample C (pH = 4) obtained at two values of ψ_d and two concentrations of $Ca(NO_3)_2$. The density of the solid is taken as 5.24.

V/m (cm^3g^{-1})	c (moles l^{-1})	100 $\Delta c/c$ (%)	coefficient of variation (%)	S_{NA} (m^2g^{-1})	
				ψ_d = 50 mV	ψ_d = 100 mV
5.03	1.1×10^{-4}	27.4	2.3	19.8	13.9
5.05	1.8×10^{-4}	7.2	9.4	9.9	7.4

tration is no longer involved in the establishment of $\Delta c/c$ and $\varkappa$ is proportional to only $\sqrt{c}$. The coefficient of variation in the activity determination by the liquid scintillation technique (BRUGGENWERT 1972), counting 4 samples of each solution, was found to be 0.5%. The ensuing coefficient of variation in S_{NA} is given in table 2–3 along with some other negative adsorption data for this experiment. Unfortunately, leakage occurred with the majority of the bags in this last experiment. Only the results of single measurements at two electrolyte concentrations can be given therefore.

The NA areas in table 2–3 have been calculated according to the procedure outlined above. There are indications that in this experiment ψ_d was of the order of, say, 50 to 100 mV. The surface potential is not higher than ca. 150 mV because the point of zero charge is around pH 6.5. Coagulation experiments (Chapter 5.) indicated that at pH 4, ψ_d is ca. 30 mV in 0.02 M solutions of $Ca(NO_3)_2$ yielding a lower limit for ψ_d of, say, 50 mV in 10^{-4} M solutions. Table 2–3 shows that the uncertainty in S_{NA} due to the assessment of ψ_d is less than the differences in S_{NA} for the two electrolyte levels. The variation in S_{NA} with c illustrates that the experimental error is still large despite the improvement in the technique.

To obtain absolute values for S_{NA} the tabulated surface areas have to be corrected for the negative adsorption of H^+. This correction has not been calculated as yet for a spherical double layer. Applying the correction for a flat double layer leads to an increase in S_{NA} of ca. 20%.

It is obvious that only a crude estimate of the NA area of sample C can be made. However, it is also clear from table 2–3 that the precise value for this NA area is likely to be smaller than that for the BET area (35 m^2g^{-1}). This result would be in accordance with the finding in section 2.5.3.3. that the surface is somewhat porous.

2.6. SURFACE STRUCTURE

For oxides, the structure of the surface always differs from that of the bulk of the solid phase as a result of surface hydration. Since it is the structure of

the surface phase rather than that of the bulk which counts in the adsorption of ions, the former will be considered in more detail.

Surface hydration studies have been reported for hematite using the analysis of water adsorption isotherms (JURINAK 1966, ZETTLEMOYER and MCCAFFERTY 1969, MORIMOTO et al. 1969) and infrared (BLYHOLDER and RICHARDSON 1962), heat of immersion (ZETTLEMOYER and MCCAFFERTY 1969) and dielectric relaxation (MCCAFFERTY et al. 1970) measurements. From these studies the rehydration of dehydrated hematite is known to occur readily. The first layer of adsorbed water is chemisorbed. That is to say the water molecules dissociate and react with the surface to form two hydroxyl groups (step 1). In the next layer water molecules adsorb physically through one or two hydrogen bond(s) with the underlying hydroxyl groups (step 2). Schematically these steps can be depicted as follows:

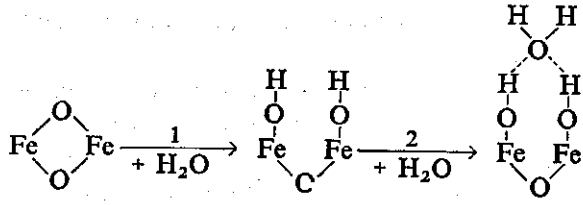

The first layer of physically adsorbed water is immobile as shown by dielectric relaxation studies (MCCAFFERTY et al. 1970), whereas successive layers undergo a gradual transition through a 'mobile' second layer to an ordered, ice-like structure in the next few layers.

The layer of chemisorbed water is particularly important in relation to the present study. In addition to hydroxyl groups, other surface groups may be present as is revealed by the discrepancy that is sometimes found between the theoretical and experimental surface coverage by hydroxyl groups. A completely hydroxylated surface would be able to accomodate ca. 9 OH's/100 Å^2 (MORIMOTO et al. 1969) whereas the experimental values vary from 4.5 through 5.9 to ca. 9 OH's/100 Å^2 as measured by JURINAK (1966), MCCAFFERTY and ZETTLEMOYER (1969) and MORIMOTO et al. (1969), respectively. The hydroxyl groups are of special interest in ion adsorption studies as they are able to dissociate and associate and to exchange against other anions. The Fe^{3+} ions on the other hand are 'buried' under the surface by hydroxyl groups and oxygen atoms and play a more indirect role.

The literature studies mentioned above have been carried out with hematite that was considered to be non-porous, in contrast to that of the present study. In this study some insight in the surface structure could be obtained from the

(D)TG analysis as described in section 2.3.1.2. As mentioned before the DTG traces indicate the release of physically adsorbed water up to a temperature of 170 °C and the loss of goethite (hydroxyl) water at a temperature around 290 °C. The remaining loss of weight, in particular above 340 °C, must be attributed mainly to the loss of chemisorbed water. For convenience, the loss of weight is expressed in terms of the weight of water released per unit (BET) area and given in table 2–4. (The small contribution to the loss of weight by amorphous oxides and impurities may be neglected).

Since the samples have been exposed to the air after drying, it may be expected that they have physisorbed water in excess of the monolayer volume. It cannot be decided therefore to which extent any physisorption of water exceeding the monolayer value for non-porous hematite is due to porosity.

Regarding the chemisorbed water, the relevant data of table 2–4 may be compared with the monolayer values for non-porous hematite to obtain information about the extent of hydration, or more properly, hydroxylation of the surface.

Converting the values for non-porous hematite as quoted above into μg m^{-2} the experimental values are calculated to vary from 67.5 to 135 μg m^{-2}. The corresponding values of table 2–4 are higher by a factor of 5 to 15, indicating that the hydroxylation is not restricted to the surface proper but extends into the interior of the solid.

The above conclusion has also been arrived at on other grounds for hematite prepared by acid hydrolysis (ONODA and DE BRUYN 1966, BÉRUBÉ et al. 1967). ONODA and DE BRUYN (1966) suggested that the surface layers of their samples had a goethite-like structure because goethite is the most stable phase in aqueous systems at pH > 1 and room temperature. Accepting a goethite-like structure for the surface layers of our samples the thickness of this layer is estimated to vary from about 15 (samples A and C) to 25 Å (sample B) which approximately corresponds to 10% of the equivalent particle radius.

TABLE 2-4. Water release for samples A, B and C as derived from thermogravimetric analysis.

temperature (°C)	predominant type of water released	water release (μg m^{-2})		
		A	B	C
20–170	physically adsorbed	322	311	394
170–240	?	126	139	108
240–340	goethite water	242	2180	214
340–950	chemisorbed	887		643

2.7. Conclusions

The synthetically prepared samples of hematite identified by various techniques contain, if any, only small amounts of crystals of other iron oxides such as goethite and amorphous oxides. Nitrogen adsorption studies reveal the samples to be slightly porous with respect to nitrogen. The precise determination of the surface area of the transitional pores was impeded by lack of appropriate standard data. In accordance with a slight degree of porosity, the negative adsorption area tends to be lower than the BET area. In this case, the accuracy is low due to the release of interfering quantities of Ca^{2+} and due to other practical complications. The surface phase of the samples is highly 'hydrated', accomodating chemisorbed water far in excess of what can be adsorbed by the surface proper.

3. SURFACE CHARGE AND COUNTER CHARGE MEASUREMENTS. EXPERIMENTAL

3.1. INTRODUCTION

The electrical double layer at solid/solution interfaces is constituted by the *surface charge* and its *counter charge* in the solution. For oxides, the surface charge and surface potential are a function of the pH and the H^+ and OH^- ions are commonly referred to as *potential-determining* (p.d.) ions (see Chapter 4.). It is impossible to distinguish experimentally between the adsorption of H^+ and the desorption of OH^- ions and *vice versa*. It is, however, convenient for the present discussion to consider both ions as being able to *ad*sorb. Their adsorption can be readily measured by potentiometric acid-base titrations of the dispersed solid. The surface charge can then be calculated from the adsorption after the *point of zero charge* has been established.

As will be shown in the next chapter surface charge–pH curves reflect many important properties of the oxide/solution interface. Of special interest is the role of the charge-compensating ions. The surface charge is compensated for by a *surface excess* of ions of opposite sign (*counterions*) and a *surface deficit* of ions of the same sign (*co-ions*). The surface charge is strongly affected by the natures and concentrations of these ions. Therefore, surface charge–pH curves are valuable tools in the study of the adsorption of counterions and co-ions at the oxide/solution interface. Thus, direct measurements of the adsorption of the counterions and co-ions are not always required. On the other hand, such measurements would furnish a means of checking the surface charge–pH curves.

In this chapter it will be shown how the adsorption of the p.d. ions at the hematite/solution interface was measured through potentiometric titrations and how the surface charge–pH curves have been established. In addition, experiments will be described in which the adsorptions of counterions, of co-ions and of p.d. ions were measured concurrently.

3.2. DETERMINATION OF SURFACE CHARGE–pH CURVES

3.2.1. *Principle*

A known amount of oxide, dispersed in a solution of an indifferent electrolyte, is titrated with acid or base, the pH being potentiometrically recorded. In addition a titration of a blank, that is a sample of the electrolyte solution of the same volume and concentration as used in the dispersion, is usually carried

out. The adsorption of the p.d. ions is then calculated from the difference in the numbers of p.d. ions necessary to produce the same change in pH of the dispersion as of the blank. Once the point of zero charge has been established, the surface charge, σ_0, is derived from the adsorption of the H^+ and OH^- ions by defining:

$$\sigma_0 \equiv F\,(\Gamma_{H^+} - \Gamma_{OH^-}) \qquad (3-1)$$

where F is the Faraday and Γ_{H^+} and Γ_{OH^-} are the numbers of equivalents of these ions adsorbed per cm^2. The surface charge is usually expressed in $\mu C\ cm^{-2}$.

3.2.2. *Experimental set-up*

The titrations were performed in a 600 ml Pyrex round bottom vessel (fig. 3–1) equipped with a Perspex cover (A) with holes for the glass electrode (E), salt bridge (G), in- and outlet tubes (H, I) for nitrogen gas and the stirrer (J). Rubber stoppers were used to locate these accessories in the cover. Preliminary experiments indicated that it was essential to maintain a small nitrogen overpressure of ca. 5 cm water in the titration cell. To that end the vessel was made gas-tight by a rubber gasket (B) between the Perspex cover and the glass wall and a waterlock (D) sealed the stirrer into the cover. Nitrogen was continuously passed over the solution and allowed to escape through the waterlock or a wash-bottle containing a solution of $Ca(OH)_2$. Before entering the system the

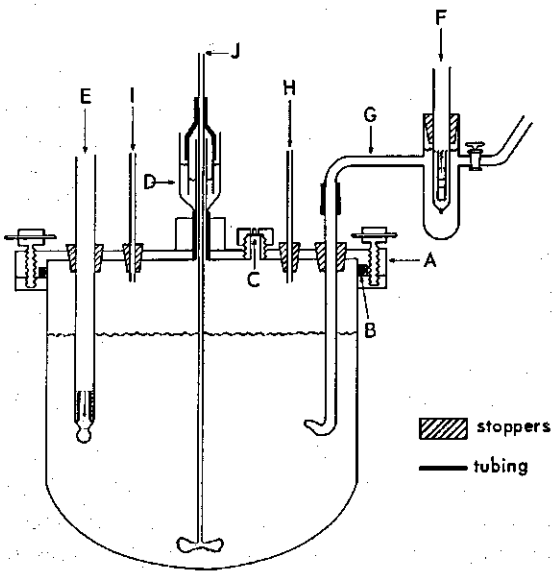

FIG. 3-1 Titration cell. For explanation see text.

nitrogen was purified over a soda-lime column and bubbled through three wash-bottles containing distilled water. Additions of acid or base were made with a Gilmont micrometer syringe *via* a rubber cap (C) in the cover. The rubber used was the same as that employed for the same purpose in gas chomatographs. The caps were frequently renewed.

The temperature was controlled at 20.0 ± 0.1 °C by pumping thermostatted water through a Perspex box surrounding the vessel. The complete apparatus was placed in a earthed metal box.

The pH was measured with a Knick pH meter, type 350 (accuracy 0.5 mV), using an Ingold glass electrode, type 201 NS (E), and an Electrofact calomel electrode, type R 113 (F). For reasons to be discussed in the next sections, the latter electrode was connected to the cell *via* a salt bridge (G) containing the same indifferent electrolyte at the same concentration as in the dispersion.

3.2.3. *Measurement of pH*

3.2.3.1. Calibration procedure

There has been a great deal of discussion with regard to the definition of pH and various scales of pH have been proposed (BATES 1964). The operational definition of pH which is perhaps the most widely used at present is:

$$\mathrm{pH} = \mathrm{pH}^s - (E - E^s) \,/\, (2.30\, RT/F) \qquad (3-2)$$

where the superscript s refers to some standard solution and E is the EMF of the cell used to measure the pH of the unknown and of the standard solution. R, T and F have their usual meaning. Buffer solutions are often used as the standards in which the pH is calculated from (BATES 1964):

$$\mathrm{pH} = -\log f_{\pm} c_{\mathrm{H}^+} \qquad (3-3)$$

where $f_{\pm}$ is the mean ion activity coefficient and c_{H^+} the concentration of the H^+ ion. The pH in the unknown solution will also be given by this equation provided the measurement has been made in a cell without a liquid junction.

However, there is a liquid junction in the cell used:

sat. calomel electrode	electrolyte solution of variable pH	glass electrode	(cell 1)

The EMF of this cell is given by:

$$E = E^0_{glass} - E_j - E_{cal} - (2.30\, RT/F)\,\mathrm{pH} \qquad (3-4)$$

where E^0_{glass} is the standard potential of the glass electrode, E_j the liquid junction potential at the boundary between the electrolyte solution and the (saturated) calomel electrode and E_{cal} the potential of the (saturated) calomel electrode.

Apart from slight day-to-day changes in E^0_{glass} which can be readily account-

ed for, E^0_{glass} and E_{cal} are constant at given temperature and pressure. Their absolute values are not required if calibrations against one or more standard solutions, such as the two NBS buffer solutions of pH 4.00 and 6.88 (20.0°C) used in this study, are carried out. The liquid junction potential, however, varies somewhat with the nature and concentration of the electrolyte and with the nature of the boundary. The extent to which the pH determined according to eqn. (3–2) now diverges from the pH expressed in eqn. (3–3), primarily depends on how much E_j varies when the standard solution is replaced by the unknown. This will be further discussed in the next section.

3.2.3.2. Liquid junction potential and salt bridge

To minimize variation in E_j, the composition of the unknown solution should approximate to that of the standards. This means here that its ionic strength should be between 0.01 and 0.1 M and its pH between 3 and 11. Although the latter condition was fulfilled in this study, the former could not because it was intended to investigate the concentration range 10^{-3} to 1 M.

In studying this possible error in the pH, other serious problems were encountered in the use of certain calomel electrodes and salt bridges in dilute solutions ($\leqslant 10^{-3}$ M). These difficulties and the method chosen to overcome them will be described below.

By way of example, E_j was studied in 10^{-3} to 1 M solutions of KCl using the cell:

calomel electrode	solution of KCl of variable pH	Ag/AgCl electrode	(cell 2)

The EMF of this cell was measured during a (blank) titration between pH 4 and 10 using KOH or HNO_3. The temperature was 20°C. The EMF was also calculated for the corresponding cell without liquid junction, taking $E^0_{Ag/AgCl}$ = 225.6 mV (BATES 1964), E_{cal} = 244.5 mV (saturated KCl) or 334.1 mV (0.1 M KCl) (CHATEAU 1954) and using the mean ion activity coefficient of KCl as reported by PARSONS (1959). The difference between the measured and calculated EMF yields E_j ($E_j = E^{cell}_{exp} - E^{cell}_{calc}$). The results for two different types of calomel electrodes in 10^{-3} M solutions of KCl are presented in table 3–1 (third to sixth column).

As can be seen from this table the saturated calomel electrode (Electrofact R 113) showed an anomalous behaviour. The liquid junction potential, $E_{j,2p}$ (defined at the bottom of table 3–1), not only changes with pH but it is also markedly affected by stirring.

As a result, the pH of a stirred solution would have been lower than that of an unstirred one, especially at high pH, if the measurements had been carried out with this electrode directly inserted in the solution. This electrode contains a ceramic plug and a gel to restrict the flow of electrolyte from the electrode compartment. CLARK (1966), using a saturated calomel electrode (L & N type) with a fiber plug, has reported similar effects. He attributed these phenomena to

the occurrence of a streaming potential in the negatively charged plug. It is therefore suggested that the variability of E_j which occurs when plug-type calomel electrodes are used in dilute solutions may be of a more wide-spread nature than seems to be recognized.

TABLE 3-1. The effect of pH and of stirring upon the liquid junction potential, E_j (in mV), in 10^{-3} M solutions of KCl in cell 2 and cell 4 (20°C).

pH		$E_{j,2s}$		$E_{j,2p}$		$E_{j,4}$	
s	u	s	u	s	u	s	u
10.092	10.097	+0.3	+0.2	+22.5	+2.5	−2.4	−2.4
9.750	9.750	−0.9	−1.4	+22.5	+2.5	−3.3	−3.3
9.247	9.250	−1.9	−2.4	+20.5	+2.5	−3.6	−3.5
8.518	8.531	−2.7	−2.7	+19.5	+2.5	−3.3	−3.4
7.720	7.730	−3.5	−3.1	+18.5	+2.5	−3.5	−3.5
7.130	7.090	−3.1	−3.0	+18.5	+0.7	−3.5	−3.5
6.660	6.655	−4.0	−3.4	+16.5	0.0	−4.0	−3.7
6.182	6.182	−3.4	−3.1	+15.5	−1.0	−3.5	−3.4
5.590	5.592	−3.6	−3.1	+14.5	+0.3	−3.5	−3.3
4.890	4.890	−3.7	−2.9	+ 9.5	−3.7	−3.4	−3.2
4.342	4.341	−3.5	−3.0	+ 4.5	−3.7	−3.8	−3.8
4.011	4.011	−4.4	−3.7	+ 0.5	−5.8	−4.3	−4.2

The symbols s and u denote stirred and unstirred solutions, respectively. The pH was measured against the sleeve-type calomel electrode.
$E_{j,2s}$: E_j in cell 2 using a sleeve-type 0.1 M KCl calomel electrode (Electrofact R 112)
$E_{j,2p}$: E_j in cell 2 using a plug-type saturated KCl calomel electrode (Electrofact R 113)
$E_{j,4}$: E_j in cell 4 using a plug-type saturated KCl calomel electrode (Electrofact R 113).

It is evident that the R 113 electrode cannot be employed for the measurement of pH with cell 1 in dilute solutions ($\leqslant 10^{-3}$ M). At higher electrolyte concentrations $E_{j,2s}$ was found to be independent of pH and unaffected by stirring.

For the sleeve-type Electrofact calomel electrode (type R 112) with 10^{-1} M KCl as the supporting electrolyte, E_j changed only slightly with pH, and stirring had no effect ($E_{j,2s}$ in table 3–1). Nevertheless, this electrode was not used in the titration of dispersions of hematite to avoid the danger of obstructions to the free flow of electrolyte from the electrode due to (partial) clogging by hematite particles. This had been observed, amongst others, with a salt bridge of the VAN LAAR-type, as modified by BIJSTERBOSCH (1965). The measurement of pH may be already affected in the manner described previously before the point is reached where the flow has become restricted so seriously that the meter response becomes oscillating and drifting.

In addition to these practical difficulties in the handling of calomel electrodes and VAN LAAR-type salt bridges, there is another fundamental problem in

their use for EMF measurements with colloidal dispersions. The EMF of cell 1 measured with the electrodes inserted in the colloidal dispersion may differ from that measured with both electrodes in the equilibrium solution only. The magnitude of this suspension or sol-concentration effect (OVERBEEK 1952) depends primarily upon the charge and indirectly upon the size and concentration of the colloidal particles and upon the nature and concentration of the indifferent electrolyte.

In principle, the most attractive procedure of arriving at the pH would be by measuring it in the equilibrium dialysate. However, this method is extremely tedious and not necessary. If the following procedure suggested by BOLT (1957) is applied, the pH measurement can be carried out as if it were for the equilibrium solution. The glass electrode is inserted in the colloidal dispersion and the calomel electrode is connected with the titration cell *via* an (agar) bridge containing the indifferent electrolyte in the same concentration, c, as in the dispersion:

calomel electrode	electrolyte solution (c)	dispersion with electrolyte (c) at variable pH	glass electrode	(cell 3)
	(bridge)	(titration cell)		

The basic idea underlying this device is that the liquid junction potential at the bridge/dispersion interface is negligible if the concentration of the p.d. ions is small in comparison with that of the indifferent electrolyte, a condition which usually holds.

BOLT's technique was employed in the present study, using two modifications. At the lowest electrolyte level the dialysate of the sol was used by BOLT to fill the bridge and higher electrolyte concentrations were obtained by adding known amounts of salt to this dialysate. In preparing the bridge agar was used to retain the solution. In the present work, the dialysate was not used for the bridge solution because the concentration of electrolyte in the dialysate was found to be negligibly small. Secondly, a special bridge (G in fig. 3–1) was designed, eliminating the use of agar, to prevent the danger of agar contamination in the titration cell. The part of the bridge that is inserted in the solution (dispersion) consists of a glass tube, the end of which is bent and pulled out in a flame to obtain a narrow opening of ca. 0.3 mm. It is constructed with a dip so that any particles which happen to penetrate into the tube do not clog the opening.

This bridge, therefore, not only facilitates the measurement of the pH without interference of the suspension effect but it also eliminates an important source of error in titrations of hematite dispersions, namely the (partial) blocking of the salt bridge. In addition, leakage of salt into the titration cell is prevented.

The question which has yet to be considered is to what extent the (total)

liquid junction potential for cell 3 deviates from that in the calibration solutions. Therefore, the liquid junction potential was determined as before, that is in standard solutions of KCl, using a Ag/AgCl-calomel electrode combination as follows:

	$E^1_{j,4}$	$E^2_{j,4}$		
sat. calomel electrode	KCl (c)	KCl (c) at variable pH	Ag/AgCl electrode	(cell 4)

with $E_{j,4} = E^1_{j,4} + E^2_{j,4}$. The EMF of this cell and of cell 2 were measured simultaneously and the liquid junction potential of cell 4, $E_{j,4}$, in 10^{-3} M solutions of KCl is given in table 3–1. It will be noticed that $E_{j,4}$ and hence the bridge/solution potential, $E^2_{j,4}$, is practically not affected by stirring and change in pH. It does not change by more than 0.4 mV except between pH 4 and 5 and between pH 9 and 10 where the change is slightly higher as could be expected in view of the fact that the concentration of the p.d. ions is no longer negligible. Replicate measurements showed that $E_{j,4} = -4.5 \pm 1.5$ mV. In 10^{-2}, 10^{-1} and 1 M solutions, E_j amounts to –3, –4 and –5 ($\pm$1.5) mV, respectively. The values in 10^{-3} and 10^{-2} M KCl are in fair agreement with the theoretical values for $E^1_{j,4}$ as calculated by PICKNETT (1968), viz. –3.9 mV and –2.8 mV, respectively, suggesting that the bridge/solution potential is very small indeed. Comparison of $E_{j,4}$ with the liquid junction potential in the NBS standard solutions used shows that the differences are small. PICKNETT (1968) has calculated $E_j = 5.4$ mV for a 0.05 M solution of potassium hydrogen phthalate (pH = 4.00) and BATES (1964) has reported that the difference in E_j using this buffer and the equimolar phosphate buffer (pH = 6.88) was less than 1 mV.

It may be concluded, therefore, that the accuracy as well as the reproducibility in the pH as measured with cell 3 will be of the order of 0.03 pH units at all the electrolyte levels studied.

3.2.3.3. Measurement of the suspension effect

The measurement of pH as described, using the indifferent electrolyte bridge, eliminates the influence of the suspension effect. On the other hand, the same technique furnishes a rapid means of determining this effect. To that end, a second calomel electrode similar to that used with the bridge is inserted in the colloidal dispersion. The difference in potential between these two electrodes is defined as the DONNAN potential and is equal to the suspension effect.

In the 2% dispersions of hematite that have been used in the titration experiments the suspension effect was only just detectable even in 10^{-3} M solutions, amounting to 1 mV or less.

3.2.3.4. Conclusions

The employment of an indifferent electrolyte bridge in the measurement of pH with a glass-calomel electrode assembly (cell 3) facilitates a reliable and rapid measurement of the pH in dispersions of hematite with an accuracy and reproducibility of 0.03 pH units at all electrolyte levels studied. The bridge primarily serves to eliminate

1. the effect of pH and stirring of the solution upon the liquid junction potential for certain plug-type calomel electrodes in dilute solutions
2. the blocking of the electrolyte flow from the calomel electrode caused by penetration of hematite into the plug
3. the entrance of salt from the calomel electrode into the titration cell.

The fundamental advantage of eliminating the influence of the suspension effect appeared to have little practical necessity.

3.2.4. *Calculation of the adsorption of the potential-determining ions*

The general procedure for measuring the adsorption of the p.d. ions as outlined in section 3.2.1. requires the amount of titrant necessary to accomplish a given change in pH to be the same for the blank as for the equilibrium solution of the dispersion. This presupposition normally holds because the concentration of the p.d. ions is small compared to that of the indifferent electrolyte. By consequence, the contribution of the negative adsorption of the co-ions to the counter charge is almost solely due to the co-ions of the indifferent electrolyte. Hence, the concentration of the p.d. ions in the dispersion is not affected by any negative adsorption of these ions.

Both the H^+ and OH^- ions may be formally considered to be able to adsorb and the difference between the number of H^+ or OH^- ions adsorbed at the surface at two pH values, pH_1 and pH_2, may be obtained from the relations:

$$m\,S\,\Delta\Gamma_{H^+} = \left[\left(n_{H^+}\right)_{pH_2} - \left(n_{H^+}\right)_{pH_1}\right]_d - \left[\left(n_{H^+}\right)_{pH_2} - \left(n_{H^+}\right)_{pH_1}\right]_b \qquad (3-5)$$

$$m\,S\,\Delta\Gamma_{OH^-} = \left[\left(n_{OH^-}\right)_{pH_2} - \left(n_{OH^-}\right)_{pH_1}\right]_d - \left[\left(n_{OH^-}\right)_{pH_2} - \left(n_{OH^-}\right)_{pH_1}\right]_b \qquad (3-6)$$

where n_{H^+} and n_{OH^-} are the total number of equivalents of these ions added to the dispersion (*d*) or the blank (*b*).

The analytically determined difference in the net adsorption of the p.d. ions, $\Delta\Gamma_{H^+} - \Delta\Gamma_{OH^-}$, is converted into absolute values, $\Gamma_{H^+} - \Gamma_{OH^-}$, with $pH_1 = pH_{p.z.c.}$ since $\Gamma_{H^+} \equiv \Gamma_{OH^-}$ at the point of zero charge (p.z.c.).

The determination of the adsorption of the p.d. ions according to equations (3–5) and (3–6) is in principle the most attractive method. However, the proce-

dure may be simplified without a significant loss of accuracy if the number of ions added to the dispersion greatly exceeds that added to the blank. Neglecting other effects such as the adsorption of p.d. ions on the glass of the titration cell, the second terms of the RHS's of equations (3–5) and (3–6) may then be approximately calculated from:

$$\left[\left(n_{H^+}\right)_{pH_2} - \left(n_{H^+}\right)_{pH_1}\right]_b = V\left[\left(c_{H^+}\right)_{pH_2} - \left(c_{H^+}\right)_{pH_1}\right]_b \qquad (3-7)$$

$$\left[\left(n_{OH^-}\right)_{pH_2} - \left(n_{OH^-}\right)_{pH_1}\right]_b = V\left[\left(c_{OH^-}\right)_{pH_2} - \left(c_{OH^-}\right)_{pH_1}\right]_b \qquad (3-8)$$

Experimental and calculated values for the 'blank correction', corresponding to the LHS's and RHS's of these equations, respectively, have been determined for solutions of KCl, K_2SO_4 and $Mg(NO_3)_2$. The calculated values were arrived at from eqn. (3–3) using the mean ion activity coefficient of the indifferent electrolyte. This activity coefficient was taken from the data compiled by PARSONS (1959) with interpolation where necessary. It was found that any differences between the calculated and the experimental values were small in comparison with the number of H^+ or OH^- ions added to the dispersion provided the solid : solution ratio was sufficiently high. This condition was always fulfilled in the titration experiments to be described.

It was therefore decided to calculate the 'blank correction' as indicated rather than to measure it.

3.2.5. *Titration procedure*

3.2.5.1. Outline

The surface charge–pH curves have normally been obtained by the following procedure.

A homogeneous stock dispersion of the hematite samples A, B or C was prepared by adjusting the pH to 4 with a solution of HNO_3 or HCl and by shaking overnight. From this dispersion, an aliquot containing about 10 g of hematite was added to the titration cell and the volume made up to 500 ml using conductivity water. The dispersion of hematite was then coagulated by adjusting the pH to 8.5–9.0 by addition of KOH solution. The supernatant was syphoned off as far as possible and replaced by the electrolyte solution desired. This procedure was repeated twice. The pH was then raised with KOH to about 10.2, unless stated otherwise, and the sol equilibrated overnight. The next day a fast titration would be made by adding small aliquots (between 50 and 200 µl) of acid at intervals of 2 to 5 minutes. About 20 additions were done to lower

the pH from 10 to 4 using the acid with the same anion as the indifferent electrolyte. If another acid titration was to be performed the dispersion would be washed again at pH 9 with electrolyte solution to adjust the salt concentration, where necessary (commonly to 10^{-3} and 10^{-2} M). At the same time the volume was adjusted to 500 ml. In the calculations the volume was taken to be constant because the amount of acid used in the titration is negligible.

3.2.5.2. Comments

Influence of CO_2

As mentioned before, in this work it was found essential to maintain a (small) nitrogen overpressure in the titration vessel. Bubbling of nitrogen gas through the solution in a vessel which is not gas-tight was insufficient to completely expel the CO_2, as was observed in titrations with low concentration of hematite and in blank titrations. There are indications that the effect of CO_2 has not always been eliminated in titrations by other investigators. BÉRUBÉ, ONODA and DE BRUYN (1967) have attributed their high values for the adsorption density on hematite obtained from equilibrium titrations to CO_2 absorption from the atmosphere. This conclusion was based on a chemical analysis of the supernatant. As adsorption of bicarbonate and carbonate ions on the solid was not taken into account in this analysis, they may have considerably underestimated the adsorption of CO_2 by the dispersion (see also below). At any rate, it is clear that CO_2 could have entered into the cell used by DE BRUYN and his coworkers despite 'flowing purified nitrogen continuously through the titration cell'. Whether ATKINSON, POSNER and QUIRK (1967) have taken the necessary precautions is not mentioned.

Fast and slow (ad)sorption

With respect to the rate of uptake of the p.d. ions on hematite two steps have been distinguished by DE BRUYN and his coworkers (BÉRUBÉ et al. 1967, ONODA and DE BRUYN 1966).

The first step is a fast one which is completed within a few minutes after the addition of acid or base. The second step is a slow process which, according to these authors, may take as long as ten days for completion. The amount taken up during the slow step was found to exceed that during the fast step by an order of magnitude. The fast adsorption was interpreted as real surface adsorption whereas the slow step was attributed to proton diffusion in the solid.

In the present study also it was useful to distinguish between a fast and slow step. However, with regard to the relative magnitudes of the two steps the current findings do not agree with those of DE BRUYN and his coworkers. In the present study the additional amount adsorbed during the slow step was only

10–20% of that adsorbed during the fast step. This followed from the comparison of the quasi-equilibrium titrations (criterion: pH readings constant for two successive periods of 15 minutes) and the fast titrations described above. To further illustrate the minor contribution from the slow step it may be added that there were no significant differences between titrations if the additions of acid were made at intervals of 20 minutes rather than 2–5 minutes. As mentioned before, the discrepancy between our results and those of DE BRUYN and coworkers may be, at least partially, due to CO_2 contamination in the titration cell employed by these authors.

For the purpose of this study, i.e. the comparison of surface charge–pH curves for different types and concentrations of electrolytes, the fast titrations were considered to be equivalent to the more time-consuming quasi-equilibrium titrations.

Conditioning of the sample

The adsorbed amount is considerably reduced by factors which promote irreversible aggregation of the samples, for example drying or shaking under coagulation conditions (some examples are given in fig. 3–2).

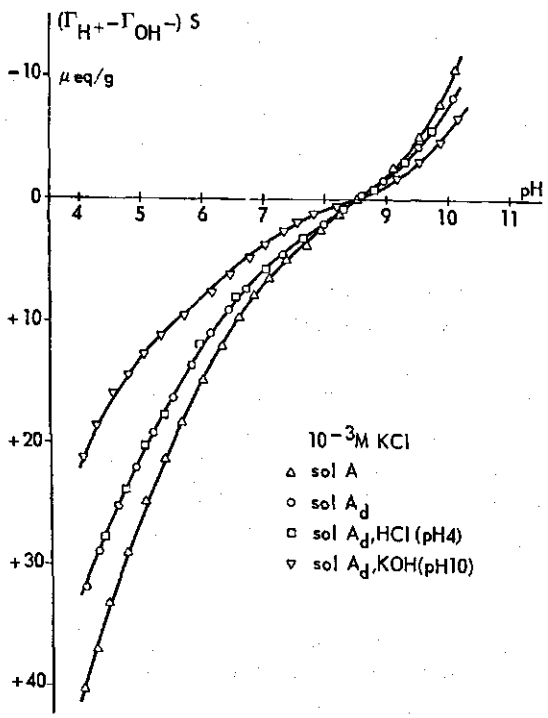

FIG. 3-2 Influence of conditioning of the sample upon the (σ_o–pH) curves of hematite in 10^{-3} M solutions of KCl. For explanation see text.

Drying at 105°C (sample A_d) leads to a reduction in the adsorption of 10–20% although the BET area was not altered. (The titration was made before the reduction in the BET area of the dry sample became apparent as shown in section 2.5.2.3.). Shaking of the dried sample with a dilute solution of an acid such as HCl (final pH ca. 4) leads to considerable repeptization, but the amount adsorbed in the fast step does not increase. If the shaking is carried out in solutions of 10^{-3} M KCl at pH 10, that is under conditions where the undried sample coagulates, aggregation is enhanced and the adsorption is lower than that for the untreated, dry sample.

Besides affecting the value of the fast adsorption, drying exerts an influence upon the p.z.c. (section 3.2.6.). Since drying also impaired the reproducibility of the titrations all the experiments reported below have been carried out without drying.

Furthermore, if a series of titrations was performed, the negative surface charge in the very first titration was occasionally found to be somewhat higher than in subsequent titrations (see for example fig. 3–3). The reason for this type of irreversibility is not known. Only the results for the second and subsequent titrations are considered here where differences did occur.

The use of KOH

It is evident that, except in the presence of KCl, the use of KOH is justified only if the amount of base added can be neglected with regard to the amount of salt which is present. For electrolyte concentrations $\geqslant 10^{-2}$ M this is always the case but in 10^{-3} M electrolyte solutions the ratio of the amount of K^+ from KOH to that of the cation of the electrolyte can become as high as 0.3–0.5 and therefore needs to be considered.

The influence of this effect on the adsorption of the p.d. ions was studied for 10^{-3} M solutions of LiCl and 5×10^{-4} M solutions of $Ba(NO_3)_2$, by comparing titration curves obtained using the appropriate base, LiOH or $Ba(OH)_2$, with titration curves obtained using KOH. The adsorption was found to be reduced using KOH only in the case of 10^{-3} M LiCl solutions. Hence, KOH could be used in place of the base with the same cation as the indifferent electrolyte, except in 10^{-3} M solutions of electrolyte with monovalent cations other than K^+. Anticipating the discussion in Chapter 4. it may be noted here that a higher preferential adsorption of Ba^{2+} compared to K^+ is indicated by the fact that K^+ does not affect the adsorption of the p.d. ions despite the high ratio (as indicated above) in the solution.

Reversibility and reproducibility

The fast adsorption of the p.d. ions is not entirely reversible when titrations are made firstly from low to high pH and then *vice versa*. There are definite

hysteresis loops in acid-base titration curves due to the contribution of the slow adsorption step which cannot be completely eliminated unless the pH range covered is kept small. For titrations performed between pH 4 and 10 the adsorption hysteresis reaches a maximum around pH 7–8 of about 0.5 μC cm^{-2} for (1–1) electrolytes and 2.5 μC cm^{-2} for asymmetric electrolytes. Hence, to acquire the best reproducibility it is necessary to compare either only acid or only base titrations. In the present study the acid titrations were considered since acid solutions are less prone to contamination by CO_2.

To improve the reproducibility the pH range was usually not extended beyond pH 4 and 10.2. The experimental error rapidly increases outside this range due to the relatively high correction for the blank and also due to the increase in liquid junction potential. Further improvements were attained by eliminating any possible heterogeneity of the sample by using the same subsample in consecutive measurements. The reproducibility of 3% thus obtained was good enough to distinguish differences between, for example, K^+ and Li^+ as is illustrated in fig. 3–3. (Note that only the second and subsequent titrations are to be compared.)

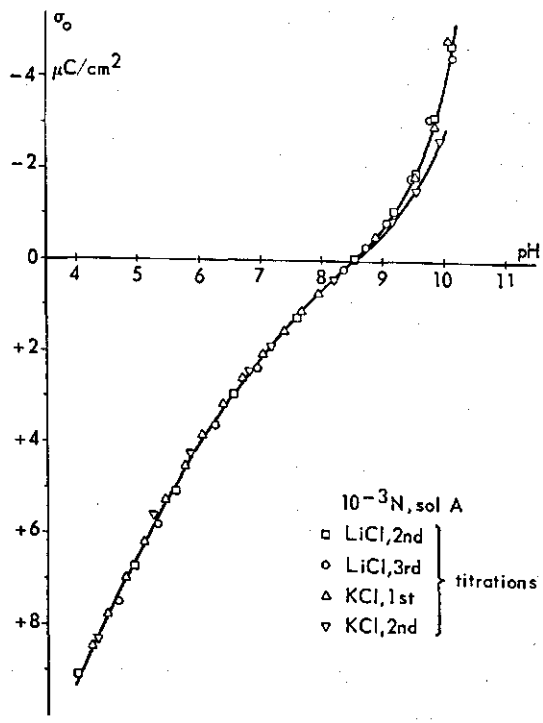

FIG. 3-3 Reproducibility of the (σ_o–pH) curves of hematite according to the standard titration procedure.

3.2.6. *Determination of the point of zero charge*

3.2.6.1. From the intersection point of surface charge–pH curves

It follows from the current GOUY-CHAPMAN-STERN-GRAHAME model of the electrical double layer (cf. OVERBEEK 1952) as well as from thermodynamics (section 4.3.6.) that the point of zero charge (p.z.c.) coincides with the intersection point of surface charge–pH curves at different ionic strengths if there is no net adsorption of ions at the p.z.c. If such adsorption does occur at high ionic strength the p.z.c. will shift and in that case should be taken as the intersection point of the σ_0–pH curve with the axis determined at low ionic strength.

Titrations are normally started at the lowest electrolyte level followed by successive titrations at higher concentrations. In the present study fast titrations were carried out over a limited pH range to minimize irreversibility effects. Between titrations at different ionic strengths the dispersion was equilibrated for half an hour after the addition of electrolyte (solution).

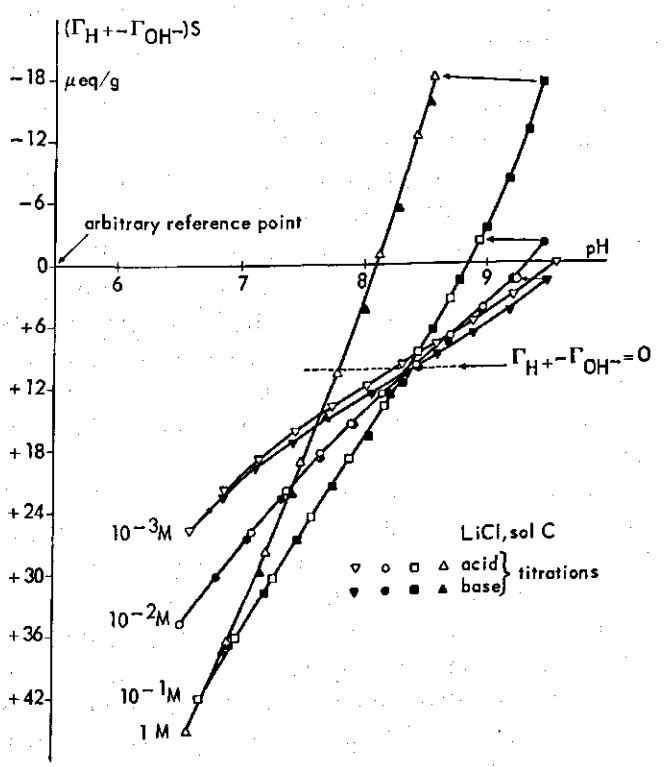

FIG. 3-4 Determination of the p.z.c. in the presence of LiCl with the intersection point method. The arrows indicate the shift in pH due to the increase in electrolyte concentration.

An example of such a short titration sequence for a normal, undried sample is given for LiCl in fig. 3–4. Ignoring the first titration in 10^{-3} M LiCl the curves at 10^{-3} and 10^{-2} M are seen to intersect one another at pH 8.40, which is identified as 'the' p.z.c. This is notably higher than the p.z.c. for the dried sample (7.5–8.0), indicating some influence of drying and, perhaps, grinding upon the p.z.c. The 10^{-1} and 1 M curve intersect the axis at pH 8.35 and 7.80, respectively, indicating adsorption of Li^+ ions at 'the' p.z.c. at high concentrations of LiCl. Replicates showed that the p.z.c. could be determined in this way with a reproducibility of ca. 0.2 pH unit.

3.2.6.2. From addition of hematite to electrolyte solutions

An alternative method of determining the p.z.c. of oxides has been proposed by BÉRUBÉ and DE BRUYN (1968a). It is based on the consideration that the pH of an indifferent electrolyte solution changes upon the addition of uncharged oxide, except at the p.z.c. Above and below this point the pH changes because of removal from the solution of an excess of OH^- or H^+ ions.

It is, of course, essential that the solid does not contain free acid or base. This condition was expected to be fulfilled in the present investigation since the samples had been washed at pH 8.5–9.0 which is around the p.z.c. To facilitate the measurements the samples have been dried at 105°C prior to use. The experiments were performed with a small titration cell that will be described in section 3.3.2. About 30 ml of electrolyte solution of known ionic strength were added to the titration cell and the pH adjusted as desired. Then a small amount of hematite was added and the pH change recorded.

Fig. 3–5 illustrates the change in pH as measured in 5×10^{-4} M solutions of $Ba(NO_3)_2$ when 100 mg of hematite (sample A) were added every two minutes. The p.z.c. thus obtained has a value of 6.65. In further experiments only one addition of 300 mg was made and the pH readings taken at five minutes after the addition of the solid. The p.z.c. was then determined from a plot of the change in pH against the initial pH. The reproducibility of this procedure was about 0.2 pH unit.

With regard to the above results two remarks may be made. Firstly, the fact that the value of 6.65 is considerably lower than the p.z.c. in the presence of low concentrations of LiCl, as determined in the previous section, is another indication for strong (specific) adsorption of Ba^{2+} (Chapter 4.). Secondly, there is good agreement between the p.z.c. in the presence of $Ba(NO_3)_2$ determined by this method and that measured by the intersection point method, namely pH 6.5. Thus it appears that drying does not affect the p.z.c. in this case.

The results for a (1–1) electrolyte, notably KNO_3, were disappointing. The p.z.c. varies with the electrolyte concentration, increasing from 7.0 in 10^{-3} M to 8.0 in 1 M solutions. As compared to the results for KNO_3 with the intersec-

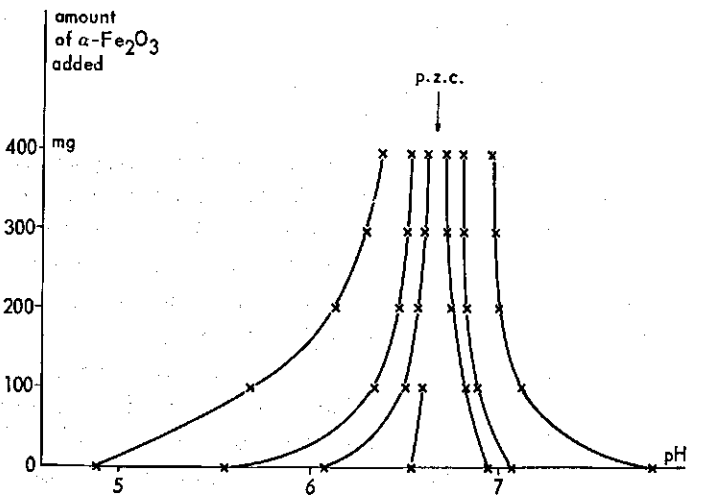

FIG. 3-5 Determination of the p.z.c. in 5×10^{-4} M solutions of $Ba(NO_3)_2$ by the addition method.

tion point method, using dry samples, the order of magnitude is the same but the apparently systematic influence of the electrolyte concentration was not shown by the latter method. A tentative explanation for this salt effect might rest in the influence of any inclusion of free acid in the samples. The higher the electrolyte concentration, the greater the adsorption of p.d. ions and the greater the change in pH, and hence, the smaller any influence of free acid. For $Ba(NO_3)_2$, as compared to KNO_3, the adsorption of p.d. ions is already high at low electrolyte concentrations, suggesting that the salt effect is ruled out even at the lowest electrolyte concentrations studied.

As a consequence of the questionable p.z.c. values obtained with the addition method, the results for (1–1) electrolytes to be reported in the following chapter are based on the intersection point measurements only.

3.3. DETERMINATION OF THE ADSORPTION OF COUNTERIONS AND CO-IONS

3.3.1. *Introduction*

The measurement of the adsorption of the counterions and co-ions cannot be performed in the way outlined for the p.d. ions because of the negative adsorption of the indifferent electrolyte which occurs in the dispersion but not in the blank.

The adsorption is now obtained from the difference between the numbers of ions added to the dispersion and those remaining in the solution as given by the relations:

$$m\,S\,(z_+\Delta\Gamma_+) = n_+ - V\Delta c \qquad (3-9)$$

$$m\,S\,(z_-\Delta\Gamma_-) = n_- - V\Delta c \qquad (3-10)$$

where the subscripts $_+$ and $_-$ denote cations and anions, respectively, z is the valency (sign not included), $\Delta\Gamma$ the change in adsorption in moles cm^{-2}, n the number of equivalents added and Δc the change in electrolyte concentration in equivalents l^{-1}. Provided that the sample itself is not contaminated with the ions added, $\Delta\Gamma_\pm = \Gamma_\pm$. The adsorption can be most suitably studied at intermediate electrolyte concentrations. At high salt concentrations, the adsorbed amount is only a small fraction of the amount remaining in solution. In dilute solutions, the contribution of the p.d. ions to the negative adsorption may no longer be negligible. For oxides, the (positive) adsorption of counterions commonly exceeds the (negative) adsorption of co-ions by an order of magnitude. In consequence, the negative adsorption is to be measured with a very high degree of accuracy if one is interested in the magnitude of the negative adsorption as such. However, in this part of our study it was primarily intended to compare surface charge and counter charge. Since the contribution of the negative adsorption to this counter charge is very small no special arrangements were made in the negative adsorption measurements.

To enable a rough check to be made of the surface charge–pH curves the adsorption of the p.d. ions and other ions should be measured concurrently. In determining the former the 'blank correction' was not estimated through eqns. (3–7) and (3–8) but directly measured.

3.3.2. *Experimental set-up*

The adsorption measurements were performed in a 50 ml Pyrex titration cell with a rubber stopper containing holes for the glass electrode and salt bridge and a rubber cap for the addition of titrant. Nitrogen gas was passed through the cell *via* holes in the glas wall. Stirring was carried out with the aid of a magnetic stirrer and a Teflon coated stirring rod. The measurement of pH, the establishment of a nitrogen atmosphere, the addition of titrant etc. was carried out as described in section 3.2.2. The temperature was controlled at 20.0 $\pm$ 0.3 °C.

3.3.3. *Experimental procedure*

An aliquot of sample B was dried prior to use at 105 °C. A 1 to 5 g portion of this hematite was added to 50 ml of a 10^{-3} N electrolyte solution and the appropriate acid or base was added by means of a micrometer syringe. The dispersion was stirred until the drift in pH was $<$ 0.02 pH unit over 15 min.

The pH was measured and a clear (equilibrium) solution for the determina-

tion of the counterion concentration was obtained by sedimentation or centrifugation.

The electrolytes studied were KCl, NaCl, $CaCl_2$ and K_2SO_4. The determination of K^+, Na^+ and Ca^{2+} was carried out with an Eppendorff flame photometer.

The concentrations of Cl^- were measured potentiometrically using Ag/AgCl electrodes and a calomel electrode connected with the cell by means of an agar bridge containing the 1.75 N KNO_3 + 0.25 N $NaNO_3$ mixture recommended by VAN LAAR (1952). The electrochemical cell was calibrated with solutions of known concentrations of chloride. The average reading of four Ag/AgCl electrodes was taken.

The concentrations of SO_4^{2-} were determined by conductometric titration with $BaCl_2$, following the procedure of VAN DEN HUL (1966). Before the titration, 7 ml of AR grade acetone were added to 10 ml of the solution that was to be analysed. The equivalence point, as determined by blank titrations, was found to be 7% lower than the stoichiometric equivalence point in the concentration range used.

The coefficient of variation was 2, 3 and 1% for the analysis by flame photometry, potentiometry and conductometry, respectively.

3.3.4. *Accuracy*

The accuracy in the adsorbed amounts of the counterions and co-ions varies from 0.2 to 0.8 $\mu C\ cm^{-2}$, depending not only on the analytical method but also on the concentration of the solid and the amount of acid or base added. The maximum negative adsorption of co-ions under the experimental conditions used is estimated to be of the order of 0.2 and 0.4 $\mu C\ cm^{-2}$ for the mono- and bivalent ions, respectively (see section 4.4.).

It follows that the relative error in the negative adsorption may be even higher than 100%. For the positive adsorption it is generally less than 10%.

3.4. CONCLUSIONS

Surface charge–pH curves for hematite can be determined from potentiometric acid-base titrations on dispersions of the solid. However, numerous precautions are necessary to obtain reliable and reproducible results.

Considerable liquid junction potential errors in the determination of the pH may be encountered when calomel electrodes or salt bridges with a restricted flow are used. These errors were eliminated in this study by the application of a specially designed salt bridge that contains the same electrolyte solution as the dispersion.

Careful exclusion of CO_2, requiring a gas-tight titration cell, and the use of well-dispersed samples is essential. The rate of adsorption has been found to vary during the adsorption, in agreement with the results of other investigators. However, in contrast to their findings the amount of p.d. ions adsorbed during the final, slow adsorption step is small as compared to that adsorbed during the initial, fast adsorption step. A so-called fast titration technique was adopted in which, after pre-equilibration, the titrant is added at intervals of 2–5 minutes. The fast adsorption is not entirely reversible and hence either base titrations or, as in the present study, acid titrations should be carried out if the effect of the indifferent electrolyte upon the surface charge–pH curves is to be studied.

The point of zero charge (p.z.c.) can be derived from successive titrations carried out at different ionic strengths. In the absence of adsorption of ions at the p.z.c. this point is given by the intersection point of the titration curves. If such adsorption does occur, e.g. for Li^+, the p.z.c. is found to shift as a function of the salt concentration. The determination of the p.z.c. by means of the addition method proposed by BÉRUBÉ and DE BRUYN gave results in close accord with the former method for (2–1) electrolytes but not for (1–1) electrolytes.

The counter charge (given by counterions and co-ions) is measured with an absolute error of about 0.5 $\mu C\ cm^{-2}$. The relative error is generally less than 10 per cent.

4. SURFACE CHARGE AND COUNTER CHARGE MEASUREMENTS. RESULTS AND DISCUSSION

In the preceding chapter it was shown how the surface charge and counter charge at the hematite/aqueous solution interface have been measured. In this chapter the results will be given and interpreted. The interpretation is based on both the well-known GOUY-CHAPMAN-STERN-GRAHAME (GCSG) model of the electrical double layer (OVERBEEK 1952) and the 'porous double layer' model recently put forward by LYKLEMA (1968). For the sake of clarity a short discussion of some basic double layer properties relevant to this study is presented first.

4.1. SOME BASIC DOUBLE LAYER PROPERTIES

4.1.1. *Structure of the electrical double layer*

Any description of the electrical double layer amounts to formulating the distribution of charge and potential. In the GSCG model the surface charge is considered to be confined to the surface plane and to be smeared out. One is thus concerned only with the distribution of charge and potential on the solution side of the interface.

In fig. 4–1 three types of distributions have been schematically depicted to illustrate the most important features of the model. First of all, a *diffuse* (or *Gouy*) *layer* is distinguished in which the free energy of adsorption per ion, ΔG_{ads}, is completely determined by the electrostatic interaction between the ion and the surface. Following GRAHAME (1947) the boundary of this layer at the solid/solution interface, that is the plane through the centres of the purely electrostatically adsorbed ions nearest to the surface, is called the *outer Helmholtz plane* (OHP). The layer between the OHP and the surface is named the molecular condensor or, as in this study, the *Stern layer*. It follows that for ions to penetrate into the STERN layer there must be some specific chemical interaction with the surface phase. The adsorption in the STERN layer will therefore be referred to in this study as *specific adsorption* and the contribution to ΔG_{ads} by 'non-electrostatic' effects as the *specific adsorption potential*, $\dot{\phi}$ [4]. The plane through the centres of the specifically adsorbed ions is called the *inner Helmholtz plane* (IHP) (GRAHAME 1947). In addition, the term *super-equivalent*

[4] It should be pointed out that although the STERN layer may be uncharged ($\sigma_m = 0$) specific effects in ion adsorption may still be encountered due to ion size effects. However, these effects are relatively small compared to chemical effects, especially for oxides, and therefore have not been included in the definition of specific adsorption.

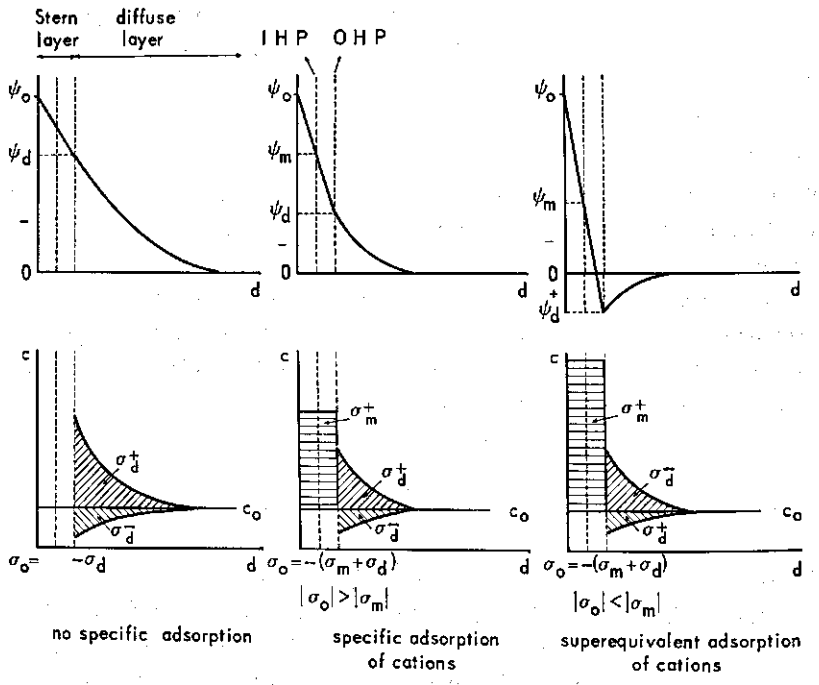

FIG. 4-1 Schematic representation for a negative surface of the potential and charge distribution in the double layer according to the GCSG model. The distance to the surface is denoted by d and the electrolyte concentration at $\psi = \psi_o$ by c_o.

adsorption will be used when the charge in the STERN layer exceeds that on the surface.

In discussing the counter charge distribution in more detail it is necessary to distinguish between

1. the composition of the counter charge, that is the extent to which the surface charge is compensated for by cations and anions, the so-called *ionic components of charge* and
2. the space distribution of the counter charge, especially the distribution over the diffuse layer and the STERN layer.

For simplicity we confine ourselves to the situation where one binary indifferent electrolyte is present in large excess of other electrolytes.

The condition for electroneutrality in case 1 reads:

$$\sigma_0 = -(\sigma^+ + \sigma^-) = -F(z_+\Gamma_+ - z_-\Gamma_-) \qquad (4-1)$$

where the symbols σ^+ $(= z_+F\Gamma_+)$ and σ^- $(= -z_-F\Gamma_-)$ denote the cationic and anionic components of charge, respectively, z_+ and z_- the valencies (sign not

included) of the cation and anion of the electrolyte and Γ_+ and Γ_- the adsorption of these ions in moles cm^{-2}.

The electroneutrality condition for the space distribution is given by:

$$\sigma_0 = -(\sigma_m + \sigma_d) = -(\sigma_m^+ + \sigma_m^- + \sigma_d^+ + \sigma_d^-) \qquad (4-2)$$

where σ_m and σ_d refer to the charge densities (of the ions indicated) in the STERN and diffuse layer, respectively.

Expressions for σ_d, as derived from the GOUY-CHAPMAN theory and relevant to this study, and for σ_m, as deduced from the treatment of STERN (1924), will be discussed below. Expressions for σ^+ and σ^- can be obtained from thermodynamics and will be considered in section 4.4.

It was already mentioned in section 2.5.4.1. that in calculating the diffuse double layer charge for spherical particles the theory for spherical double layers (LOEB et al. 1961) must be used when $\varkappa a < 20$, where $\varkappa$ is given by:

$$\varkappa = \sqrt{\frac{4\pi N_{Av} e^2 \sum_i c_i z_i^2}{1000\, \varepsilon k T}} \qquad (4-3)$$

N_{Av} is AVOGADRO's number, c_i and z_i are the molar concentration and valency of ion i, respectively, and ε is the di electric constant. (The other constants have been mentioned on page 24). It was shown in Chapter 2., that the hematite particles under study have a more or less globular habit and an equivalent radius varying between about 200 and 400 Å. Since in this study $1/\varkappa$ will often be higher than 10–20 Å and thus $\varkappa a < 20$, it was decided to use the spherical double layer equations throughout this study.

If σ_d^+ and σ_d^- are explicitly expressed as a function of the electrolyte concentration in equivalents per litre, eqn. (2–27) of LOEB et al. may be rewritten as:

$$\sigma_d^{\pm} = \pm \sqrt{\frac{\varepsilon k T N_{Av}}{2000\, \pi}} (\sqrt{z_{ct} c})\, I_{\pm} \qquad (4-4)$$

where the $_+$ and $_-$ sign apply to a negative and positive surface, respectively. I_+ (and I_-) depend on the reduced potential, y_d, and the reduced particle radius, q_0, and on the valencies z_{co} and z_{ct} of the co-ions and the counterions, respectively (cf. page 24). Defining $I = I_+ + I_-$ the net (absolute) diffuse double layer charge can be written as:

$$\sigma_d = \sqrt{\frac{\varepsilon k T N_{Av}}{2000\, \pi}} (\sqrt{z_{ct} c})\, I \qquad (4-5)$$

which on inserting the numerical constants at 20 °C yields:

$$\sigma_d = 5.89 (\sqrt{z_{ct} c})\, I \qquad (\mu C\ cm^{-2}) \qquad (4-6)$$

The specifically adsorbed charge σ_m is commonly calculated from a LANGMUIR type equation:

$$\frac{\theta_m}{1-\theta_m} = \frac{c}{55.5} \exp\left(-\frac{\Delta G_{ads}}{kT}\right) \tag{4-7}$$

where the concentration c is expressed in moles l^{-1}. $\theta_m = \sigma_m/\sigma_m^{max}$ is the degree of charge compensation in the STERN layer. In the treatment by STERN (1924) the maximum number of available surface sites per cm^2 (σ_m^{max}/e) has been taken as constant and equal to the number of water molecules per cm^2 that can be accomodated in a monolayer. The adsorption free energy per ion, ΔG_{ads}, is defined by:

$$\Delta G_{ads} = \pm ze\psi_m - \phi \tag{4-8}$$

where ψ_m is the potential in the inner HELMHOLTZ plane. The + sign refers to a negative surface and *vice versa*.

4.1.2. *Point of zero charge and iso-electric point*

As was mentioned in Chapter 3. the *point of zero charge* (p.z.c.) is defined for oxides as the pH value (pH^0) for which $\Gamma_{H^+} = \Gamma_{OH^-}$. It was also noted that the p.z.c. is not a unique parameter for a particular oxide/solution interface as such because it may be affected by e.g. the composition of the solution. Because this has not always been recognized and because it is one of the important features of this study this subject will be treated in more detail in section 4.3.6. Here we confine ourselves to the physics of the adsorption process.

The shift in p.z.c. with electrolyte concentration is attributed to specific adsorption at the p.z.c. Generally, with increasing relative contribution of the charge compensation in the STERN layer (i.e. increasing σ_m/σ_d) the surface charge is promoted. This equally applies to the p.z.c., where in the absence of specific adsorption $\sigma_m^+ = \sigma_m^- = 0$ and $\sigma_d^+ = \sigma_d^-$. Thus, if for example (specific) adsorption of cations occurs at the p.z.c., a negative surface charge would be created and for oxides the pH would have to be lowered to bring σ_0 back to zero.

The notions *point of zero charge* and *iso-electric point* have sometimes been used interchangeably. The latter quantity is usually determined from electrokinetic methods and therefore represents the point of zero electrokinetic potential. In the absence of specific adsorption both points should coincide. However, in the presence of specific adsorption at the p.z.c. they do not. In fact they move into opposite directions. In the example of specific adsorption of cations σ_0 becomes negative but at the same time ψ_d and hence the electrokinetic potential become positive. (Note that σ_0 cannot increase more rapidly than σ_m. Thus the specific adsorption at the original p.z.c. is actually super-equivalent.) It follows that the pH has to be raised to bring the electrokinetic potential back to zero.

4.1.3. *Surface potential*

It is well-known that the potential of a reversible electrode ideally obeys the NERNST relation. This equation can be derived from thermodynamics with the assumptions of (1) equilibrium within and between the solid and liquid phase and (2) invariability of the chemical potential(s) of the p.d. ion(s) in the solid phase with change in solution composition. Since the surface is incorporated in the solid phase the chemical potential at the surface is also taken to be constant[5]. For solids such as AgI where the p.d. ions (Ag^+ and I^-) are constituents of the lattice this is thought to be justified. This is because the composition of the solid (surface) does not change upon adsorption of the p.d. ions. From thermodynamics the change in GALVANI potential difference ($\Delta\varphi$) between the solid and liquid phase is then related to the activity of the p.d. ions in the solution, $a_{p.d.}$, by the expression:

$$\mathrm{d}(\Delta\varphi) = \pm \frac{RT}{F} \mathrm{d} \ln a_{p.d.} \tag{4-9}$$

the + and − sign referring to p.d. cations and anions, respectively. Taking the p.z.c. as a reference point the surface potential, ψ_0, may be defined by the relation:

$$\psi_0 \equiv \Delta\varphi - \Delta\varphi_{p.z.c.} \tag{4-10}$$

and combination of eqns. (4–9) and (4–10) yields:

$$\psi_0 = \pm \frac{RT}{F} \ln \frac{a_{p.d.}}{(a_{p.d.})_{p.z.c.}} \tag{4-11}$$

Since $\mathrm{d}(\Delta\varphi)$ may be measured, provided electrodes can be constructed of the solid, the surface potential is a well-defined, experimentally accessible parameter.

Unfortunately for oxides $\mathrm{d}(\Delta\varphi)$ is not open to measurement because, so far, electrodes of simple oxides such as α-Fe_2O_3 have not been constructed. Moreover it is not known to what extent eqn. (4–9) holds. This arises from the fact that the composition of the surface, and hence the chemical potentials of the surface constituents, are in principle no longer independent of the solution composition. As a result, for oxides eqn. (4–11) is replaced by:

$$\psi_0 = \frac{RT}{F} \ln \frac{a_{H^+}}{(a_{H^+})_{p.z.c.}} - \frac{\mu^s_{H^+} - (\mu^s_{H^+})_{p.z.c.}}{F} \tag{4-12}$$

[5] This does not exclude any difference in chemical potential between surface and bulk of the solid but merely implies invariability of these potentials with solution composition.

if expressed in terms of H^+ ion activity. The symbol $\mu^s_{H^+}$ denotes the chemical potential of the H^+ ion at the surface. It is clear that $\mu^s_{H^+}$ cannot be obtained without non-thermodynamic assumptions.

The differential form of eqn. (4–12) has been given by BÉRUBÉ and DE BRUYN (1968a and 1968b). From their experiments, these authors have suggested that, at least for small surface charges, $\mu^s_{H^+}$ may be taken constant. However, their results are not conclusive as will be shown in the next section. LEVINE and SMITH (1971) have recently given a further analysis of the problem by calculating $\mu^s_{H^+}$ using a statistical mechanical model. They have divided $\mu^s_{H^+}$ into a standard chemical potential (denoted by the superscript ^{0}) and an entropic part:

$$\mu^s_H = (\mu^{0,s}_{X^+} - \mu^{0,s}_X) + RT \ln \frac{n_{X^+}}{n_X} = (\mu^{0,s}_X - \mu^{0,s}_{X^-}) + RT \ln \frac{n_X}{n_{X^-}} \qquad (4-13)$$

where X, X^+ and X^- denote uncharged, positive and negative surface sites, respectively, and n their number per unit area. On introducing the equilibrium constants of the association and dissociation reactions:

$$X + H^+ \overset{K_a}{\rightleftarrows} X^+ \qquad\qquad X \overset{K_d}{\rightleftarrows} X^- + \quad ^+ \qquad (4-14)$$

and the fractions $\theta_{X^+} = n_{X^+}/n_s$ and $\theta_{X^-} = n_{X^-}/n_s$, where n_s is the total number of surface sites, eqn. (4–12) becomes:

$$\psi_0 = \frac{RT}{F}\left(\ln \frac{a_{H^+}}{(a_{H^+})_{p.z.c.}} - \frac{1}{2} \ln \frac{\theta_{X^+}}{\theta_{X^-}}\right) \qquad (4-15)$$

In the first expression of LEVINE and SMITH (1971) (their eqn. 2–13) θ_{X^+} and θ_{X^-} are expressed in terms of σ_0, n_s and θ_0, where the latter quantity is the fraction of surface sites charged at the p.z.c. This quantity is a function of 'the' equilibrium constants K_a and K_d (neglecting discreteness-of-charge effects). Thus, if one type of surface site is involved in both the association and dissociation reactions, and if one were able to find K_a and K_d by independent means, ψ_0 could be calculated. This is not possible as yet. In principle, θ_0 can also be directly obtained from counter charge measurements at the p.z.c., provided there is no specific adsorption, since then $\Gamma_{H^+} = \Gamma_{OH^-} = z_+\Gamma_+ = -z_-\Gamma_-$. However, the counter charge measurements made in this study (section 4.4.) show that the experimental error in the determination of Γ_+ and Γ_- at the p.z.c. is so large that even the order of magnitude of θ_0 cannot be established. It is therefore concluded that at the moment this approach of LEVINE and SMITH (1971) does not solve the problem.

In view of the facts mentioned above our data will be presented in the form of (σ_0–pH) curves rather than (σ_0–ψ_0) curves.

4.1.4. *Differential capacity*

The differential capacity, C, is a useful characteristic of the double layer. It is defined by the expression:

$$C = \frac{d\sigma_0}{d\psi_0} \tag{4-16}$$

It will be evident from the preceding section that for oxides it is convenient to define an experimental differential capacity:

$$C_{exp} \equiv -\frac{F}{2.30RT}\left(\frac{d\sigma_0}{dpH}\right) \tag{4-17}$$

By combination of eqns. (4–12), (4–16) and (4–17) the following relation between C and C_{exp} is found:

$$\frac{1}{C} = \frac{1}{C_{exp}} - \frac{d\mu^s_{H^+}}{F\,d\sigma_0} \tag{4-18}$$

If we assume that $d\mu^s_{H^+}/d\sigma_0$ is positive, as implied by eqn. (4–13), then $C \geqslant C_{exp}$.

This result is of interest because it may give the possibility to detect specific adsorption. In the absence of specific adsorption ($\sigma_0 = -\sigma_d$) the differential capacity of the STERN layer, C_m, may be defined:

$$C_m = \frac{d\sigma_0}{d(\psi_0 - \psi_d)} \tag{4-19}$$

and since the differential capacity of the diffuse layer, C_d, is given by:

$$C_d = -\frac{d\sigma_d}{d\psi_d} \tag{4-20}$$

the total capacity, C, may be calculated from:

$$\frac{1}{C} = \frac{1}{C_m} + \frac{1}{C_d} \tag{4-21}$$

As the capacities are positive it follows from eqn. (4–21) that $C \leqslant C_d$. Formally, eqn. (4–19) can be applied also in the presence of specific adsorption. From eqns. (4–2), (4–19) and (4–20):

$$\frac{1}{C} = \frac{1}{C_m} + \frac{1}{C_d} + \left(\frac{d\sigma_m}{d\sigma_0}\right)\frac{1}{C_d} \tag{4-22}$$

Since $d\sigma_m/d\sigma_0$ is negative C may now exceed C_d. Therefore, in the GCSG model $C_{exp} \geqslant C_d$ certainly indicates specific adsorption. (An alternative explanation will be considered in section 4.3.4.).

It may be noted, finally, that BÉRUBÉ and DE BRUYN (1968a and 1968b) have considered $C > C_d$ to be unlikely on physical grounds which they do not specify. Their result that $C_{exp} \simeq C_d$ has therefore been taken by them to be 'more logically explained by a model which justifies the independence of $\mu^s_{H^+}$ of σ_0'. In other words, $C \simeq C_{exp}$ because otherwise C would be greater than C_d. It will be clear from the discussion above that this reasoning is not justified.

Furthermore, it is of interest that when C is predominantly determined by C_d (at low c_{salt}) the p.z.c. can be found from the point of minimum differential capacity, that is the inflection point of the (σ_0–ψ_0) or (σ_0–pH) curves. This is true for symmetrical electrolytes. For the asymmetrical electrolytes used in this study, a difference between the p.z.c. and the inflection point corresponding to ca. 20 mV has been calculated but not always observed (LYKLEMA and OVERBEEK 1961).

4.2. SURFACE CHARGE–pH CURVES. RESULTS

The (σ_0–pH) curves to be presented below have been determined in the presence of 10^{-3}, 10^{-2}, 10^{-1} and 1 M solutions of the chlorides of Li^+, K^+ and Cs^+ and in the presence of 5×10^{-4}, 5×10^{-3} and 5×10^{-2} M solutions of K_2SO_4 and the nitrates of Mg^{2+}, Ca^{2+}, Sr^{2+} and Ba^{2+}. To facilitate the discussion and comparison of these curves for different types of electrolyte the concentrations will be expressed below in normalities (N) rather than in molarities (M). For (2–1) and (1–2) electrolytes the normality is twice the molarity.

4.2.1. *Surface charge–pH curves in the presence of alkali chlorides*

In the course of this study it became clear that the (σ_0–pH) curves for the various sols which have been prepared did not coincide within the experimental error. This is demonstrated in table 4–1, showing the ratio's of the surface charge of sol A and C to that of sol B at different concentrations of KCl. The ratio's vary with pH as well as with electrolyte concentration. Furthermore the ratio's increase with increasing difference in surface area, S_{BET} being 35 and 31 m^2g^{-1} for sol C and sol A, respectively. In comparing the (σ_0–pH) curves for sol C with those of other authors who have used the fast titration method, it is noticeable that the σ_0's reported by ATKINSON et al. (1967) (KCl) and PARKS and DE BRUYN (1962) (KNO_3) are higher by a factor of about 1.5 and 3.5, respectively. (As was mentioned in Chapter 2. the mode of preparation of the samples by these authors differs from that followed in the present study). Similar differences in surface charge density exist for different samples of SiO_2 (LYKLEMA 1971).

For hematite, the differences obtained by the various authors may be partly due to variations in experimental technique. However, the differences in σ_0

TABLE 4-1. Ratio of the surface charges of sols A and C to that of sol B at different concentrations of KCl.

	c_{KCl}	pH						
	(M)	4	5	6	7	8	9	10
$\frac{(\sigma_0)_A}{(\sigma_0)_B}$	10^{-3}	1.36	1.28	1.19	1.00	0.95	0.96	0.90
	10^{-2}	1.32	1.25	1.18	1.15	1.07	0.93	0.83
	10^{-1}	1.19	1.14	1.13	1.25	1.22	1.04	1.08
	1	1.16	1.10	1.13	1.19	1.08	1.05	1.11
$\frac{(\sigma_0)_C}{(\sigma_0)_B}$	10^{-3}	1.64	1.60	1.51	1.26	1.00	0.93	1.00
	10^{-2}	1.56	1.53	1.46	1.39	1.24	1.01	0.86
	10^{-1}	1.38	1.33	1.32	1.41	1.41	1.15	1.17
	1	1.24	1.18	1.21	1.34	1.33	1.20	1.21

between sol A, B and C clearly indicate that, in addition, there must be some variations between samples playing a role. For SiO_2, LYKLEMA (1971) has attributed the differences in σ_0 to the ability of p.d. ions and counterions to penetrate into the solid. This could also apply to hematite and will be discussed in more detail in section 4.3. In addition, one might consider possible 'chemical' differences in surface structure not associated with ion-porosity. In principle such variation could affect the p.z.c. and $\mu^s_{H^+}$. However, the sols studied did not have significant differences in p.z.c. and the question as to the variability of $\mu^s_{H^+}$ with sample is a matter of speculation.

In order to study the influence of the nature and concentration of different electrolytes it is necessary to exclude the variability between one sample and the other. For this reason the results to be discussed have been obtained with the same sol (sol B) unless stated otherwise. In passing, it should be stressed that defining $pH \equiv -\log a_{H^+}$ means that the conversion of pH into c_{H^+} varies with c_{salt}. This does not influence the position of the p.z.c. In principle the intersection point should be sharper than with $pH = -\log c_{H^+}$ but this may be masked by the experimental error.

The (σ_0–pH) curves for KCl are given in fig. 4–2. The p.z.c. has been established from the intersection point method. It does coincide with the inflection points of the curves in 10^{-3} and 10^{-2} N as expected. (At higher c_{salt} this point is not clearly located). The pH^0 of 8.5 ($\pm$ 0.2) compares well with that found by PARKS and DE BRUYN (1962). The data of ATKINSON et al. (1967) tend to be somewhat higher (pH^0 8.5–9.3). In the case of the addition method and also with the counter charge measurements (using dried samples) lower pH^0 values have been found, suggesting some influence of drying and perhaps grinding. The fact that the curves at different c_{salt} have a common intersection point indicates either the absence of any specific adsorption of K^+ and Cl^-, or an

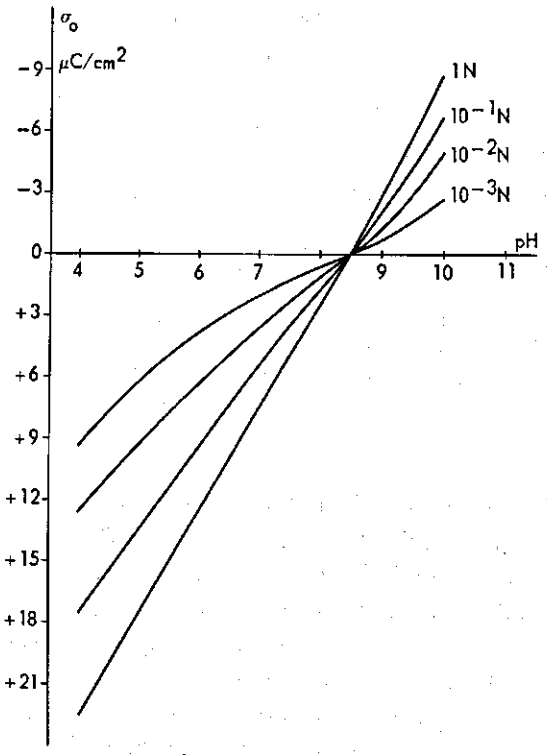

FIG. 4-2 Surface charge of hematite (sol B) as a function of pH in the presence of different concentrations of KCl.

(almost) identical specific adsorption potential for these ions. These facts will be further discussed in section 4.3.4.

The (σ_0–pH) curves in LiCl (fig. 4–3) show some differences compared to those in KCl. Especially at high concentrations the curves are much steeper on the negative side of the p.z.c. and there is a distinct shift of the p.z.c. from pH^0 8.5 in 10^{-3} and 10^{-2} N to 8.2 in 10^{-1} N and 7.8 in 1 N LiCl. As shown in section 4.1.2., both trends indicate specific adsorption of Li^+. As far as we are aware this is the first reported case where specific adsorption of a monovalent cation shows up in a shift of the p.z.c. (BREEUWSMA and LYKLEMA 1971). To date no completely comparable studies have been published. BÉRUBÉ and DE BRUYN (1968) have given differential capacity curves for rutile in the presence of 10^{-3} and 10^{-1} N solutions of the nitrates of Li^+, Na^+ and Cs^+. The highest values of σ_0 were obtained for Li^+, but any shift in p.z.c. was not reported, although the occurrence of such a shift would perhaps have been detectable at higher electrolyte concentrations than those studied by these authors.

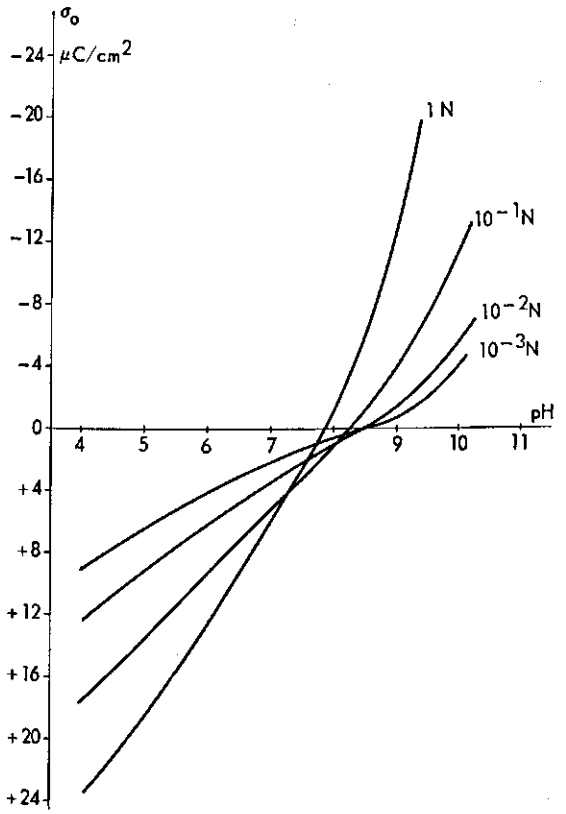

FIG. 4-3 Surface charge of hematite (sol B) as a function of pH in the presence of different concentrations of LiCl.

In comparing the adsorption of Li^+, K^+ and Cs^+ it is convenient to study the (σ_0–pH) curves at constant c_{salt}. Results are shown in fig. 4–4 for the chlorides. The curves in 10^{-3} N solutions show the same features as those in 10^{-2} N solutions and have therefore been omitted. It is seen that at low c_{salt} ($\leqslant 10^{-2}$ N) the lyotropic sequence in σ_0 is:

$$Li^+ > K^+ > Cs^+$$

whereas above this concentration:

$$Li^+ >> K^+ \simeq Cs^+.$$

The latter result is of particular interest and will be dealt with in the discussion (section 4.3.).

4.2.2. *Surface charge–pH curves in the presence of alkaline earth nitrates*

The (σ_0–pH) curves in Ca^{2+} and Mg^{2+} nitrates are given in figs. 4–5 and 4–6, respectively. These curves are typical for the alkaline earth nitrates. The p.z.c. was determined by the intersection point method and by identification

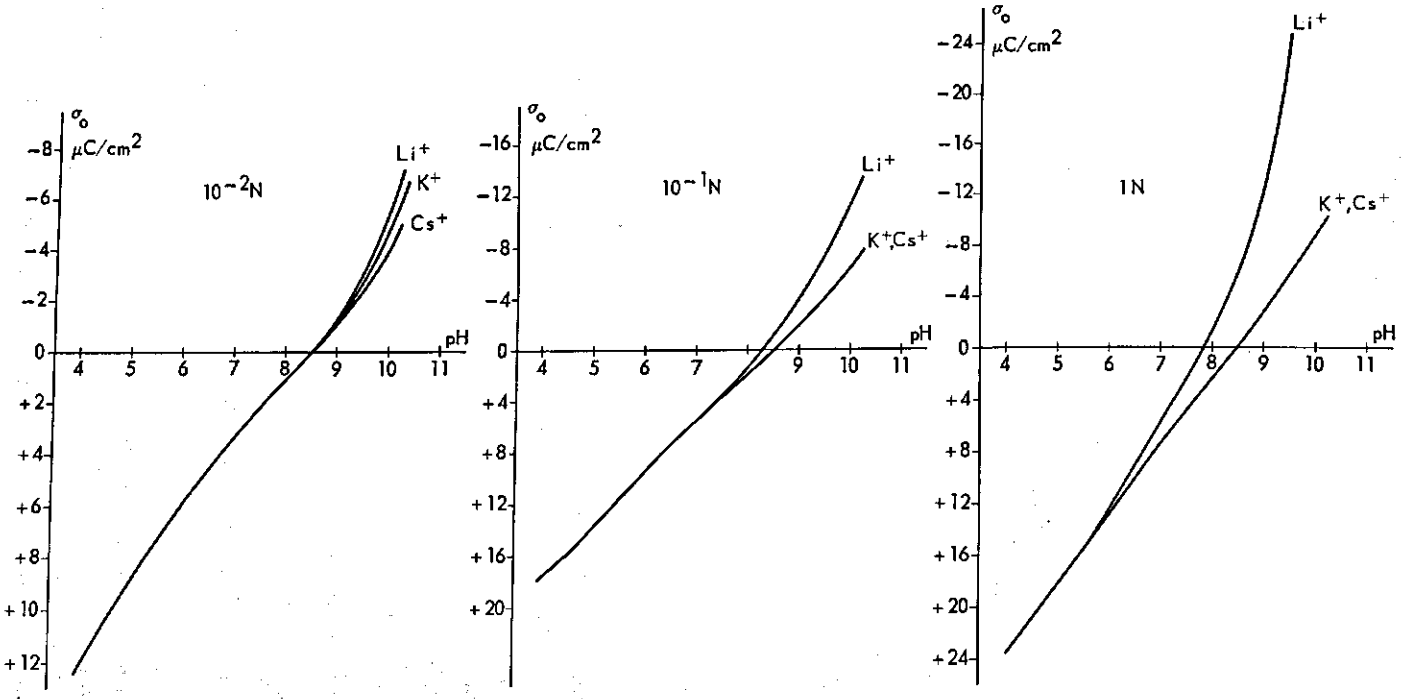

FIG. 4-4 Surface charge of hematite (sol B) as a function of pH in the presence of 10^{-2}, 10^{-1} and 1 N solutions of the chlorides of Li^+, K^+ and Cs^+.

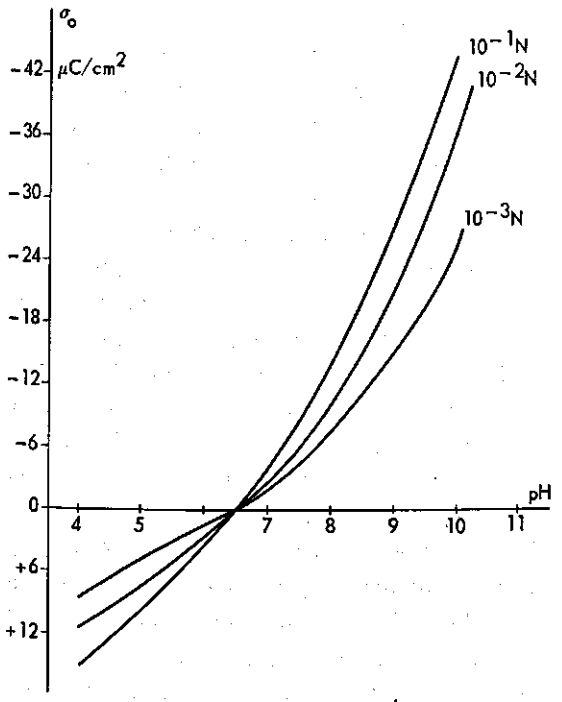

FIG. 4-5 Surface charge of hematite (sol B) as a function of pH in the presence of different concentrations of $Ca(NO_3)_2$.

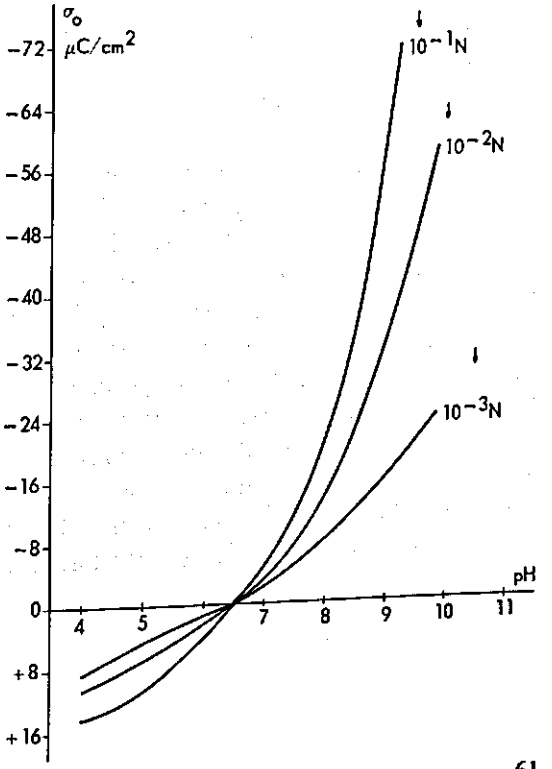

FIG. 4-6 Surface charge of hematite (sol B) as a function of pH in the presence of different concentrations of $Mg(NO_3)_2$. The arrows indicate the pH where ideal solutions of Mg^{2+} salts are saturated with respect to $Mg(OH)_2$. The solubility product is taken to be $10^{-10.6}$.

with the inflection points. The former method is less accurate in this case due to the steepness of the curves. The identification of the p.z.c. with the inflection point (in 10^{-3} and 10^{-2} N solutions) is considered to be permitted because the theoretical difference between these points for (2–1) electrolytes is only slightly beyond the experimental error. The value obtained was corroborated by the addition method and by counter charge measurements.

As compared to the results for KCl the negative surface charges attained in the presence of $Ca(NO_3)_2$ are much higher whereas the positive surface charges approach each other at low pH (see also BREEUWSMA and LYKLEMA 1973). The p.z.c. has shifted from pH^0 8.5 to 6.5 $\pm$ 0.2. Both features indicate strong specific adsorption of Ca^{2+}. Furthermore it is to be noted that this shift is already produced at a concentration of 10^{-3} N and that further increase of c_{salt} has no influence. In another experiment in the presence of 10^{-3} N KNO_3 and of $Ca(NO_3)_2$ concentrations increasing from 10^{-6} to 10^{-3} N the inflection point was found to gradually shift from pH^0 8.5 to 6.5.

The (σ_0–pH) curves in $Mg(NO_3)_2$ show the same features as those in $Ca(NO_3)_2$ except that the negative surface charge at high c_{salt} ($> 10^{-3}$ N) is markedly higher with Mg^{2+} than with Ca^{2+}. This is further illustrated in fig. 4–7 which gives the (σ_0–pH) curves at constant c_{salt} for all the alkaline earth nitrates studied. In 10^{-3} N solutions the (σ_0–pH) curves in the various electrolytes practically coincide. In 10^{-2} N and especially in 10^{-1} N solutions the following sequence is found for σ_0:

$$Mg^{2+} >> Ca^{2+} > Sr^{2+} \simeq Ba^{2+}.$$

4.2.3. *Surface charge–pH curves in the presence of potassium sulphate*

The (σ_0–pH) curves in the presence of K_2SO_4 are shown in fig. 4–8. For the same reasons as discussed above for the alkaline earth nitrates, the p.z.c. was identified with the pH of the inflection points at low ionic strength (10^{-3} and 10^{-2} N). The p.z.c. thus determined is $pH^0 = 9.6 \pm 0.2$. As in the presence of (1–1) electrolytes, the addition method and the counter charge measurements gave lower values (ca. 8). Besides a positive shift in p.z.c. the (σ_0–pH) curves in K_2SO_4 indicate a considerable increase in positive surface charge compared to that in KCl. As with the alkaline earth nitrates, the p.z.c. shifts below 10^{-3} N but not at higher concentrations.

In conclusion, the SO_4^{2-} ion appears to be strongly specifically adsorbed and its behaviour resembles that of the alkaline earth ions.

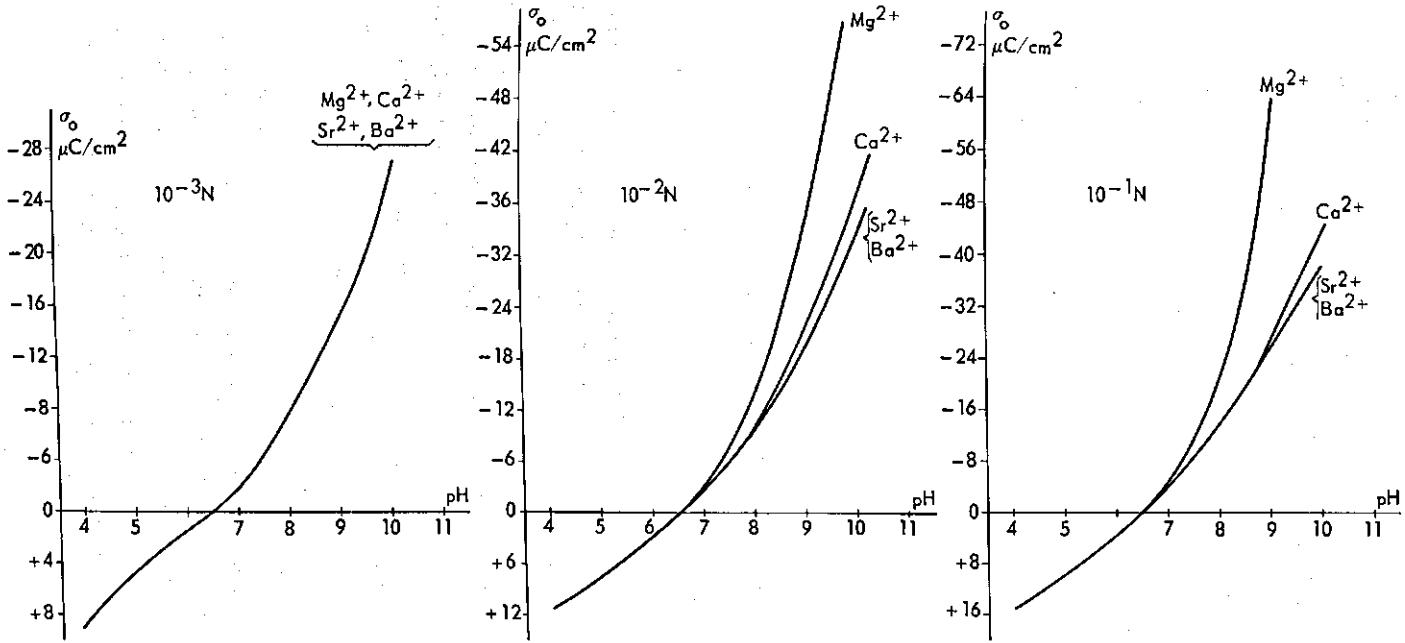

FIG. 4-7 Surface charge of hematite (sol B) as a function of pH in the presence of 10^{-3}, 10^{-2} and 10^{-1} N solutions of the nitrates of Mg^{2+}, Ca^{2+}, Sr^{2+} and Ba^{2+}.

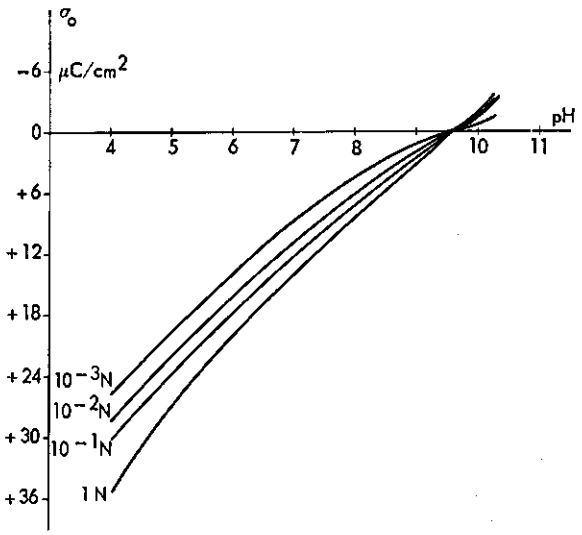

FIG. 4-8 Surface charge of hematite (sol A) as a function of pH in the presence of different concentrations of K_2SO_4.

4.3. SURFACE CHARGE MEASUREMENTS. DISCUSSION

4.3.1. *Comparison of (σ_0–pH) curves with (σ_0–ψ_0) curves for mercury and silver iodide*

It is worthwhile to start the discussion of the results reported above by comparing the (σ_0–pH) curves for hematite with the corresponding (σ_0–ψ_0) curves for systems such as mercury (GRAHAME 1947) and silver iodide (LYKLEMA 1963). In so doing there is one obvious similarity. At given pH or ψ_0 the surface charge increases with increasing concentration of *indifferent* (i.e. not potential-determining) electrolyte as expected from eqns. (4–2), (4–6) and (4–7). In the GCSG model this demonstrates the screening effect of the counterions on the surface charge. The lateral interaction between the charged surface groups decreases with increasing c_{salt} enabling more charged surface groups to become accommodated at the interface at given surface potential.

There are conspicuous differences between the (σ_0–pH) curves for hematite (and for oxides and oxidic materials in general) and the (σ_0–ψ_0) curves for mercury and silver iodide. In order to compare surface charge curves on different substrates it is necessary to do so at high c_{salt} because in that case the charge-compensating ions are primarily situated in the non-diffuse part of the double layer. The adsorption in this region is more affected by the properties of the solid/solution interface and hence reflects these properties to a greater extent than at lower c_{salt}.

For negative surfaces some surface charge curves in the presence of 10^{-1} N electrolyte have been compiled in fig. 4–9. Two facts clearly emerge from these figures. Firstly, the (σ_0–ψ_0) curves for Hg and AgI are slightly *concave* towards the potential axis whereas the (σ_0–pH) curves are highly *convex* towards the pH-axis, indicating progressive increase in OH^- adsorption with increasing pH. Secondly, the (negative) values for σ_0 are much higher for the oxides and glass ($\sim$ tens of $\mu C\ cm^{-2}$) than for mercury and silver iodide (a few $\mu C\ cm^{-2}$). Similar results have been found by several authors for silica (BOLT 1957, ABENDROTH 1970, AHMED 1966), hematite(ATKINSON et al. 1967, PARKS and DE BRUYN 1962, AHMED and MAKSIMOV 1968) and for other oxides such as TiO_2 (BÉRUBÉ and DE BRUYN 1968, AHMED and MAKSIMOV 1969), ZnO (BLOK 1968), Al_2O_3 (SADEK et al. 1970), SnO_2 (AHMED and MAKSIMOV 1969), ZrO_2 (AHMED 1966) and ThO_2 (AHMED 1966).

A further notable feature of the (σ_0–pH) curves for oxides, not shown in the

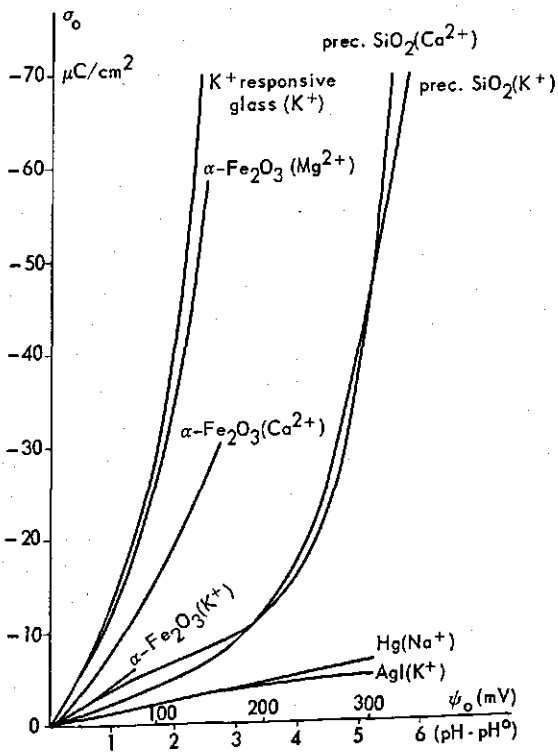

FIG. 4-9 Surface charge curves for various materials in the presence of 10^{-1} N electrolyte. K^+-responsive glass in KCl (TADROS and LYKLEMA), precipitated silica in KCl and $CaCl_2$ (TADROS and LYKLEMA), hematite in KCl, $Ca(NO_3)_2$ and $Mg(NO_3)_2$ (this study), mercury in NaF (GRAHAME, after integration of differential capacity) and silver iodide in KNO_3 (LYKLEMA).

figure, is that they are generally more or less symmetrical with respect to the p.z.c. Thus for positive surfaces the (σ_0–pH) curves are also convex towards the pH axis. For Hg and AgI the (σ_0–ψ_0) curves on positive surfaces have this same shape. The order of magnitude of σ_0 developed on the positive side of the p.z.c. is still much higher for the oxides, though.

4.3.2. *Porous double layer model*

It appears from the foregoing section that oxides have some common characteristics not shown by mercury and silver iodide. It has been pointed out recently by TADROS and LYKLEMA (1968 and 1969a) that for precipitated silica the high surface charges may be due to penetration of ions into the solid. Direct evidence for this type of surface porosity was derived from the charge-build up (at high pH and high c_{salt}) beyond the surface density of silanol groups. The idea of these authors was confirmed by their study of the (σ_0–pH) curves for glass powders (TADROS and LYKLEMA 1969b). Glass surfaces are well-known to exhibit extensive swelling upon immersion in aqueous solutions, especially at low pH. The negative surface charges of these materials markedly exceed the monolayer capacity based upon the BET areas after soaking. Both the silica and the glass samples used in these studies were found to be porous with respect to nitrogen. This does not *a priori* imply that the surface would be porous for ions. The latter type of porosity may solely exist in (aqueous) solutions where the surface structure has been affected by processes such as swelling and leaching or other processes connected with the finite solubility of the solid, whereas the 'nitrogen porosity' is always measured on dried materials. On the other hand, the origin of both types of porosity might be related. LYKLEMA (1971) has shown that indeed for silica the surface charge does increase with increasing degree of 'nitrogen porosity'. It was also noted that despite their high surface charge silica sols, as a rule, are not particularly stable.

It is essential in the (qualitative) explanation of the high surface charges that, in addition to p.d. ions, counterions are able to penetrate as well. Otherwise high surface charges cannot exist because of the high potential which would then develop. (It is convenient to maintain the term 'surface charge' although it is clear that the charge is no longer confined to the surface proper). Moreover, penetration of both p.d. and counterions explains the normal stability found with oxide sols because the high surface charge is for the greater part compensated for inside the solid so that no excessively high diffuse double layer charges are encountered.

LYKLEMA (1968) has also given a quantitative elaboration of the porous double layer model. The principal assumptions are

1. The surface charge density decreases exponentially with increasing distance x from the surface into the solid phase:

$$n(x) = n(0) \exp(-px) \qquad (4-23)$$

where $n(x)$ denotes the number of surface charges per unit volume at a distance x and $n(0)$ that at the surface. The symbol p refers to the penetration depth, defined as the reciprocal distance over which the charge density decreases to 1/e times its value at the surface.

2. The adsorption of counterions in the solid follows a LANGMUIR-type equation:

$$\left(\frac{\theta}{1-\theta}\right)_x = \left(\frac{c}{55.5}\right) \exp\left(\pm \frac{ze\psi(x)}{kT} - \frac{\phi}{kT}\right) = B \exp y(x) \qquad (4-24)$$

with

$$B = \left(\frac{c}{55.5}\right) \exp\left(-\frac{\phi}{kT}\right) \qquad (4-25)$$

in which θ is the fraction of the surface charge that is compensated for by counterions in the solid and $y(x)$ is the dimensionless reduced potential defined as $\pm ze\psi(x)/kT$. Again the + sign refers to a negative surface and *vice versa*. For the potential – distance relationship the following equation is derived:

$$\frac{d^2y}{du^2} = \frac{\alpha e^{-u}}{1+Be^y} \qquad (4-26)$$

in which u is the dimensionless reduced distance px and

$$\alpha = \frac{4 \pi e z \sigma_0}{\varepsilon kT p} \qquad (4-27)$$

Finally, an equation is given for the fraction of the surface charge that is compensated for by the counter charge:

$$\frac{\sigma_m^s}{\sigma_0} = B \int_0^\infty \frac{e^{y-u}}{1+Be^y} du \qquad (4-28)$$

In his paper, LYKLEMA (1968) gives some numerical solutions of eqns. (4–26) and (4–28), showing several interesting features. Two of them may be mentioned here. Firstly, with increasing surface charge the quantity $\sigma_0 - \sigma_m$ i.e. the charge effective in colloid stability, soon becomes independent of σ_0 even at low penetration depths ($\sim$ 1 Å). In other words, at high surface charge further adsorption of p.d. ions is completely compensated for by adsorption of counterions inside the solid. It is therefore clear that the theory does account for high surface charges as well as for normal stability. Secondly, the numerical solutions indicate that the counterion penetration is much more sensitive towards $1/p$ (the penetration depth) than to B. This could mean that the radii of the counterion

and the pores are more important in counterion adsorption than the concentration and specific adsorption potential of the counterions.

Finally, it is noted that the shape of the (σ_0–ψ_0) curves, calculated from the complete set of computer data, is indeed convex (see below). As a result the differential capacity also passes through a minimum at the p.z.c.

4.3.3. *Other double layer models for oxides*

Besides the porous double layer theory several other models and theories for the double layer on oxide surfaces have been proposed, all based upon non-penetration.

First of all, though not presenting a quantitative treatment, the interesting model for the rutile/solution interface developed by BÉRUBÉ and DE BRUYN (1968) is mentioned. These authors have drawn the attention to the effect of highly polarizing oxide surfaces on the water structure. It is discussed how this may influence the location of the surface charge and ion specificity.

The first attempt at a quantitative approach is due to ATKINSON et al. (1967). The equation of these authors for the adsorption of the p.d. ions as a function of the pH and electrolyte concentration has the advantage of being open to experimental verification. However, the derivation is questionable. For the chemical potential of the adsorbed H^+ ions these authors have essentially used eqn. (4–13) written in terms of relative rather than absolute quantities:

$$\mu^s_{H+} = \mu^{0,s}_{H+} + RT \ln \frac{\theta_{X+}}{1-\theta_{X+}} \qquad (4-29)$$

For the counterion an analogous equation was used. It has been argued earlier that this splitting of μ^s_{H+} is necessarily arbitrary, that is, it is based upon a (non-thermodynamic) model. This model can only be tested if its use does not involve important additional assumptions. In the treatment by ATKINSON et al. (1967) it is assumed that (1) the diffuse double layer can be ignored ($\theta_{X+} = \theta_{anion}$), (2) the double layer capacity is constant ($\psi_0 - \psi_{anion}$ = constant), (3) $\sigma_0 \simeq F\Gamma_{H+}$ (below the p.z.c.) or $\sigma_0 \simeq F\Gamma_{OH-}$ (above the p.z.c.) and (4) $\theta_{X+}/(1-\theta_{X+}) \simeq \theta_{X+}$. These simplifications are not really justified (2) nor always substantiated by the experimental facts (1 and 4). It is therefore not surprising that in the present study, except for KCl below the p.z.c., poor agreement was obtained between this theory and experiment.

Another approach has been described by BLOK (1968) in a study of the double layer on ZnO in the presence of (1–1) electrolytes. The assumptions are as follows: 'NERNST behaviour' of the surface potential, specific adsorption both of cations and anions and constant capacities for the inner and outer HELMHOLTZ layer. Thus (σ_0–ψ_0) curves can be calculated and one may attempt, by trial and error, to match the experimental curves with theoretical ones.

Except for the 'NERNST behaviour' the same assumptions made by BLOK (1968) have been used by LEVINE and SMITH (1971). As was mentioned in section 4.1.3. they have also considered the variation in $\mu^s_{H^+}$.

As a result two additional parameters appear in their model, namely the total number of chargeable surface sites and the fraction of surface sites charged at the p.z.c. Unfortunately, the models of BLOK (1968) and LEVINE and SMITH (1971) cannot be verified as yet owing to the many experimentally inaccessible parameters.

Finally, the simplified 'polyelectrolyte model' proposed by STUMM et al. (1970) is mentioned. The association-dissociation behaviour of amphoteric oxides is related to that of polyelectrolytes. Assuming a bifunctional character of the surface groups, as in eqn. (4–14), and considering the dissociation equilibrium, these authors define a 'microscopic' acidity constant which for the present purpose is written as:

$$K_d^m = \frac{[X^-]\,[H^+]_s}{[X_T] - [X^-]} \qquad (4-30)$$

where $[X^-]$ is the concentration of negative surface sites in moles l^{-1} and $[X_T]$ the total concentration of dissociable surface sites in moles l^{-1}. The concentration of the H^+ ions at the surface in moles l^{-1} is denoted by $[H^+]_s$. In the elaboration by STUMM et al. (1970) it is stated that $[X^-]$ can be obtained from acid-base titrations. Since $[X^-]$ is proportional to Γ_{OH^-} it is thus assumed that Γ_{H^+} can be ignored. Provided that $[H^+]_s$ can be calculated, K_d^m and X_T can be derived from a plot of $[H^+]_s$ against $[X^-]^{-1}$. With the aid of the BOLTZMANN factor, $[H^+]_s$ is expressed in the concentration in the solution, $[H^+]$, by:

$$[H^+]_s = [H^+] \exp\left(-\frac{e\psi_s}{kT}\right) \qquad (4-31)$$

where ψ_s is the difference in potential between surface and solution. As a first approximation STUMM et al. (1970) assume $\psi_s = \psi_d$ and $\sigma_0 = -\sigma_d$ and calculate ψ_d from σ_d by diffuse double layer theory. Obviously this is a crude approximation because it ignores specific adsorption and even the presence of a STERN layer. At the same time it does illustrate that the 'polyelectrolyte model' requires a knowledge of the double layer structure and hence ultimately encounters the same problems as the GCSG model.

It is thus concluded that the current double layer models for oxides based upon non-penetration of ions suffer either from being too simple or from being too rigorous. In other words, as yet we do not have an acceptable theory, with experimentally accessible parameters, to describe the electrical double layer on oxides in the absence of ion penetration.

4.3.4. *Porous double layer model applied to hematite*

The (σ_0–pH) curves for hematite exhibit several features that can be qualitatively explained in terms of the porous double layer model (BREEUWSMA and LYKLEMA 1971).

Over the pH range studied, σ_0 does not attain such high values as found for precipitated SiO_2 and glass. However, the range studied is limited and under certain conditions extension towards higher pH might well give rise to σ_0 values exceeding those corresponding to full dissociation of all surface hydroxyl groups. For hematite with ca. 4.5 to 5.9 OH^- groups per 100 Å^2 (section 2.6.) full dissociation would amount to a surface charge of 70–90 μC cm^{-2}. In fact in the presence of 10^{-1} N $Mg(NO_3)_2$, σ_0 does approach this maximum without any sign of saturation (fig. 4–6). It has been noted that at high c_{salt}, Li^+ and Mg^{2+} exhibit exceptionally strong adsorption as compared to the other alkali and alkaline earth ions[6]. In the porous double layer model this indicates a high degree of penetration for these ions. Because penetration is higher the smaller the counterion and because Li^+ and Mg^{2+} are the smallest unhydrated ions studied, this suggests that they adsorb in a partly or completely dehydrated form. This suggestion is reinforced if one considers the crystal ionic radii of these elements in 6-co-ordination, viz. 0.60 Å for Li^+ and 0.65 for Mg^{2+} (WELLS 1945). These values are almost equal to that for Fe^{3+} (0.60 Å) (WELLS 1945) indicating that Mg^{2+} and Li^+ ions are able to occupy octahedral Fe^{3+} sites. This is not possible with the other alkali and alkaline earth ions studied (having a crystal ionic radius $\geqslant$ 0.99 Å) and, hence, would explain the exceptional behaviour of Li^+ and Mg^{2+}. The situation is thus analogous to that in clay minerals and other layer silicates where also Li^+ and Mg^{2+} are the sole alkali and alkaline earth ions occurring in the octahedral hydroxyl layers (DEER et al. 1962).

To our knowledge complete dehydration of counterions upon adsorption has hitherto not been described. If the suggestion of penetration of dehydrated Li^+ and Mg^{2+} ions into the solid is correct it should also be found with other oxides where these ions do fit into the crystal structure. It has been argued (QUIRK 1971, TADROS 1971) that indeed complete dehydration is unlikely to occur at ambient temperature. However, this cannot be stated *a priori* since the (unknown) gain in free energy due to adsorption may well exceed the dehydration energy. It is furthermore important to note that on the swollen surfaces of precipitated silica (TADROS and LYKLEMA 1968 and 1969a) and glass (TADROS and LYKLEMA 1969b) the behaviour of Li^+ and Mg^{2+} is not exceptional. It is

[6] Mg^{2+} and the other alkaline earth ions are considered to be adsorbed as such. That is to say, under the experimental conditions hydrolysis of these ions is considered to be unlikely. Firstly, in the pH range studied hydrolysis in the bulk solution is negligible, even for Mg^{2+} which shows the strongest tendency to hydrolyse (SILLÉN and MARTELL 1964). Secondly, the degree of hydrolysis at the surface may be expected to be even lower than that in the solution.

therefore not likely that this behaviour can be explained in terms of (promotion of) swelling as has been suggested elsewhere (QUIRK 1971). Last but not least an alternative explanation in terms of the GCSG model should be examined. The behaviour of specifically adsorbed ions could be interpreted in terms of the specific adsorption potential, ϕ. For (partly) dehydrated counterions this parameter might be expected to increase with decreasing ionic radius. However, it is not easy to explain why there should be a discontinuity in ϕ with ionic radius in going from Li^+ to the other alkali ions, and from Mg^{2+} to the other alkaline earth ions.

With regard to the possibility of penetration of Li^+ and Mg^{2+} at high c_{salt}, it was thought worthwhile to transform the (σ_0–pH) curves into (α–$y(0)$) curves and to compare them with the theoretical ones given in fig. 4–10. For lack of

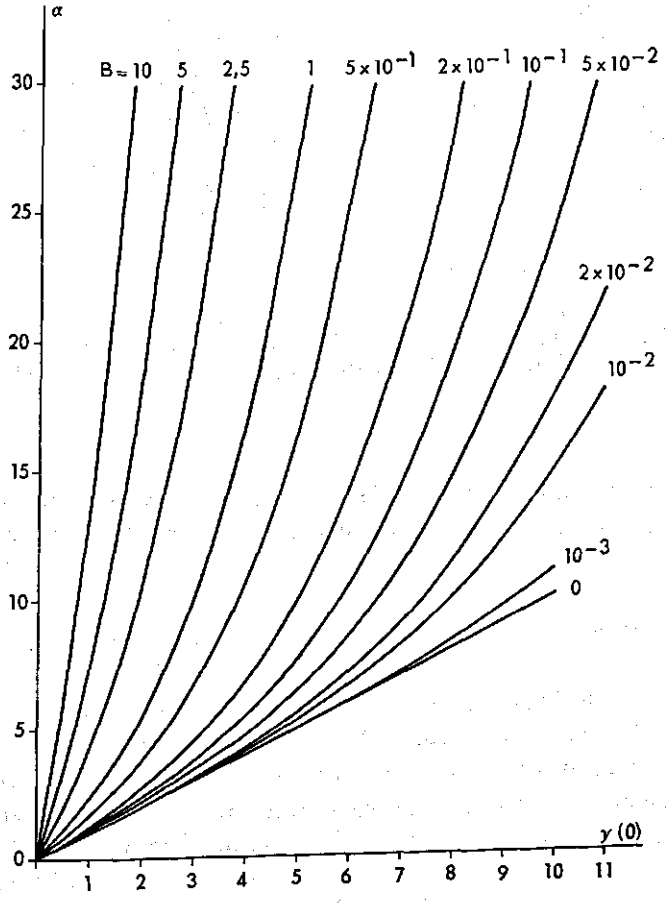

FIG. 4-10 Plots of α as a function of $y(0)$ for fixed values of B, calculated from the porous double layer theory.

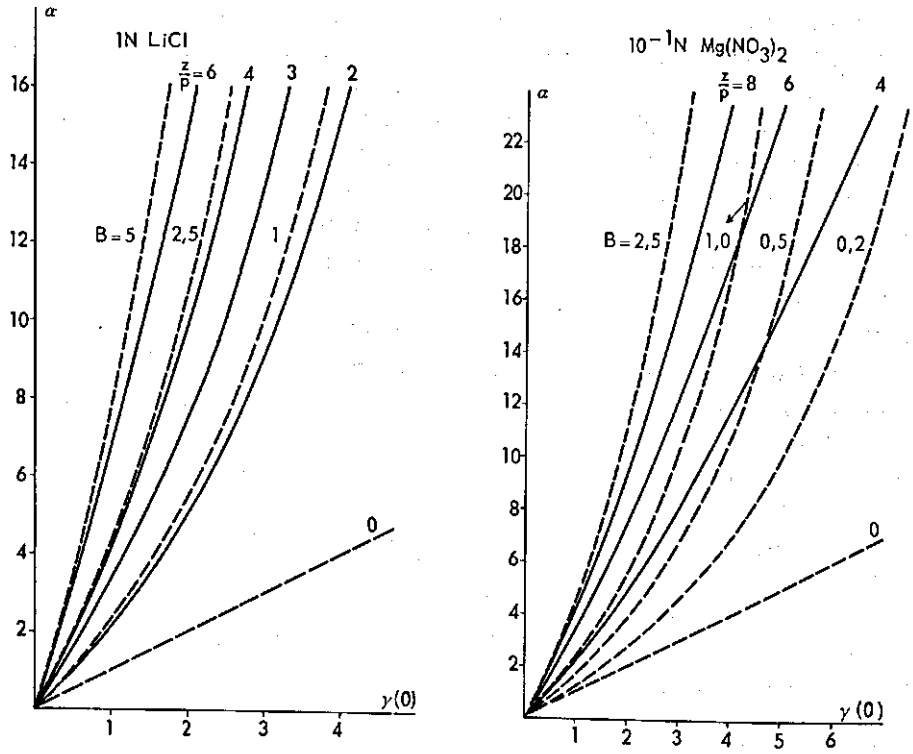

FIG. 4-11 Theoretical curves of α as a function of $y(0)$, and experimental ones for hematite in the presence of 1 N LiCl and 10^{-1} N $Mg(NO_3)_2$. Theoretical and experimental curves are represented by broken lines and full lines, respectively. For explanation of B and (z/p) see text.

anything more rigorous, eqn. (4–11) was used in the calculation of $y(0)$ from pH. The values for α have been calculated from eqn. (4–27) which at 20 °C, taking $\varepsilon = 15$ [7], reads:

$$\alpha = 0.29 \left(\frac{z}{p}\right) \sigma_0 \qquad (4-32)$$

The results for the highest concentrations of Li^+ and Mg^{2+} studied are given in fig. 4–11. The shapes of the curves for Li^+ most closely resemble those of the theoretical ones. It is true that the values of the three adaptable parameters ε, p and ϕ cannot be independently determined in this manner but the order of magnitude found for $1/p$ (less than a few Å) in combination with that for ϕ

[7] This value has not been established for the samples in this study. It is however close to the value of 14.2 that has been reported by MELLOR (1934).

(3–5 kT), as calculated from eqn. (4–25), is not unrealistic. For Mg^{2+} the shape of the experimental curves is clearly less convex than for the theoretical ones. One possible reason for this might be that the NERNST-type equation (4–11) may not be applied because $d\psi_0/dpH$ decreases with increasing surface charge. Another possibility is the fact that the electrolyte concentration studied (0.1 N) may have been too low because the experimental curves tend to become more convex at higher c_{salt}. On extrapolating the results for Mg^{2+} towards higher concentrations a (crude) estimate for the specific adsorption potential at penetration depth's of several Å gives values between 5 and 10 kT. It is concluded that, in view of the assumptions that had to be made, the porous double layer theory does satisfactorily describe the experimental results for Li^+ and Mg^{2+} at high c_{salt}.

At low c_{salt}, Li^+ and Mg^{2+} no longer behave exceptionally, probably indicating that with decreasing c_{salt} the relative contribution of charge compensation outside the solid increases. The question yet to be answered is whether the other ions do penetrate, if not in octahedral positions. The (σ_0–pH) curves for all electrolytes at low c_{salt} are not convex enough to match with theoretical ones. As before, this may be due to deviations from 'NERNST behaviour' of the surface potential. From the point of view of the porous double layer model it may also indicate that charge compensation takes place both inside and outside the solid. It seems useful to see whether or not the results can be completely described in terms of adsorption in the STERN layer and the diffuse layer. As mentioned in section 4.3.3. there is as yet no appropriate 'non-porous' double layer theory from which really conclusive results may be expected. However, it is possible to demonstrate that complete charge compensation outside the solid is questionable.

To that end a comparison is made between the experimental differential capacities, C_{exp}, and those calculated from the diffuse double layer theory, C_d. It is convenient to make comparisons at the p.z.c. because C_d is a function of ψ_d, and ψ_d is only known at this point: $\psi_d^{p.z.c.} = 0$ (in the absence of specific adsorption). The results for KCl will be given as an example. The differential capacity for spherical double layers has been calculated from eqns. (4–5) and (4–20) using the DEBYE-HÜCKEL approximation for I as given by LOEB et al. (1961). To demonstrate the influence of the particle radius, $C_d^{p.z.c.}$ has been calculated for two values of a, corresponding with the upper (400 Å) and lower (200 Å) limit of the particle size range. For sake of comparison, $C_d^{p.z.c.}$ has also been calculated for a flat double layer according to OVERBEEK (1952, page 131). Because no significant differences are present between the values of $C_{exp}^{p.z.c.}$ for the different sols studied (A, B and C) the average value has been used.

It can be seen from the results in table 4–2 that the calculated values of

TABLE 4-2. Experimental capacities on hematite at the p.z.c. compared with those calculated according to diffuse double layer theory.

c_{KCl}	$C_{exp}^{p.z.c.}$	$C_{flat\ d.l.}$ [1]	$C_{spherical\ d.l.}$ [2]	
			$a = 200$ Å	$a = 400$ Å
(moles l^{-1})	($\mu F\ cm^{-2}$)			
10^{-3}	21.0 ± 0.5	7.3	9.12	10.9
10^{-2}	35.5 ± 0.7	23.2	25.0	26.7
10^{-1}	70 ± 2	73.4	75.2	76.9
1	88 ± 5	232.0	233.8	235.5

[1] $C_d^{p.z.c.} = \frac{\varepsilon\kappa}{4\pi}$ [2] $C_d^{p.z.c.} = \frac{\varepsilon}{4\pi}\left(\kappa + \frac{1}{a}\right)$

$C_d^{p.z.c.}$ for spherical double layers are somewhat higher than those for flat double layers, especially at low ionic strength. However, even for $a = 200$ Å at low ionic strength $C_{exp}^{p.z.c.} > C_d^{p.z.c.}$. The same feature was found with the alkaline earth nitrates and potassium sulphate. As was shown in section 4.1.4. this observation implies also that $C^{p.z.c.} > C_d^{p.z.c.}$. It was furthermore shown in that section that, in terms of the GCSG model, the fact that $C > C_d$ is indicative of specific adsorption. For the asymmetrical electrolytes and LiCl this was already inferred from the shift in p.z.c. and from the increase in surface charge. Since for KCl the p.z.c. does not shift with increasing c_{salt}, it has to be concluded that both K^+ and Cl^- are specifically adsorbed and that they have approximately identical specific adsorption potentials. (As a result the assumption of $\psi_d = 0$ may be a reasonable approximation). Because for the alkaline earth nitrates and K_2SO_4 the p.z.c. also does not shift above 10^{-3} N one is forced to assume approximately identical ϕ values in these cases as well. Since for KNO_3 (not shown here) also no shift in p.z.c. was found this would lead to the unrealistic conclusion of approximately equal specific adsorption potentials for all the ions involved. Ion penetration on the other hand offers a simple explanation for $C > C_d$. Because the surface charge is (partly) compensated for inside the solid, at a given ψ_0 more charge can be accomodated on a porous than on a non-porous surface.

It is concluded from the discussion above that the (σ_0–pH) curves for hematite are compatible with a partial penetration of p.d. ions and counterions, especially of Li^+ and Mg^{2+}. It may be added that in view of the magnitude of the surface charges, there is only a slight penetration as compared to precipitated silica and glass. The hematite samples were found to be also only slightly porous with respect to nitrogen adsorption. This fits therefore in the trend of increasing surface charge with increasing 'nitrogen porosity' observed for silica-like surfaces (LYKLEMA 1971).

4.3.5. *Ion specificity*

In view of the conclusions of the preceding sections it would seem that ion specificity on oxides can be discussed merely in a qualitative manner. Because counterion penetration may occur it should be realized that ion specificity may be affected by other factors than those usually taken into account.

As was mentioned in the foregoing section, the sequences in the adsorption of alkali and alkaline earth ions at high salt concentrations can indeed most readily be interpreted in terms of penetration of (partially) dehydrated ions and non-penetration of other ions. At low c_{salt} ion penetration need not be invoked to explain the increase in adsorption of the alkali ions in the order:

$$Li^+ > K^+ > Cs^+$$

The same sequence has been found on rutile by BÉRUBÉ and DE BRUYN (1968). From stability studies of hematite sols, DUMONT and WATILLON (1971) reported the reverse order for the coagulation concentration of these ions. Since ψ_d decreases with increasing σ_m this is in accord with our observation. The specific effects may be interpreted in terms of the effect of the water structure upon counterion adsorption as has been done by these authors, ignoring counterion penetration into the solid. Another *ad hoc* explanation could be given in terms of the 'crystal field strength' model proposed by STUMM et al. (1970). In that case partial dehydration has to be assumed to explain the sequence reported above. This model is compatible with ion penetration so that experimental results can be explained assuming penetration or not.

It was furthermore noted that the (σ_0–pH) curves reveal a considerable influence of the valency of the counterions, the bivalent ions being more strongly adsorbed than the monovalent ones. It may be mentioned that this is also predicted by the porous double layer theory. From eqn. (4–27) it is seen that z affects σ_0 in the same manner as the penetration depth $1/p$ does. This implies that σ_d is more sensitive to a change in the valency than to a change in the specific adsorption potential (section 4.3.2.).

4.3.6. *Shift in p.z.c. and the Esin-Markov coefficient*

The shift in p.z.c. with increasing electrolyte concentration has been dealt with in a number of studies on the electrical double layer on mercury. ESIN and MARKOV (1939) found that the experimental shift was larger than predicted from STERN's theory. This anomaly was later referred to by GRAHAME (1955) as the 'ESIN-MARKOV effect'. PARSONS (1957) has discussed the shift in p.z.c. with c_{salt} from a thermodynamic point of view for polarizable interfaces and extended the theory to include any shift in surface potential caused by a change in c_{salt}. Recently LYKLEMA (1972) has worked out the thermodynamic theory for reversible interfaces.

For oxides he defines the ESIN-MARKOV coefficient β as:

$$\beta = \left(\frac{\mathrm{dpH}}{\mathrm{d}\log f_{\pm}c}\right)_{\sigma_0} \tag{4-33}$$

The relationship between this coefficient and the adsorption of, for example, cations is found to be:

$$\beta = \frac{1}{z_-} + \frac{z_+ + z_-}{z_+ z_-}\left(\frac{\delta\sigma^+}{\delta\sigma_0}\right)_{f_{\pm}c} \tag{4-34}$$

where the sign is not included in the valencies. Strictly speaking, expression (4–34) applies to the region where the relative variation of the individual activity coefficients equals that of the mean activity coefficient. At higher c_{salt} it is no longer exact.

Some values for $(\delta\sigma^+/\delta\sigma_0)_{f_{\pm}c}$ and β for the electrolytes used in this study have been compiled in table 4–3. In the absence of specific adsorption $\delta\sigma^+/\delta\sigma_0$ can be calculated from diffuse double layer theory. At the p.z.c. it can also be derived from simple electroneutrality conditions in this case. For example, for a (1–1) electrolyte at the p.z.c. the positive and negative surface charges are neutralized by an equal amount of anions and cations, respectively. It follows that under these conditions $\delta\sigma^+/\delta\sigma_0 = -\frac{1}{2}$ and $\beta = 0$. In the presence of specific adsorption of e.g. cations at the p.z.c. the value of $\delta\sigma^+/\delta\sigma_0 < -\frac{1}{2}$ and hence $\beta < 0$. The limiting values of $\delta\sigma^+/\delta\sigma_0$ far below and far above the p.z.c. are also readily determined if one considers that the negative adsorption becomes constant at high surface charge. Any change in σ_0 is thus completely compensated for by a change in the positive adsorption, that is, below the p.z.c. by the adsorption of anions and above the p.z.c. by the adsorption of cations. (In practice this holds even when the negative adsorption is not entirely constant because the negative adsorption is (very) small as compared to the positive

TABLE 4-3. ESIN-MARKOV coefficient β as a function of surface charge and electrolyte type. The assumptions are: no specific adsorption at the p.z.c. and no super-equivalent adsorption.

surface charge	type of electrolyte					
	(1–1)		(2–1)		(1–2)	
	$\left(\frac{\delta\sigma^+}{\delta\sigma_0}\right)_{f_{\pm}c}$	β	$\left(\frac{\delta\sigma^+}{\delta\sigma_0}\right)_{f_{\pm}c}$	β	$\left(\frac{\delta\sigma^+}{\delta\sigma_0}\right)_{f_{\pm}c}$	β
>>0	0	1	0	1	0	$+\frac{1}{2}$
0	$-\frac{1}{2}$	0	$-\frac{2}{3}$	0	$-\frac{1}{3}$	0
<<0	−1	−1	−1	$-\frac{1}{2}$	−1	−1

adsorption). It is obvious that this is also valid in the presence of specific adsorption, provided the adsorption is not super-equivalent. Thus at high positive and negative surface charges $\delta\sigma^+/\delta\sigma_0 = 0$ and -1, respectively. In the case of super-equivalent adsorption $\delta\sigma^+/\delta\sigma_0 < -1$.

As shown in section 4.2., the p.z.c. was found to shift with increasing c_{salt} towards a lower pH in the presence of LiCl and the alkaline earth nitrates, and towards a higher pH in the presence of K_2SO_4. Remarkably enough, for the asymmetrical electrolytes no further shift was observed above 10^{-3} N. This suggests that the specific adsorption at the p.z.c. takes place with a limited amount of special surface groups. It follows from the discussion above that the negative shifts of the p.z.c. (i.e. towards lower pH) are indeed to be attributed to specific adsorption of cations (Li^+ and the alkaline earth ions) rather than of anions. This has not always been recognized by other authors. For example, PARKS (1965) erroneously interpreted OVERBEEK's work (1952) by concluding that specific adsorption of anions would lead to a negative shift of the p.z.c. Part of this misunderstanding may be due to the fact that no proper distinction was made between p.z.c. and i.e.p. As mentioned before, these points move in opposite directions with specific adsorption. Furthermore, a different definition

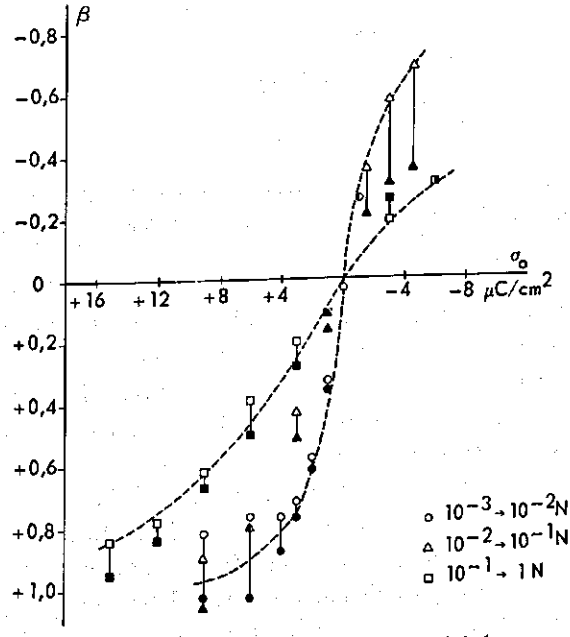

FIG. 4-12 ESIN-MARKOV coefficient β as a function of σ_0 for sol A (open symbols) and sol B (solid symbols) in the presence of KCl. The shape of the symbol gives the concentration change as indicated in the figure.

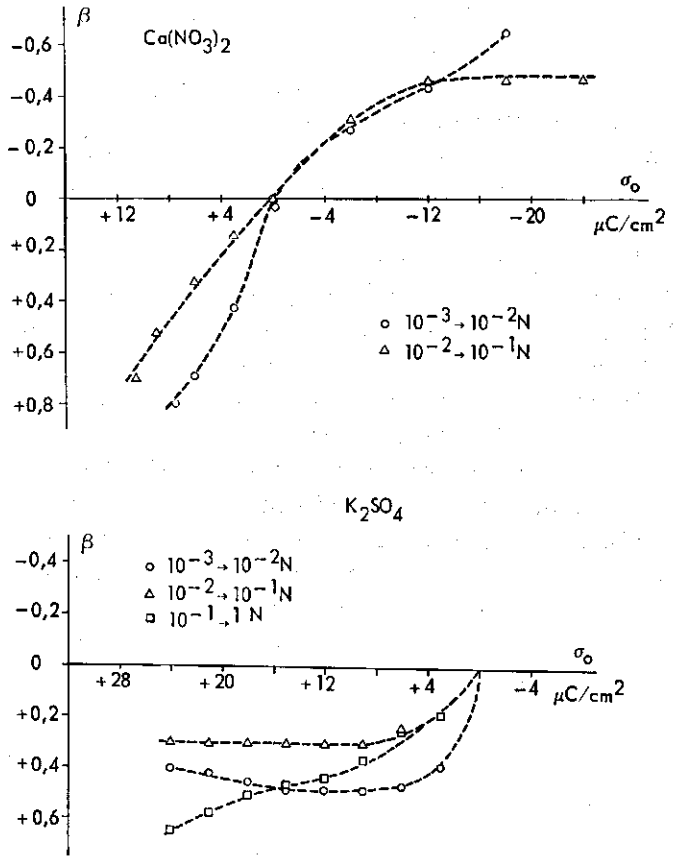

FIG. 4-13 ESIN-MARKOV coefficient β as a function of σ_0 for sol A in the presence of $Ca(NO_3)_2$ and K_2SO_4. The shape of the symbol gives the concentration change as indicated in the figure.

of specific adsorption has led HINGSTON et al. (1967) to the same conclusion as PARKS (1965). The former authors use the term specific adsorption for adsorption occurring through a ligand exchange reaction with surface hydroxyl groups. In that case the anion behaves as a p.d. ion if it carries 'residual' charge ($z_- \geqslant 2$) and the conclusion is now correct. It follows from this discussion that one is able to distinguish between 'counterion behaviour' and 'p.d. ion behaviour' from the direction in which the p.z.c. shifts. In connection with this it may be noted that AYLMORE et al. (1967) have suggested that adsorption of SO_4^{2-} on hematite occurs by ligand exchange. This would imply a negative shift of the p.z.c. and is therefore at variance with the current results (see also section 4.4.).

It is of interest to compare the experimental values for β at 'high' positive

and 'high' negative surface charges with those predicted by eqn. (4–34) and given in table 4–3. To that end ($\beta - \sigma_0$) plots for KCl, $Ca(NO_3)_2$ and K_2SO_4 are presented in figs. 4–12 and 4–13. The results for KCl have been plotted for two different sols (A and B). The spread in β due to the use of different samples is considerable. Furthermore, β varies also with the concentration. It can be seen however that, as far as data at sufficiently high surface charge are available, β does approach or does not exceed the theoretical values within experimental error.

This conclusion thus lends credit to the methods that have been used to relate the (σ_0–pH) curves to each other. It is interesting that for Li^+ and especially for Mg^{2+} (not shown here) β definitely exceeds the limiting values for high negative surface charges. For Mg^{2+}, β increases regularly with negative surface charge from 0 at the p.z.c. to a value of about – 1.3 at the highest pH attained, whereas the limiting value is $-\frac{1}{2}$. This may be tentatively interpreted in terms of super-equivalent adsorption. As can be seen from eqn. (4–34), for a (2–1) electrolyte the fact that $\beta < -1$ implies $\delta\sigma^+/\delta\sigma_0 < -1$. In other words, at high pH where $\beta < -1$ the positive counter charge increases more rapidly with pH than the surface charge so that eventually super-equivalent adsorption should occur. It should be realized however that if Mg^{2+} penetrates into the solid, as suggested above, complications may arise with respect to the applicability of eqn. (4–34). It has been noted by LYKLEMA (1972) for porous surfaces that β tends to be too low as soon as σ_0 becomes very high (say higher than 50–100 $\mu C\ cm^{-2}$).

4.4. COUNTER CHARGE MEASUREMENTS. RESULTS AND DISCUSSION

In the present study the ionic components of charge, σ^+ and σ^-, have been obtained from direct measurements of the counter charge. This was made possible by the relatively high surface area of the order of 20 –30 $m^2 g^{-1}$. For substances with low surface area direct measurements are difficult. LYKLEMA has shown how in general σ^+ and σ^- may be derived from (σ_0–ψ_0) curves (1963) and (σ_0–pH) curves (1972) provided these can be very accurately determined. As can be seen from eqns. (4–33) and (4–34) one can in principle obtain σ^+ by integration of eqn. (4–34):

$$\sigma^+ = -\frac{z_+\sigma_0}{z_+ + z_-} + \frac{z_+ z_-}{z_+ + z_-}\int_0^{\sigma_0} \beta\, d\sigma_0 \qquad (4-35)$$

and for σ^- an analogous equation can be obtained (LYKLEMA 1972).

As a result of the rather large error in β reported above this procedure is not very accurate in the present case. However, the main reason for performing

direct measurements rather than using the indirect procedure was to have an independent measurement of σ^+ and σ^- and also of the p.z.c.

Figures 4–14 and 4–15 show the surface charge and counter charge for sol A and sol B in the presence of 10^{-3} N solutions of Ca^{2+} salts and K_2SO_4. The results clearly illustrate the manner in which the surface charge is compensated for by positive and negative adsorption. Consider for example fig. 4–14. At high pH ($\sigma_0 < 0$) the surface charge is largely compensated for by a positive adsorption of Ca^{2+} and to a small extent by a negative adsorption of Cl^-. At low pH ($\sigma_0 > 0$) the situation has reversed. It can be seen that commonly the charge balance $\sigma_0 = -(\sigma_{Ca^{2+}} + \sigma_{Cl^-})$ is well obeyed within the experimental error of about 0.5 $\mu C\ cm^{-2}$. (The results for sol A have been included to show that the slight tendency of $\sigma_{Ca^{2+}}$ to exceed σ_0 at high pH found for $CaCl_2$ is

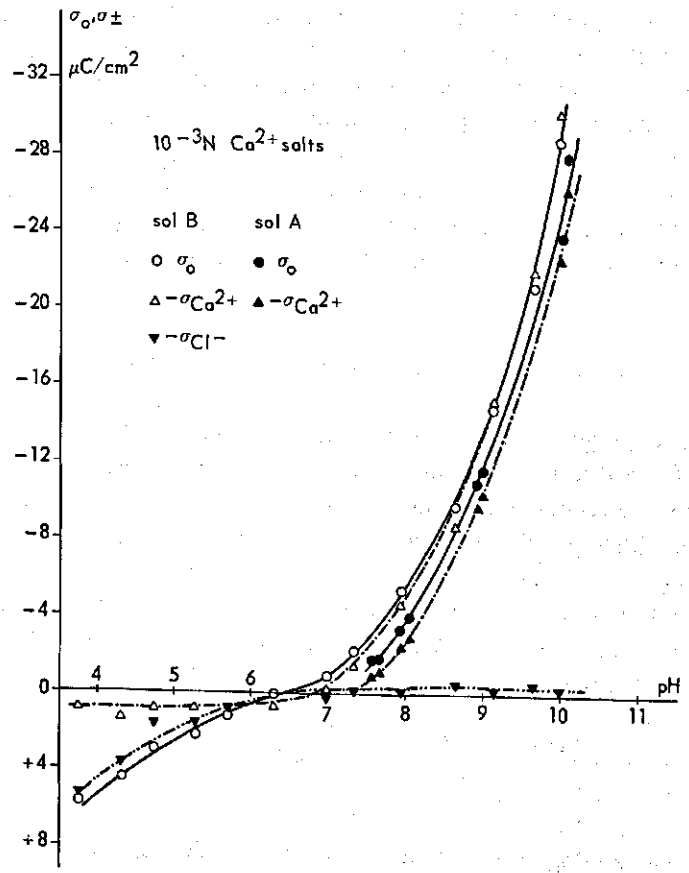

FIG. 4-14 Ionic components of charge in the electrical double layer on hematite in the presence of 10^{-3} N $CaCl_2$ (sol B) and 10^{-3} N $Ca(NO_3)_2$ (sol A).

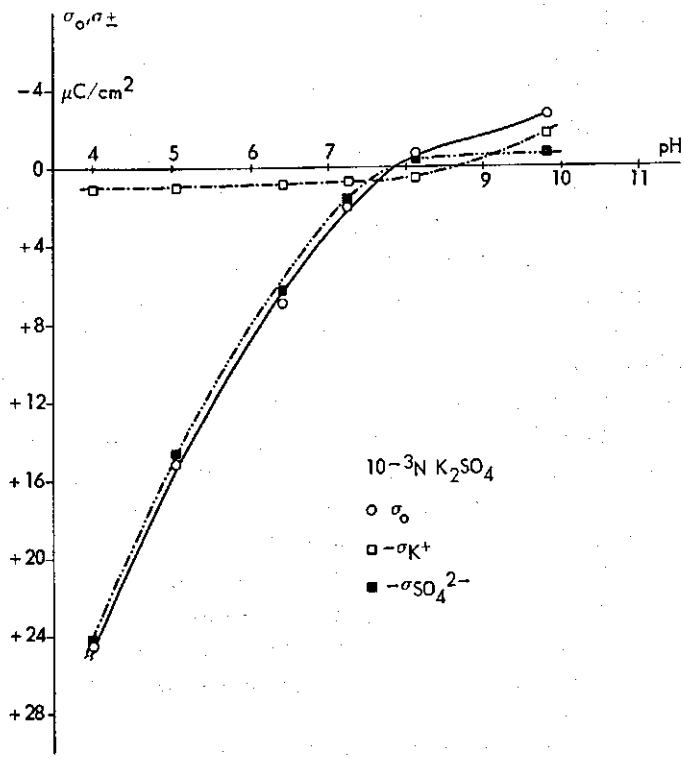

FIG. 4-15 Ionic components of charge in the electrical double layer on hematite in the presence of 10^{-3} N K_2SO_4 (sol B).

not significant). The p.z.c. indicated by the direct counter charge measurements is between pH 6 and 7, confirming the pH^o obtained by the potentiometric titration method. Also for K_2SO_4 the general trends are evident.

With respect to the magnitude of the maximum negative adsorption it is noted that the experimental values for Cl^- and SO_4^{2-} are in fair agreement with estimates of the maximum values predicted by eqn. (4–4), taking $a = 350$ Å (sol B) and $\psi_d = 100$–200 mV. These values are of the order of 0.2–0.4 $\mu C\,cm^{-2}$. The negative adsorption of K^+ and Ca^{2+} ($\simeq 1\ \mu C\ cm^{-2}$) is somewhat higher than expected. This is due to the release of traces of these ions retained by the samples during their preparation (see also section 2.5.4.2.). Furthermore, the crossing of the σ^+ and σ^- curves around the p.z.c. is not in agreement with the theory because it would imply negative rather than positive adsorption of electrolyte at this point. However, in view of the experimental error the crossing is not considered to be significant. It also follows that the amount of positively adsorb-

ed Ca^{2+} required to shift the p.z.c. is less than, say, 1 $\mu C\ cm^{-2}$. As will be shown in Chapter 5., for wet samples in the presence of $Ba(NO_3)_2$ restabilization of coagulated sols occurs at pH 7 and 8. This indicates super-equivalent adsorption of Ba^{2+} ($|\sigma_{Ba^{2+}}| > |\sigma_0|$). For the dry samples in the presence of (2–1) electrolytes no restabilization was found and, as fig. 4–14 shows, there is also no significant super-equivalent adsorption. The reason for this difference in behaviour of wet and dry samples is not known, but it supports the idea that for oxidic adsorbents the structure of the solid surface is an important parameter.

The (σ_0–pH) curves of fig. 4–14 and 4–15 and those of fig. 4–5 and 4–8 show some differences that are related to variations in pretreatment of the samples, in preparation of the sols and in the titration procedure. In particular, the difference in p.z.c. in the presence of K_2SO_4 between fig. 4–15 ($pH^0 \simeq 8$) and fig. 4–8 ($pH^0 \simeq 9.6$) is noteworthy. This also seems due to the use of dry and wet samples. For the (1–1) electrolytes studied the counter charge measurements on dry samples also indicated a lower pH^0 (7–8) than the potentiometric titrations on wet samples. Thus, drying shifts the p.z.c. towards somewhat lower pH^0 values for the (1–1) and (1–2) electrolytes but not for the (2–1) electrolytes. This is perhaps also due to surface structure effects.

The results of the surface and counter charge measurements for the (1–1) electrolytes studied, KCl and NaCl, are not shown here. The trends are the same as in figs. 4–14 and 4–15.

It is concluded that the ions studied do behave as (normal) counterions. The ligand exchange adsorption of SO_4^{2-} on hematite proposed by AYLMORE et al. (1967) was based upon the observation of almost complete irreversibility of the adsorption (with respect to concentration). In an attempt to clarify the reasons for the difference in opinion between these authors and the present one, the reversibility of the adsorption of Ca^{2+} and SO_4^{2-} was studied in a few experiments. In both cases full reversibility of the adsorption (with respect to pH) was found, as expected for counterions. It seems therefore that the difference in opinion is caused by conflicting experimental results.

4.5. CONCLUSIONS

The double layer properties of hematite show notable differences with preparation, pretreatment and type of electrolyte which are tentatively attributed to variations in surface structure. The (σ_0–pH) curves for hematite in the presence of alkali chlorides and alkaline earth nitrates exhibit some features also found with other oxides: they are more or less symmetrical with respect to the p.z.c., and the surface charge is of the order of tens of $\mu C\ cm^{-2}$. It was verified whether this could be attributed to penetration of potential-determining ions and coun-

terions into the solid, as has been reported for silica (TADROS and LYKLEMA 1968, 1969a) and glass (TADROS and LYKLEMA 1969b).

The high preferential adsorption of Li^+ and Mg^{2+} over the other alkali and alkaline earth ions, respectively, does suggest penetration of these ions. It was inferred that Li^+ and Mg^{2+} may adsorb in a *de*hydrated form in the octahedral positions of the solid, which would be compatible with the fact that the crystal ionic radii of these ions approximate to that of Fe^{3+}. The porous double layer theory (LYKLEMA 1968) gives reasonable agreement in this case. At low c_{salt} the high experimental differential capacities at the p.z.c. are consistent both with a slight penetration of counterions and, though less convincingly, with a high specific adsorption of both cations and anions. A quantitative treatment is impeded by the uncertainty with respect to the 'NERNST behaviour' of the surface potential and by lack of 'non-porous' double layer theories based upon plausible assumptions or amenable to experimental verification.

Besides the strong specific adsorption of Li^+ and Mg^{2+} at high c_{salt} the strong specific adsorption of bivalent ions over monovalent ions is notable. An interesting feature of this study is the shift in p.z.c. which is brought about by the strong specific adsorption. In the presence of (predominant) specific adsorption of cations or anions at the p.z.c., pH^0 shifts towards a lower or higher pH, respectively. These shifts are predicted by the ESIN-MARKOV coefficient which describes the change in pH with a change in c_{salt}, as a function of the charge compensation by cations and anions. In the cases where theoretical and experimental ESIN-MARKOV coefficients could be compared (at high surface charge) fair agreement was obtained. The counter charge measurements indicate that the surface charge-counter charge balance is obeyed well, provided that the presence of small amounts of K^+ and Ca^{2+} in the samples and the experimental error of ca. 0.5 $\mu C\ cm^{-2}$ are taken into account.

5. STABILITY MEASUREMENTS

5.1. INTRODUCTION

Besides being important from a practical point of view, measurements of the stability of colloidal dispersions against electrolyte provide useful information regarding the distribution of the counter charge. In the DLVO theory of the stability of lyophobic colloids (DERYAGIN and LANDAU 1941, VERWEY and OVERBEEK 1948) the repulsion is governed by the *diffuse double layer potential*, ψ_d, that is the potential in the outer HELMHOLTZ plane (cf. fig. 4–1). The theory provides a means of calculating this potential from the so-called *coagulation concentration*, that is the electrolyte concentration above which the sol is no longer stable. From ψ_d, σ_d can then be calculated as described in the preceding chapter and σ_m is obtained from the difference $\sigma_m = \sigma_0 - \sigma_d$.

The criterium chosen for stability is somewhat arbitrary and coagulation concentrations depend on the experimental procedure (LYKLEMA 1970). The simple *classical* method (KLOMPÉ 1941), whereby the degree of coagulation is determined at some fixed time after the addition of the coagulant, was used in this work. Since the time-scale involved is much larger than in the *kinetic* method (REERINK and OVERBEEK 1954), it is arguable that any parameters derived from the classical method (e.g. diffuse layer charge and potential) should be comparable to those from adsorption measurements (total charge and potential). The reproducibility is less than that for the kinetic method.

It is nevertheless satisfactory for our purpose since σ_d was found to be small as compared to σ_m and hence the error in σ_d is not critical.

5.2. CALCULATION OF ψ_d AND σ_d

The basis for the derivation of ψ_d from the coagulation concentration, c_c, has been given by VERWEY and OVERBEEK (1948). It was shown that c_c can be calculated if the assumption is made that, at the coagulation concentration, the maximum in the total interaction free energy between any two particles becomes zero. The interaction free energy, V_t is made up of the repulsive free energy, V_R, and the attractive free energy, V_A. The repulsive free energy is calculated from the GOUY-CHAPMAN theory and applies therefore to the diffuse part of the double layer. VERWEY and OVERBEEK (1948) considered the double layer to be completely diffuse and, consequently, the origin of the repulsive and attractive forces were taken to be the same. For these conditions the authors have given a

relation between ψ_0 and c_c. To find the relation between ψ_d and c_c the thickness of the STERN layer has to be taken into account as noted by VINCENT et al. (1971). These authors have calculated this relation for flat double layers as well as for spherical ones. In the latter case an approximative equation for V_A was used. It holds when the distance between the particles is very small compared to the particle radius. Since this is not a very good approximation (as noted by these authors) the complete HAMAKER equation will be used here.

For small interaction ($\varkappa d \geqslant$ ca. 2) the repulsive free energy, V_R, between the double layers of two spherical particles is (VERWEY and OVERBEEK, page 140):

$$V_R = \frac{8\,\varepsilon\,(kT)^2}{(ze)^2}\,\gamma^2 a \exp(-\varkappa d) \qquad (5-1)$$

where d is the distance between the outer HELMHOLTZ planes (OHP's) of the two interacting particles and:

$$\gamma = \tanh\left(\frac{ze\psi_d}{4kT}\right) \qquad (5-2)$$

Since for spherical particles under coagulation conditions $\varkappa d$ is somewhat less than 2 (see also section 5.4.) eqn. (5–1) is rather approximate. Eqn. (5–1) was derived with the assumption that the surface potential be constant. In view of the time-scale of our experiments this assumption should be valid. Moreover, FRENS (1968) has shown that it is irrelevant whether the potential or the charge is assumed to be constant as long as $\varkappa d > 0.5$. As can be seen from table 5–2 (page 90) this is always the case in the present study.

The expression for the attractive free energy of two spherical particles derived by HAMAKER (1937) is:

$$V_A = -\frac{A}{6}\left[\frac{2}{s^2-4} + \frac{2}{s^2} + \ln\frac{s^2-4}{s^2}\right] \qquad (5-3)$$

where A is the Hamaker constant, $s = R/a$ and R the distance between the centres of the particles. If Δ is the thickness of the STERN layer (from OHP to surface) $R = 2a + 2\Delta + d$.

Following VERWEY and OVERBEEK (1948) the coagulation conditions may be defined as:

$$V_R^{max} = -V_A^{max} \qquad (5-4)$$

$$\frac{dV_R^{max}}{dd} = -\frac{dV_A^{max}}{dd} \qquad (5-5)$$

where the superscript ^{max} refers to the distance at which $V_t = V_t^{max}$. Strictly speaking these conditions apply better to the kinetic method than to the classical

method. With the latter method there is plenty of time for interacting particles to overcome a small energy barrier. However, in practice (for AgI) the c_c values with this method as compared to the kinetic method are lower only by ca. 30% (LYKLEMA 1970). The ensuing difference in ψ_d is even less.

We now have 4 equations with 7 unknown quantities, viz. V_R, V_A, A, a, Δ, d and ψ_d. If some value can be assigned to A, a and Δ these equations may be solved for ψ_d. First the relation between s and $\varkappa$ under coagulation conditions can be obtained by combination of eqns. (5–4) and (5–5) and substitution of eqns. (5–1) and (5–3):

$$(\varkappa a)_{c_c} = 64\left[4\, s_{max}^5 - 24\, s_{max}^3 + 32\, s_{max} + (s_{max}^7 - 8\, s_{max}^5 + 16\, s_{max}^3) \ln \frac{s_{max}^2 - 4}{s_{max}^2}\right]^{-1} \qquad (5-6)$$

This relationship is plotted in fig. (5–1). Subsequently γ may be calculated from:

$$\gamma^2 = \frac{(ze)^2}{48\,\varepsilon\,(kT)^2} \cdot \frac{A \exp(\varkappa d)}{a}\left[\frac{2}{s_{max}^2 - 4} + \frac{2}{s_{max}^2} + \ln \frac{s_{max}^2 - 4}{s_{max}^2}\right] \qquad (5-7)$$

where $\dfrac{(ze)^2}{48\,\varepsilon\,(kT)^2} = 3.65 \times 10^4\ \mathrm{cm\,erg^{-1}}$ for (1–1) electrolytes at 20 °C. Finally, ψ_d is obtained from eqn. (5–2) and σ_d from eqn. (4–6).

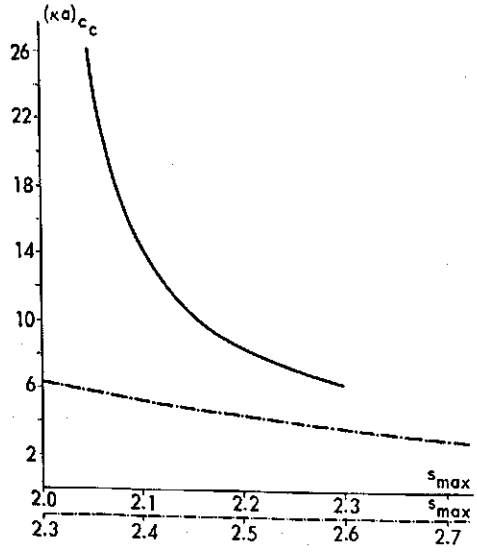

FIG. 5-1 Relation between $\varkappa a$ at the coagulation concentration and s_{max} as given by eqn. (5-6).

5.3. Experimental

The stability measurements were carried out in coagulation tubes. The tubes were cleaned with concentrated HCl (when contaminated with hematite) and chromic acid and then thoroughly rinsed with tap water and distilled water, respectively. Prior to the measurement, portions of dilute stock suspension (sol A, stored at pH 4) were brought to and equilibrated at the desired pH value. 2.5 ml of electrolyte solution plus distilled water were then mixed with 10 ml of sol in the coagulation tubes to give a final sol concentration of 2 mmole l^{-1}. The pH was subsequently readjusted with KOH or HNO_3. Measurements were taken after 24 hours. The coagulation concentration, c_c, was identified with the electrolyte concentration required to just produce a clear supernatant. Where restabilization was being studied the restabilization concentration was taken to be the electrolyte concentration above which a clear supernatant was no longer observed. The concentration decade ($10^{-x} - 10^{-(x+1)}$ N) in which c_c was found, was scanned in duplicate in 5 to 10 steps. The occurrence of restabilization was studied over the concentration range $10^{-7} - 10^{-1}$ N. The reproducibility was ca. 10%. The electrolytes studied were KNO_3, $Mg(NO_3)_2$, $Ba(NO_3)_2$, K_2SO_4 and sodium phosphate (pH range 4–11). The results for phosphate will be discussed in Chapter 6.

5.4. Results

5.4.1. *General considerations*

The coagulation concentrations are given in table 5–1 and fig. 5–2. For the sake of clarity the data are expressed in meq l^{-1} rather than mmole l^{-1}. The

Table 5-1. Coagulation concentration in meq l^{-1} for hematite (sol A, 2 mmoles l^{-1}) in the presence of the salts indicated.

	KNO_3	$Ba(NO_3)_2$		$Mg(NO_3)_2$		K_2SO_4
pH		1st	2nd	1st	2nd	
4	54	53		52		0.4
5	42	42		40		0.6
6	28	28		28		0.7
7	10	$<10^{-4}$	7	$<10^{-4}$	10	0.6
8	0.9	$<10^{-4}$	3.5	$<10^{-4}$	5	0.6
9	$<10^{-2}$	$<10^{-4}$		$<10^{-4}$		$<10^{-4}$
10	0.9	0.05				2
11	8.0	0.05				9

N.B. For the (1–2) and (2–1) electrolytes, c_c in meq $l^{-1} = 2\ c_c$ in mmole l^{-1}.
In the case of restabilization both the first (1st) and second (2nd) coagulation concentration have been reported.

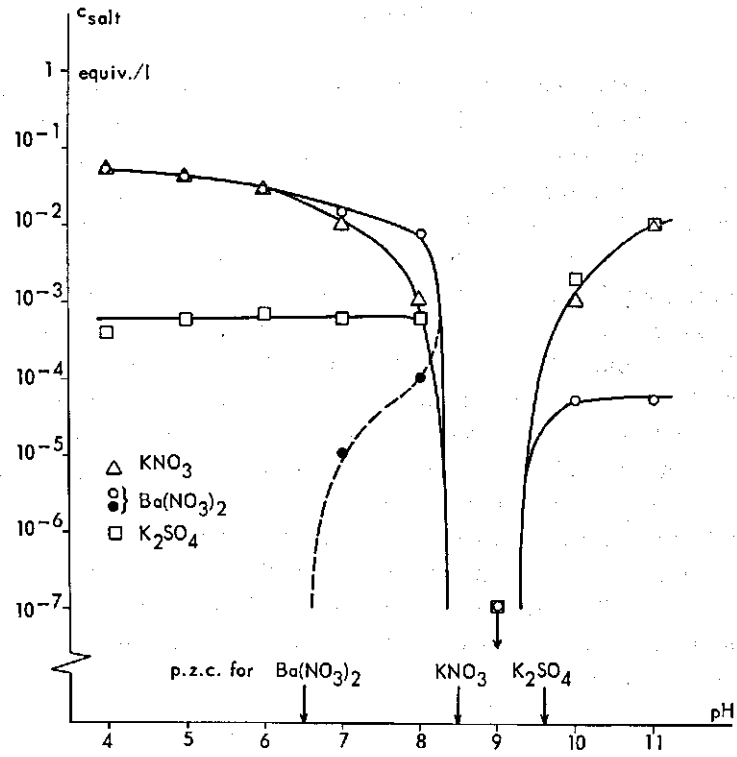

FIG. 5-2 Stability regions of hematite sol (sol A, 2 mmoles l^{-1}) in the presence of KNO_3, $Ba(NO_3)_2$ and K_2SO_4. Open and solid symbols indicate concentrations above which the sol is unstable and stable, respectively.

results for $Mg(NO_3)_2$ have not been included in the figure because they are very close to those for $Ba(NO_3)_2$.

The c_c's for KNO_3 are lower than those reported by DUMONT and WATILLON (1971). The differences increase from 50% at pH 4 to ca. 300% at pH 7. At pH 11 the difference is ca. 100%. DUMONT and WATILLON (1971) prepared their hematite by acid hydrolysis (section 2.2.) and used the kinetic method to study stability. The differences observed are therefore partly due to the analytical method. In addition, there is probably some influence of the sample. It is seen that at 'high' surface charge the effect of the co-ion vanishes, as anticipated. The values for c_c in KNO_3 and $Ba(NO_3)_2$ are identical at pH $\leqslant 6$ and for KNO_3 and K_2SO_4 at pH > 10. For KNO_3 the negative sol is less stable than the positive sol. This is contrary to what has been found for AgI. Furthermore, the bivalent counterions have c_c's considerably lower than the monovalent

ones. As the c_c values for $Ba(NO_3)_2$ are so low, the amount of p.d. ions can no longer be neglected. If the pH was increased with $Ba(OH)_2$ rather than with KOH, no stable sols could be made at all above pH 8. It follows again that Ba^{2+} ions are very strongly adsorbed.

The point of minimum stability ($\psi_d \simeq 0$) in the presence of KNO_3 approximately coincides with the p.z.c. This was corroborated by measurements of the settling time of the suspension in the titration vessel which was found to be minimal between pH 8.5 and 9.0. The coincidence of i.e.p. and p.z.c. is in accord with the absence of a shift in p.z.c. with changing c_{KNO_3} (unpublished results).

The most conspicuous feature of the stability measurements is the irregular coagulation series for the alkaline earth nitrates at pH 7 and 8. As can be seen from table 5–1 and figure 5–2, with $Ba(NO_3)_2$ the hematite is coagulated at very low concentrations, restabilized at 10^{-5} and 10^{-4} N (at pH 7 and 8, respectively) and recoagulated at 7×10^{-3} and 3.5×10^{-3} N. Provided that the p.z.c. has already shifted to its final value of about 6.5 in very dilute solutions, this phenomenon can be viewed as a reversal of charge due to super-equivalent adsorption of Ba^{2+} in the STERN layer.

It is notable that restabilization cannot be detected above pH 8.5, the p.z.c. in the absence of specific adsorption. In other words, we do not find a positive shift (i.e. towards a higher pH) of the i.e.p. This shift was expected because the p.z.c. showed a negative shift and i.e.p. and p.z.c. move into opposite directions. Indeed several workers (MODI and FUERSTENAU 1957, HEALY et al. 1968, WIESE et al. 1971) who used electrokinetic methods, have reported such a shift of the i.e.p. for oxides in the presence of (2–1) (MODI and FUERSTENAU 1957, HEALY et al. 1968) or (3–1) (WIESE et al. 1971) electrolytes.

It is suggested that this apparent discrepancy is due to the use of different experimental methods. It may be that restabilization is not observed at high pH due to the fact that the (high) electrolyte level, necessary to produce a sufficiently high STERN layer charge, at the same time prevents repeptization.

Finally, it may be noticed that no restabilization was found with SO_4^{2-}. In addition, the shift in p.z.c. was found to be lower than for Ba^{2+}, whereas the c_c for SO_4^{2-} is higher than for Ba^{2+}. All of this indicates that Ba^{2+}, and alkaline earth ions in general, are more strongly adsorbed than SO_4^{2-}.

5.4.2. *Distribution of counter charge over σ_d and σ_m*

It is evident from the foregoing section that in the presence of bivalent counterions the surface charge is (almost) fully compensated for in the non-diffuse part of the double layer. Below we shall deal with the distribution of the counter charge over σ_d and σ_m for monovalent counterions. The procedure is approximate because surface charges are compared with diffuse layer charges obtained

under different conditions. Moreover the calculation of σ_d requires a knowledge of the HAMAKER constant, the STERN layer thickness and the 'average' particle radius, all of which can only be assessed within certain limits. The outcome is nevertheless interesting.

First of all, ψ_d and σ_d were calculated for KNO_3 as outlined in section 5.2. According to FOWKES (1964) the HAMAKER constant, A, for hematite in water is 4.5×10^{-13} erg. This is perhaps an overestimation because according to the macroscopic theory, following NINHAM and PARSEGIAN (1970), the HAMAKER constant for water is closer to that of hematite than would seem from FOWKES' picture. The equivalent particle radius for sol A was calculated from $S = 3/\rho a$. Taking into account a surface area of the pores of 6 m^2g^{-1}, the outer area equals 26 m^2g^{-1}. This gives $a = 220$ Å. The thickness of the STERN layer, Δ, was taken to be 5 Å. This is perhaps the lower limit because in the presence of the (minimum) number of one water molecule between surface and counterion the sum of $r_{O^{2-}} + 2\,r_{water} + r_{ion}$ is even for K^+ and NO_3^- larger than 5 Å. However, in view of the uncertainties in the packing and in the surface roughness any further refinement is not considered. Furthermore it is not certain whether the same Δ for K^+ and NO_3^- may be used.

It is noted that because the values assigned to A and Δ are upper and lower limits, respectively, the values calculated for ψ_d are maximum values. On the other hand, the ψ_d's thus calculated are too low for the reasons discussed in section 5.2.

The surface charge corresponding to a given σ_d was established by interpolation of the (σ_0–pH) curves. To facilitate this procedure, σ_0 was replotted against c_{salt} at given pH on a semi-logarithmic scale.

The results are compiled in table 5–2. It is seen that for NO_3^-, $|\sigma_m/\sigma_0| \times 100$ increases from 82% in the vicinity of the p.z.c. to 92% at pH 4. For K^+ it is

TABLE 5-2. Distribution of the counter charge over σ_d and σ_m for hematite in the presence of KNO_3.

pH	c	$10^2\kappa$	d	ψ_d	σ_d	σ_m	$\left\|\frac{\sigma_m}{\sigma_0}\right\| \times 100$
	(mmole l^{-1})	$(Å)^{-1}$	(Å)	(mV)	($\mu C\ cm^{-2}$)		
4	54	7.58	7.2	23.8	1.45	17.9	92.5
5	42	6.70	10.2	22.8	1.22	12.7	91.2
6	28	5.47	13.7	21.2	0.95	7.4	88.7
7	10	3.27	44.6	16.5	0.50	3.5	87.5
8	0.9	0.98	303	4.6	0.11	0.5	81.7
10	0.9	0.98	303	4.6	0.11	2.2	95.2
11	8	2.93	52.7	13.6	0.40	7.1	94.7

already ca. 95% close to the p.z.c., indicating that K^+ is somewhat more strongly adsorbed than NO_3^-. It is evident that under coagulation conditions even the monovalent counterions, irrespective of sign, are primarily situated in the non-diffuse part of the double layer. The uncertainties in the calculations do not detract from this conclusion. If follows that the conclusion arrived at in the previous chapter, that the counterions are highly specifically adsorbed and/or penetrating into the solid, is corroborated by these results. It may also be concluded that the high values of σ_m/σ_0 relative to those for AgI (VINCENT et al. 1971) may be expected to be another characteristic for oxides.

6. PHOSPHATE ADSORPTION ON HEMATITE

6.1. INTRODUCTION

The adsorption of phosphate on hematite deserves special treatment as a separate chapter because the nature of the adsorption process differs in principle from that for the anions and cations considered in the preceding chapters. As will be shown there are indications that phosphate ions may exchange with surface ions. Depending on pH, the phosphate ion itself may thus act as a potential-determining ion. Therefore (σ_0–pH) curves as such do not provide decisive information about the phosphate adsorption. Direct adsorption measurements are required instead. Stability measurements on the other hand retain their value and indeed may become even more valuable. Before considering these experiments a short discussion will be given of the phosphate adsorption mechanisms envisaged by other workers and of one which results from this study.

6.2. MODELS FOR THE ADSORPTION MECHANISM

6.2.1. *Earlier models*

In dilute solutions (concentration $<$ ca. 10^{-3} M), phosphate ions (OLSEN and WATANABE 1957, RENNIE and MCKERCHER 1959, BACHE 1964, HSU 1964, DE HAAN 1965, MULJADI et al. 1966, HINGSTON et al. 1967, 1968 and 1970) and other weak acid anions, e.g. molybdate (REISENAUER et al. 1962, REYES and JURINAK 1967) borate (SIMS and BINGHAM 1968) and silicate (HINGSTON et al. 1967, 1968 and 1970), are generally considered to be adsorbed by (iron) oxides and clay minerals *via* a chemisorption process. In this concentration region most authors have found their adsorption data to conform to normal (OLSEN and WATANABE 1957, RENNIE and MCKERCHER 1959, HSU 1964, HINGSTON et al. 1967, 1968 and 1970 REYES and JURINAK 1967) or composite (DE HAAN 1965, MULJADI et al. 1966) LANGMUIR isotherms. However, when the adsorption measurements were extended up to intermediate concentrations (between ca. 10^{-3} and 10^{-1} M) no saturation was usually attained. Instead a linear (MULJADI et al. 1966) or FREUNDLICH-type (OLSEN and WATANABE 1957, BACHE 1964, REISENAUER et al. 1962) isotherm was obtained. This has led to the postulate that other sorption mechanisms, such as precipitation (BACHE 1964) and penetration into an amorphous region of the solid (MULJADI et al. 1966) may be operative. Finally, at very high concentrations ($>$ 10^{-1} M) decomposition of

the oxide and subsequent precipitation of (iron) phosphates have been clearly demonstrated (see Chapter 1.).

As to the nature of the chemisorption process at low concentrations little is known. It is generally held that it involves exchange of phosphate ions with surface groups, but which groups are taking part and how this process depends upon the pH is not well established. MULJADI, POSNER and QUIRK (1966) have postulated the following reaction with Al-OH groups of hydrous aluminium oxides and of (the edges of) clay minerals:

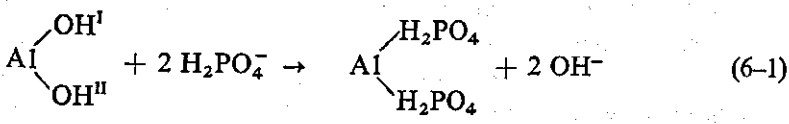

(6–1)

The two hydroxyl groups -OH^{I} and -OH^{II} are thought to represent two different LANGMUIR adsorption sites with a distinct difference in adsorption energy. Below a concentration of, say, 10^{-4} M the first hydroxyl group is taken to be completely exchanged whereas exchange of the second type of -OH group is said to be accompanied by surface penetration. Above ca. 10^{-2} M only penetration would occur. This splitting of the adsorption isotherm is speculative and not supported by other measurements. Moreover, in addition to Al-$(OH)_2$ groups other groups occur, probably more frequently, e.g. Al-OH and Al-OH_2^+ (at low pH). Furthermore, there is no evidence at present that the $H_2PO_4^-$ ion does adsorb and the HPO_4^{2-} ion does not.

In later publications, HINGSTON et al. (1967, 1968 and 1970) discussed the exchange reactions further. They determined the adsorption on goethite and gibbsite of i.a. phosphates, selenite and silicate. The concentrations are not explicitly given but are probably below 10^{-3} M. Anyhow, according to the authors the LANGMUIR equation describes their data satisfactorily. Their interpretation is based upon a plot of the adsorption maxima against the pH. These plots show humps and breaks for mono- and polybasic acids, respectively, at pH = pK. It is not easy to see how the authors explain this result. The essential feature appears to be that phosphate adsorbs by exchange against -OH_2^+ groups formed from -OH groups, not only by adsorption of protons from the solution, but also directly by proton transfer from one of the phosphate ions, namely the conjugate acid of the anion. The authors state that proton release from the acid is at a maximum at pH = pK and this would explain the hump or break. For phosphate adsorption on iron oxides at intermediate pH this 'proton-mediated' mechanism may be schematically depicted by:

$$FeOH + H_2PO_4^- \leftrightarrows FeOH_2^+ + HPO_4^{2-} \leftrightarrows FeHPO_4^- + H_2O \qquad (6\text{–}2)$$

The overall reaction is between $H_2PO_4^-$ and hematite. Since the concentration of $H_2PO_4^-$ increases monotonically on lowering the pH one would also expect a

continuous, rather than an irregular, increase of the phosphate adsorption in this direction. In our opinion, reaction (6–2) is nevertheless of interest because it illustrates that the buffer mechanism can play a role *via* the kinetics of the adsorption process. If reaction (6–2) is true then the rate of adsorption depends upon the concentrations of both phosphate ions. In other words, the hump or break around pH = pK might be inherent to a non-equilibrium situation.

The break around pH = pK in the curves of the adsorbed amount against pH was not found by HUANG (1971) in a study of the phosphate adsorption on γ-Al_2O_3 (direct measurements). The phosphate adsorption model given by this author is entirely different from the ones discussed above because it presumes release of H^+ ions instead of OH^- ions or H_2O molecules. However, on closer inspection this model seems to be based upon a faulty interpretation of experimental results. The potentiometric titration technique was used to measure the adsorption of phosphate indirectly from the shift in pH with increasing phosphate concentration. The decrease in pH upon addition of phosphate to the oxide suspension in the absence of acid or base was tacitly taken to be caused by release of H^+ ions. If the author had compared the pH of the suspension with that of a blank (phosphate solution of the same concentration as in the suspension) he might have noticed that the initial pH is highest for the suspension. Thus the experiments of HUANG also indicate release of OH^- ions rather than of H^+ ions.

A significantly different point of view with respect to the phosphate adsorption mechanism has been proposed by JACOBS (1968). He suggested that phosphate adsorption occurs by hydrogen bonding to surface $-OH_2^+$ and -OH groups because the heat of phosphate adsorption (at pH 4.6) is of the same order as the heat of formation of a hydrogen bond.

6.2.2. *Present model*

The above discussion illustrates the lack of agreement, as well as the lack of information, regarding the phosphate adsorption mechanism. This is not surprising in view of the complexity of the situation. Amongst the many problems, one would mention the distinction between physical, chemical and other sorption mechanisms, the occurrence of different phosphate species as a function of pH, the possible shift in the dissociation equilibria at the surface and the rate and reversibility of the adsorption processes. In the present study of phosphate adsorption on hematite we had to confine ourselves to a limited number of techniques in an attempt to elucidate the problem.

Below a simple model for the adsorption mechanism is described that satisfactorily served as a working-hypothesis in this study. It should however be emphasized that more work is needed to verify the model.

In the pH range studied (pH 4–11) phosphate occurs in solution as the

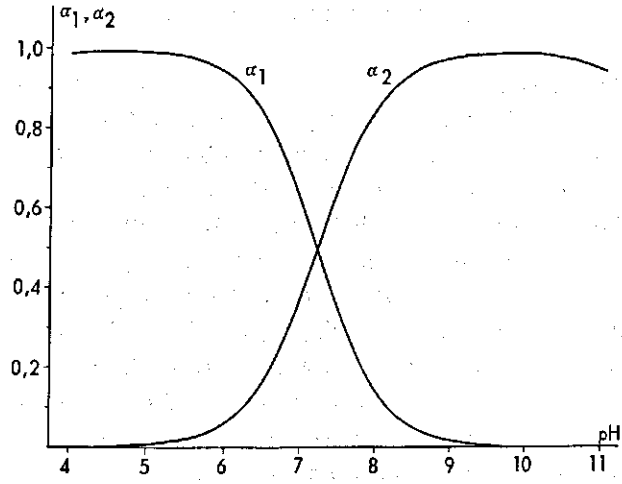

FIG. 6-1 Fractions of total phosphate of monovalent (α_1) and bivalent (α_2) phosphate ions as a function of pH. The pK values used are pK_1 = 2.13, pK_2 = 7.21 and pK_3 = 12.32.

$H_2PO_4^-$ and/or the HPO_4^{2-} ion as can be seen in fig. 6–1 (calculated with pK_1 = 2.13, pK_2 = 7.21 and pK_3 = 12.32 (KNCV 1962), cf. DE HAAN (1965) and VAN DEN HUL (1966). We have therefore restricted ourselves to possible overall reactions between hematite and these two phosphate species only. It is assumed that on the surface of hematite -OH_2^+, -OH and -O^- groups occur, the relative amounts of which depend upon the pH. It is likely that the affinity of these groups for phosphate decreases in the order given. On this basis the following reactions can be envisaged:

$$FeOH_2^+ + H_2PO_4^- \leftrightarrows FeH_2PO_4 + H_2O \quad (1)$$
$$FeOH_2^+ + HPO_4^{2-} \leftrightarrows FeHPO_4^- + H_2O \quad (2)$$
$$FeOH + H_2PO_4^- \leftrightarrows FeH_2PO_4 + OH^- \quad (3)$$
$$FeOH + HPO_4^{2-} \leftrightarrows FeHPO_4^- + OH^- \quad (4)$$
$$FeO^- + H_2PO_4^- \leftrightarrows FeHPO_4^- + OH^- \quad (5)$$
$$FeO^- + HPO_4^{2-} \leftrightarrows FePO_4^{2-} + OH^- \quad (6)$$

In the next sections we shall discuss the consequences of this model with respect to phosphate adsorption, stoichiometry of the exchange equations and colloidal stability. To study possible changes in the sorption mechanism with the phosphate concentration, adsorption experiments have been performed covering the range of dilute to moderate concentrations ($0–7\times10^{-3}$ M).

6.3. Adsorption isotherms

6.3.1. *Experimental*

The phosphate adsorption measurements have been carried out with the specially prepared sol D ($S_{BET} = 21$ m^2g^{-1}). An aliquot of this sol containing ca. 1.5 g of hematite was added to a 50 ml glass bottle. The volume was made up to 35 ml, the pH adjusted with KOH or HNO_3 and the suspension left overnight. Then 5 ml of a known NaH_2PO_4 or Na_2HPO_4 solution (at pH 4–7 and 7–11, respectively) were added to give an initial concentration of phosphate of 0.3–9 mmoles l^{-1}. The pH was readjusted directly after the addition of phosphate, and again after 30 and 120 minutes. The pH measurements were carried out with a combined glass-calomel electrode (Electrofact 7 Gr 111) and a Knick pH meter. The dispersions were stirred during the measurement of the pH and then placed in a thermostat bath at 20.0 $\pm$ 0.5 °C. After 3 hours the dispersions were filtered through a 0.1 μm Sartorius membrane filter and the first 5 ml of filtrate (in which the concentration of phosphate was not yet constant) were discarded.

The concentration of phosphate, c_p, in the filtrate was determined by the molybdenum blue method using hydrazine sulphate as the reducing agent (Charlot and Bézier 1957). The reagents were:

A. 10.75 g of $(NH_4)_6Mo_7O_{24}.4H_2O$ dissolved in 170 ml of 36 N H_2SO_4 and made up to 500 ml

B. 0.75 g of $(NH_2)_2H_2SO_4$ dissolved in 500 ml water (freshly prepared each week).

Standard series with $c_p = 0–4 \times 10^{-5}$ M were prepared by addition of 4 ml of reagent A and 3 ml of B to a known amount of phosphate in 50 ml flasks. The solutions were made up to volume with water and heated on a (boiling) water-bath for 10 minutes. After cooling to ambient temperature the optical density was measured at 830 nm using a Unicam SP 600 spectrophotometer. The unknown solution was similarly treated after appropriate dilution.

The adsorption of phosphate was calculated from the difference between the initial and final c_p. The accuracy was 5–10%.

The amount of acid required to keep the pH constant during adsorption of phosphate was measured in separate experiments in which the pH of the phosphate solution had been adjusted prior to use. To exclude CO_2 the measurements at pH 4–9 were performed in the titration cell described in section 3.3.2. In addition some experiments at pH 4 and 7 were carried out in glass bottles. The duration of the adsorption was limited to 10 minutes to minimize the acid consumption by the hematite dispersion itself. (There is always a drift in the pH of a hematite suspension, the magnitude being dependent upon the pretreatment. The drift during 10 minutes was negligible).

6.3.2. *Results and discussion*

The adsorption isotherms obtained are shown in fig. 6–2. Before discussing them in detail something should be said about the rate and reversibility of the adsorption process. The rate of adsorption is high in the initial stages of the process but decreases in the later stages. In fact, the slow adsorption continues, at least for many weeks. The initial rate of desorption is also fast whereas the final desorption is either slow or does not occur at all. This can be seen from fig. 6–2 by comparing the adsorption isotherm, obtained after 3 hours of adsorption at pH 4 followed by 2 hours of desorption at pH 11, with the normal isotherm at pH 11. These facts suggest the presence of a considerable energy of activation which is indicative for chemisorption.

It is clear that the isotherms in fig. 6–2 present a 'snapshot picture' because the adsorption is not yet complete. Some changes in the position of the isotherms relative to each other can therefore not be precluded. However, some preliminary experiments showed that drastic changes with time do not occur.

The adsorption isotherms are of the 'high-affinity' type. The affinity – as judged from the length of the vertical part – increases with decreasing pH. The isotherms leave the ordinate axis far below saturation. (Taking an area of 21.6 Å^2 per phosphate ion (JURINAK 1966) the saturation value would amount to

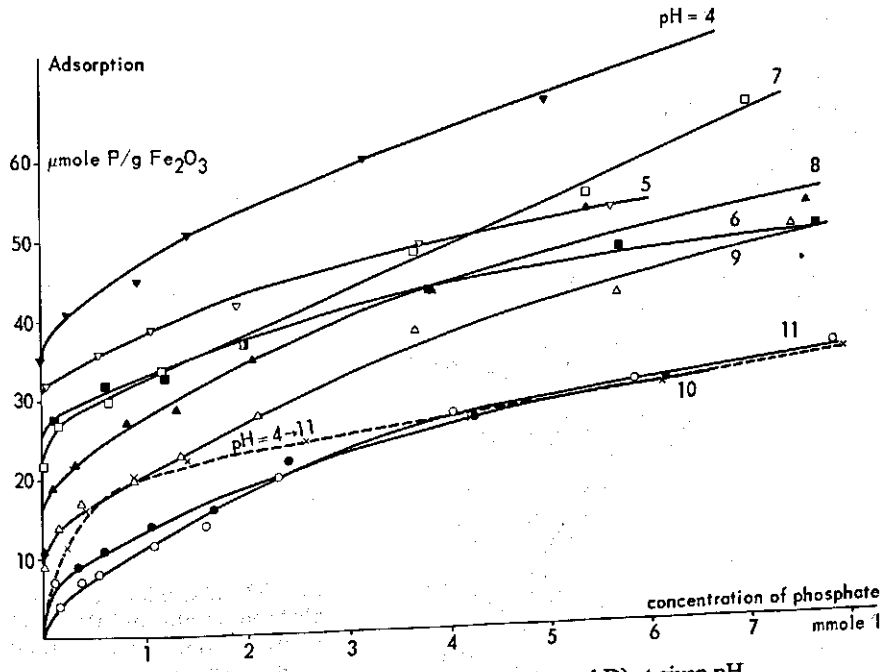

FIG. 6-2 Adsorption isotherms of phosphate on hematite (sol D) at given pH.

161 μmol g^{-1}). Obviously the surface groups with a high affinity for phosphate are already exhausted at low c_p ($<10^{-4}$ M). At higher concentrations the adsorption does not level off to a plateau as required in LANGMUIR adsorption but continues to increase with concentration. The highest surface occupancies attained (c_p high, pH 4 or 7) are still $<50\%$ of the available surface area. Therefore, interpretation in terms of even a modified LANGMUIR adsorption is dangerous.

Regarding the influence of the pH it is noticeable that there is also adsorption of phosphate above pH 8.5, that is above the p.z.c. in absence of specific adsorption. Even at pH 10 and 11 significant adsorption occurs showing that, in this respect also, phosphate behaves differently from the anions studied before. In terms of the proposed adsorption model it indicates exchange with -OH and/or $-O^-$ groups. To study the influence of pH in more detail it is expedient to replot the data of fig. 6–2 in the manner shown in fig. 6–3. It is seen that the adsorption generally increases with decreasing pH. This is a logical feature in view of the increase in the number of $-OH_2^+$ groups (or, more properly, of the ratio $-OH_2^+/-OH$).

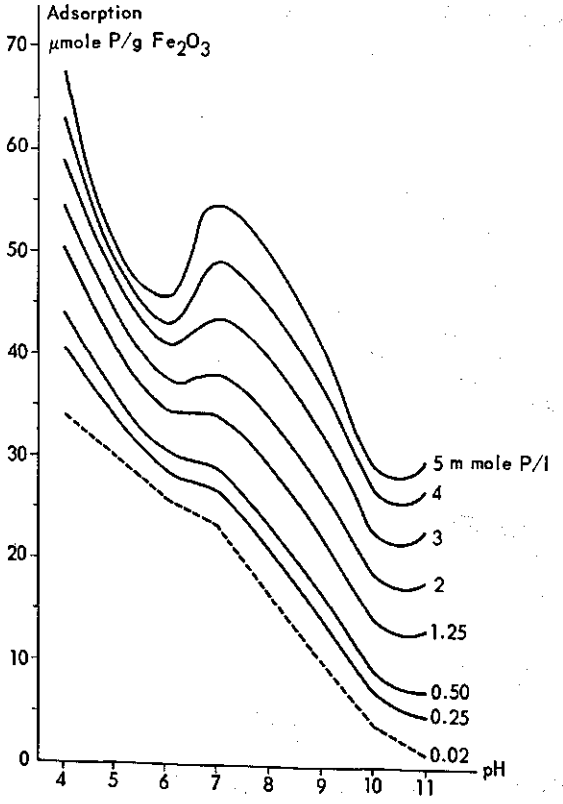

FIG. 6-3 Adsorption of phosphate on hematite (sol D). Effect of pH at various concentrations of phosphate (cross-sections of fig. 3).

In addition to this general trend, the adsorption–pH curves exhibit a break at low c_p which develops into a hump at higher c_p. It is striking that this break or hump occurs around pH = pK_2, in agreement with the results of HINGSTON et al. (1967, 1968 and 1970). Moreover, the shape of the curves at high pH suggests a similar feature at pH = pK_3. That the break and humps occur at the same pH suggests that there is no difference in adsorption mechanism for dilute solutions (2×10^{-5} M) and solutions at intermediate concentrations ($1–5 \times 10^{-3}$ M). As noted before, the occurrence of breaks and humps may be inherent to the quasi-equilibrium character of the phosphate adsorption but this needs further experimental verification. At any rate, other processes such as incipient precipitation of iron phosphate compounds at the surface and surface-induced dimerisation or polymerisation cannot be as readily correlated with the pK values.

Further information concerning the adsorption mechanism comes from the study of the amount of acid required to keep the pH constant during adsorption of phosphate. The ratio, R, of this amount to the amount of phosphate adsorbed is plotted against the pH in fig. 6–4. The values at pH 4 and 7 were obtained with "wet" samples. They are average values from five observations. The standard deviation of the average is shown in the figure. The other data were obtained from duplicate experiments with dried samples of sol A and the standard deviation is considerably larger (see fig. 6–4).

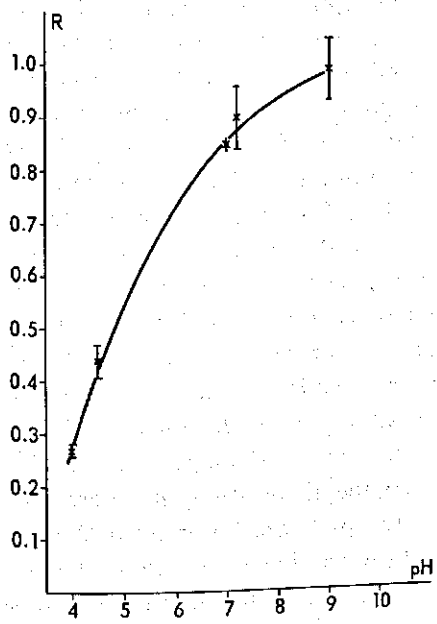

FIG. 6-4 Ratio R in mole/mole of the amount of acid, which is required to keep pH constant during the adsorption of phosphate on hematite, and the amount of phosphate adsorbed.

The general trends are clear. First of all, it is noticeable that there is no hump present around pH = pK_2, indicating that the adsorption process at this pH does not deviate from that at other pH values. Moreover, it was also found that R is independent of c_p over the concentration range studied (up to 2 mmoles l^{-1}). This suggests again that also the adsorption mechanisms at high and low c_p are the same. Finally, the magnitude of R, as well as its relation to pH, is satisfactorily explained by the proposed adsorption reactions. According to reactions (1) to (6), H_2O molecules are released from positive surface groups and OH^- ions from uncharged or negative groups. This means that R should decrease with pH from 1 at the (normal) p.z.c. to 0 at the completely positively charged surface. This trend is observed closely in the experiments. It is realized that the experimental R is affected by shifts in the phosphate equilibria. These shifts may be caused by a change in the (intrinsic) pK upon adsorption or by preferential adsorption of one of the phosphate species. However, both effects appear to be unlikely. Firstly, potentiometric titrations of hematite dispersions in the presence of phosphate showed that the pK_2 of the adsorbed phosphate was essentially the same as that in the solution. Secondly, the continuous and c_p-independent variation of R with pH seems to argue against the possibility of a shift in the phosphate equilibria. Finally, not only the R values but also the results of the stability experiments support the idea that no major changes take place in the degree of dissociation. It is thus concluded that the gradual shift from reaction (1) to (4) for pH 4 to 9 is supported by the measurement of R.

An interesting feature of the phosphate adsorption on hematite and other oxide surfaces is that under special conditions the phosphate ion itself becomes a p.d. ion because it is bound to the surface and affects its charge. See reactions (1), (2), (4) and (6). This is supported by measurements of the phosphate adsorption as a function of the concentration of indifferent electrolyte. These measurements have been carried out with sol A and KCl. The results are given in table 6–1 along with the concomitant R values. It is seen that the adsorption of phosphate increases with increasing c_{KCl}, especially at pH 7.2 and 9.0. This is characteristic for p.d. ions and is due to screening of the negatively charged phosphate groups at the surface. (The stability experiments indicate that under the stated experimental conditions the (surface) charge is also negative at pH 7.2). The effect cannot be explained in terms of mass law equations. It can also be seen from table 6–1 that, apart from a slight increase of R from 0 to 10^{-3} M KCl, R decreases with increasing c_{KCl} over the entire pH range studied. This cannot be ascribed to the influence of c_{salt} upon the dissociation. In the presence of the highest concentration of KCl used the pK's are lower by 0.22 units (PARSONS 1959). As can be seen from fig. 6–1 this would alter the ratio $H_2PO_4^-/HPO_4^{2-}$ at pH 7.2 but not at pH 4.5 and 9.0, whereas R changes irrespective of

TABLE 6-1. Phosphate adsorption (P_{ads}) and R values for sol A as a function of c_{KCl} and pH. The initial c_p was 2 mmoles l^{-1}.

c_{KCl}	pH 4.5			pH 7.2			pH 9.0		
	c_p (mmole l^{-1})	P_{ads} (μmole g^{-1})	R	c_p (mmole l^{-1})	P_{ads} (μmole g^{-1})	R	c_p (mmole l^{-1})	P_{ads} (μmole g^{-1})	R
0	0.98	51	0.44	1.25	37.5	0.90	1.45	27.5	0.99
10^{-3}	1.00	50	0.41	1.25	37.5	0.95	1.47	26.5	1.13
10^{-2}	0.98	51	0.16	1.05	47.5	0.57	1.45	27.5	1.07
10^{-1}	0.92	54	–0.08(?)	0.95	52.5	0.34	1.26	37.0	0.75

pH. It has been suggested previously (BREEUWSMA and LYKLEMA 1973) that this change could be due to increased dissociation of the negatively charged phosphate groups at the surface. However, this would imply that in the absence of indifferent electrolyte the dissociation would be suppressed, whereas it was demonstrated above that there is no significant difference between the degree of dissociation at the surface and in the bulk of the solution. The decrease of R with c_{salt} at low pH can be qualitatively understood as being due to the (normal) increase in the number of positive surface groups ($-OH_2^+$) leading to increased adsorption according to (1) rather than (3).

6.4. STABILITY MEASUREMENTS

The experimental method for the stability experiments has been described in section 5.3. The coagulation and restabilization concentrations are summarized in table 6–2 and the stability regions, determined by the c_p and pH for which the sol is stable, are shown in fig. 6–5.

In very dilute solutions ($<10^{-5}$ M) the sol is only coagulated around pH 8.5, that is the p.z.c. in the absence of specific adsorption. Obviously, the adsorption of phosphate is insufficiently high to cause coagulation and/or restabilization. The first coagulation concentration in the pH range 6–8 is exceedingly low (ca. 10^{-4} M) and increases below pH 6 to only ca. 10^{-4} M at pH 4. In other words, phosphate is under these conditions a very effective coagulant for hematite. It can, on the other hand, also act as a powerful stabilizer. In the first place, phosphate markedly increases the stability of the hematite sol above pH 8.5, as can be seen from a comparison of the c_c values with those for KNO_3

TABLE 6-2. Coagulation (c_c) and restabilization (c_{rest}) concentrations for hematite (sol A) in the presence of phosphate.

pH	1st c_c	c_{rest}	2nd c_c
	(mmole l^{-1})		
4	0.16		
5	0.033		
6	0.013	3.3	33
7	0.010	0.023	30
8	0.016	0.030	23
8.5	<0.0003	0.023	
9	20		
10	20		
11	20		

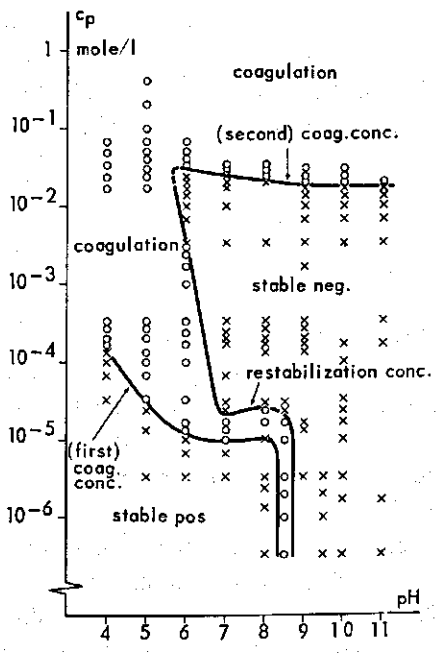

FIG. 6-5 Stability regions of hematite sol (sol A, 2 mmoles l^{-1}) in the presence of phosphate. Open points and crosses indicate unstable and stable sols, respectively.

and K_2SO_4 at the same pH (table 5–1). Secondly, the hematite sol is readily (re)stabilized (especially between pH 7 and 8.5), and the second coagulation concentration is again higher than that in the presence of KNO_3 (and K_2SO_4).

These facts are in general agreement with the proposed adsorption mechanism. The increased stability above pH 8.5 can be ascribed to reactions (4) and (6). In terms of the proposed model the restabilization is essentially due to the adsorption of bivalent phosphate. According to reactions (2) and (4) this bivalent phosphate is able to reverse the charge and hence to restabilize the sol. As long as more than about 40% of the phosphate ions is present in the bivalent form (pH 7–8.5) restabilization occurs at the very low concentration of $2-3 \times 10^{-5}$ M. With increasing ratio of monovalent to bivalent phosphate the restabilization concentration rapidly increases until no further restabilization occurs at a pH where practically all the phosphate is monovalent (see fig. 6–1). This is in agreement with the fact that according to reactions (1) and (3) no reversal of charge takes place with monovalent phosphate.

The reversal of (the diffuse layer) charge between pH 6 and 8.5 implies that the i.e.p. ($\psi_d \simeq 0$) has shifted towards a lower pH. It was pointed out in Chapters 4. and 5. that such a shift was to be expected in the case of specific adsorption of anions at the p.z.c. It may now be added that the same holds true when the anions become incorporated in the surface since, in this respect, it is immaterial whether the sign of ψ_d is determined by the surface charge or by the counter

charge in the STERN layer. In other words, the shift of the i.e.p., in contrast to that of the p.z.c., is not a characteristic for either counterion or p.d. ion behaviour. That phosphate does give rise to a shift of the i.e.p., whereas the alkaline earth ions do not, emphasizes the exceptionally strong adsorption of phosphate ions at the hematite surface.

6.5. CONCLUSIONS

The essential features of the proposed adsorption mechanism are

1. exchange of phosphate ions against $-OH_2^+$ and $-OH^-$ groups at the surface
2. no major changes in the dissociation equilibria of phosphoric acid upon adsorption.

The results reported above generally support this model. A notable exception is the influence of the concentration of indifferent electrolyte on the R values at high pH. There are no indications for the occurrence of more than one adsorption mechanism in the concentration range studied (c_p : 0 – 7 mmoles l^{-1}).

Further investigations are needed to clarify the roles of time and of indifferent electrolytes. It is of special interest to establish whether or not the hump at pH = pK_2 reflects quasi-equilibrium conditions.

SUMMARY

This study is primarily intended to provide a better understanding of the adsorption of ions on hematite (α-Fe_2O_3). In addition, due attention is given to the relation between the ionic adsorption and the colloidal stability of hematite sols.

Chapter 1. is concerned with the motivation and outline of the present study. The role of iron oxides in soils is discussed as an example of the practical importance of these materials. Several important plant nutrients (e.g. N, S, P, Mo and B) may be adsorbed on iron oxides in anionic form. Furthermore, the adsorption of cations by the soil and also the soil structure may be directly or indirectly affected by the iron oxides. When this study was started only a few fundamental colloid-chemical studies had been made on the iron oxide system. In particular, studies were lacking in which both the adsorption of ions and the colloidal stability had been discussed. Such investigations had been made, for example with silver iodide, and these studies served as a model for the present one. Hematite was chosen to represent the group of iron oxides because it plays an important role in (lateritic) soils and because it can be readily identified and also prepared and handled as a sol.

Chapter 2. deals with the preparation of the samples and their characterization, with special emphasis on the surface properties. A reasonably fast method was developed for the preparation of hematite. The samples contained little or none of the other forms of iron oxides but did contain traces of (strongly adsorbed) Ca^{2+} and Mg^{2+} ions. The electron micrographs indicated more or less globular particles with diameters between 400 and 700 Å. The specific surface area was determined with the BET method using a continuous flow technique and N_2 as adsorbate. Efforts to measure the surface area also by the negative adsorption method (at pH 4 with Ca^{2+} as co-ion) encountered serious practical problems. In particular the release of Ca^{2+} ions by the samples hampered the measurements. By using Ca^{45} this difficulty was largely overcome. The negative adsorption area was lower than the BET area, suggesting some degree of porosity.

Evidence for surface porosity was also obtained from N_2 adsorption data measured by the static method. The adsorption isotherm exhibits a hysteresis loop. It is a type IV isotherm implying that the pores have a width between 20 and 200 Å. Porosity is also evident, although less clearly, from the *t*-plot method. A quantitative estimate of the degree of porosity from the *t*-plot method is not possible (as yet) because of the lack of standard data for non-porous hematite.

Thermogravimetric data indirectly revealed that the surface layers of the hematite particles are hydrated or, more precisely, hydroxylated.

Measurements and calculations of the surface charge (due to adsorption of potential-determining ions) and of the counter charge (due to the distribution of indifferent ions), as a function of pH and salt concentration are described in Chapter 3. The surface charge, σ_0, was determined by potentiometric acid-base titrations. Preliminary measurements had indicated that the system could only be kept free of CO_2 by means of a gas-tight cell with a controlled N_2 atmosphere. The pH was measured with a glass electrode. A reference calomel electrode was connected with the solution (or the sol) in the titration vessel by means of a salt bridge. This construction led to fewer practical problems than the use of a 'VAN LAAR bridge' and the direct insertion of the calomel electrode in the solution. The fact that, using this device, the suspension effect does not interfere with the measurement of pH was of minor importance in this study.

The standard titration procedure used was a fast acid titration from pH 10 to 4. The 'wet' samples (always kept in contact with solution) were equilibrated at pH 10 before each titration. The amount of acid adsorbed during the slow adsorption step following the initial fast process did not amount to more than 20% of the total adsorption. The reproducibility was about 3 %.

The point of zero charge (p.z.c.) was determined from the intersection point of the (σ_0–pH) curves at different salt concentrations. To check the p.z.c.'s obtained in this way, the 'addition method' was also employed, i.e. the change in pH caused by the addition of (dried) hematite was recorded. Good agreement was obtained for the (2–1) electrolytes. For the other electrolytes studied the addition method gave lower values, possibly due to the drying of the samples.

At the end of Chapter 3. it is described how for some electrolytes both the surface charge and the counter charge have been measured under the same conditions.

The results and discussion of the surface charge and counter charge measurements are given in Chapter 4. The electrolytes studied were the chlorides of Li^+, K^+ and Cs^+, the nitrates of Mg^{2+}, Ca^{2+}, Sr^{2+} and Ba^{2+}, and K_2SO_4. The (σ_0–pH) curves on hematite resemble those on other (iron) oxides. The curves are generally convex with respect to the pH axis and the surface charge attains much higher values (several tens of $\mu C\ cm^{-2}$) than on, for example, silver iodide and mercury. The very high surface charge values for precipitated silica and for glass reported by other workers have been attributed to penetration into the solid by the potential-determining ions as well as by the counterions. It was therefore checked whether this was also the case for hematite.

The results for Li^+ and Mg^{2+} at high salt concentration do indeed point in this direction. Under these conditions both ions are strongly preferentially adsorbed compared to the other alkali or alkaline earth ions. This is presumably

related to the fact that of the cations studied only Li^+ and Mg^{2+} fit in the octahedral holes of the hematite lattice. Finally, it appears that the (σ_0–pH) curves for Li^+ and Mg^{2+} are fairly well described by the porous double layer theory of LYKLEMA. For the other ions the indications for porosity are less clear. However, on the basis of the current double layer models for oxides it is equally impossible to demonstrate that the (σ_0–pH) curves should be explained *without* assuming penetration.

A conspicuous feature of the (σ_0–pH) curves is the fact that the p.z.c. shifts due to the presence of certain electrolytes. This phenomenon has hitherto not been described for oxides. In the presence of KCl the p.z.c. occurs at pH 8.5. In the presence of LiCl and the alkaline earth nitrates a shift of the p.z.c. towards lower pH values was found. In contrast to this, the p.z.c. shifted towards a higher pH in the presence of K_2SO_4. These shifts are the result of (specific) adsorption of cations and anions, respectively, at the p.z.c. The direction in which the p.z.c. shifts was found to be in accordance with the thermodynamically derived ESIN-MARKOV coefficient. When verifiable, namely at high surface charge, fair quantitative agreement was also found between the theoretical and experimental values for this coefficient.

The measurements of the surface charge and the counter charge under the same conditions gave the expected results regarding both the distribution of the counter charge over cations and anions and the surface charge-counter charge balance.

Chapter 5. deals with the method and results of the stability experiments. The classical method of visually determining the coagulation concentration in a series of coagulation tubes was applied. The diffuse double layer potential was calculated from the coagulation value using the DLVO theory for spherical particles. The diffuse layer charge was then calculated and, by substraction of this charge from the surface charge, the charge in the STERN layer (and/or the solid phase) was obtained.

It is shown that the monovalent cations and anions in the double layer are for the greater part (more than 85% under coagulation conditions) located in the STERN layer and/or the solid phase. For the alkaline earth ions (and presumably also for the sulfate ion) this percentage rises to virtually 100% as is apparent from the instability of the hematite sol when these ions are present as counterions. With the alkaline earth ions reversal of charge occurs between pH 8.5 and pH 6.5. The expected shift in the iso-electric point towards a higher pH was not observed, possibly because the stability measurements were not sensitive enough in this respect.

It appears that with the electrolytes discussed so far the ions act as normal counterions, even though they may be strongly specifically adsorbed. This is not the case with phosphate. The adsorption of this ion is therefore treated separate-

ly in Chapter 6. There the relevant literature is briefly discussed first. A working-hypothesis is then postulated which implies that adsorption of phosphate ions occurs by exchange reactions (as given in Chapter 6.) of these ions with surface groups, in particular -OH and $-OH_2^+$. It is furthermore assumed that the phosphate dissociation equilibria do not alter upon adsorption. The experiments performed concern the direct measurement of (1) the adsorption of phosphate (2) the amount of acid required to keep the pH constant during this adsorption and (3) the stability of the hematite sols in the presence of phosphate.

Regarding the adsorption of phosphate the proposed exchange reactions explain the adsorption on the negative hematite surface and the increase in adsorption with decreasing pH and increasing concentration of indifferent electrolyte. It was not possible to explain the relatively strong increase in adsorption around pH = p*K*. (It was suggested that this feature might be related to incomplete equilibration with the solution). The amount of acid consumed during the adsorption of phosphate is also in accordance with the exchange reactions. However, the influence of the concentration of indifferent electrolyte was not always clear. The adsorption of phosphate and the stoichiometry of the exchange reactions could thus partially be explained in terms of the proposed reactions. Further verification is needed. The stability measurements indicated, i.a., that after coagulation of the hematite sol at very low concentrations only polyvalent phosphate ions (i.c. the bivalent ions) could produce restabilization. With regard to the exchange reactions this means that these ions act as potential-determining ions. It is finally noted that there are no definite indications for the occurrence of more than one adsorption mechanism.

Summarizing it is concluded that the adsorption of ions on hematite appears to be characterized by a large variety of interactions with the surface. In order of increasing degree of interaction, the following sequence can be set up:

1. the chlorides of K^+ and Cs^+. More than 85% of the ions in the STERN layer and/or the solid phase. No shift in p.z.c. ($pH^0 = 8.5$).
2. LiCl. Behaviour at low salt concentrations similar to KCl. At high salt concentrations penetration into the solid phase and shift in the p.z.c. ($pH^0 = 7.8$ in 1 M).
3. K_2SO_4. The p.z.c. shifts to a higher pH ($pH^0 = 9.6$). No restabilization.
4. the nitrates of Ca^{2+}, Sr^{2+} and Ba^{2+}. (Almost) completely in the Stern layer. The p.z.c. shifts to a lower pH ($pH^0 = 6.5$). Reversal of charge between pH 8.5 and 6.5.
5. $Mg(NO_3)_2$. Behaviour at low salt concentrations similar to the other alkaline earth ions. At high salt concentrations penetration as with Li^+.
6. Phosphate. Exchange against surface groups (mainly -OH and $-OH_2^+$). Reversal of charge between pH 8.5 and 6.0. Polyvalent ions potential-determining.

A further conclusion is that a better understanding of the adsorption of ions on iron oxides, and on oxides in general, can be achieved by using a combination of surface-chemical and colloid-chemical techniques, in particular the measurements of the surface charge and the stability.

ACKNOWLEDGEMENTS

This work was performed in the Laboratory of Physical and Colloid Chemistry of the Agricultural University, Wageningen.

The author is greatly indebted to Prof. Dr. J. LYKLEMA for his guidance and support. His fascinating lectures and the cordial atmosphere which he creates in his laboratory are gratefully acknowledged.

Many thanks are due to the friends and colleagues in the laboratory for their help and advice. The assistance of AB J. VAN DER LINDE in most of the experiments is particularly appreciated.

The author wishes to express his thanks to the Board of Directors of the Netherlands Soil Survey Institute for permitting the manuscript to be written while he was at this Institute.

Much credit is also due to Dr. B. VINCENT (Bristol) for his critical reading of the English text.

SAMENVATTING

Het belangrijkste doel van dit onderzoek was een beter inzicht te krijgen in de adsorptie van ionen aan hematiet (α-Fe_2O_3). Daarnaast is ook de nodige aandacht besteed aan de samenhang tussen deze adsorptie en de kolloïdale stabiliteit van hematietsolen.

Hoofdstuk 1. is gewijd aan de motivering en opzet van dit onderzoek. Als voorbeeld van het praktisch belang van ijzeroxiden zoals hematiet wordt de rol van deze oxiden in de bodem besproken. Hieruit blijkt dat de adsorptie door ijzeroxiden, en ook de kolloïdale wisselwerking met deze verbindingen, in de bodem van veel belang is. Zo kunnen allerlei voor de plant belangrijke voedingselementen (bijv. N, S, P, Mo en B) in de vorm van anionen door ijzeroxiden worden geadsorbeerd. Verder kan ook de adsorptie van kationen door de bodem direct of indirect worden beïnvloed, evenals de bodemstructuur. Bij de aanvang van dit onderzoek was er op deze terreinen slechts weinig fundamenteel kolloïdchemisch onderzoek verricht. Met name zijn er geen onderzoekingen geweest waarin zowel de adsorptie van ionen door ijzeroxiden als de kolloïdale stabiliteit van deze oxiden werd bestudeerd. Dergelijke onderzoekingen zijn wel verricht voor bijvoorbeeld zilverjodide en deze hebben dan ook model gestaan voor het huidige onderzoek. Hematiet is als vertegenwoordiger uit de groep van ijzeroxiden gekozen, omdat het een belangrijke rol speelt in de bodem (bijv. in laterietgronden) en omdat het gemakkelijk is te identificeren en als sol te bereiden en te bewerken.

In hoofdstuk 2. wordt de bereiding van de monsters en hun karakterisering, in het bijzonder die van het oppervlak, besproken. Mede op grond van hetgeen uit de literatuur bekend was, werd een betrekkelijk snelle methode voor de bereiding van hematiet ontwikkeld. De aldus verkregen monsters bevatten weinig of geen andere vormen van ijzeroxiden en sporen van sterk door hematiet geadsorbeerde Ca^{2+} en Mg^{2+}-ionen. Uit electronenmicroscoopfoto's bleek, dat de deeltjes min of meer bolvormig zijn, terwijl de diameters meestal tussen de 400 en 700 Å liggen. Het specifiek oppervlak werd bepaald met behulp van de BET-methode. De metingen werden verricht met een dynamische methode met N_2 als adsorbaat. Bij pogingen het oppervlak eveneens met behulp van de negatieve adsorptie-methode te bepalen (bij pH 4 met Ca^{2+} als co-ion) werden enkele grote praktische problemen ondervonden. Vooral de door het monster afgegeven Ca^{2+}-ionen bleken de meting te bemoeilijken. Door gebruik te maken van Ca^{45} kon deze moeilijkheid voor een belangrijk deel worden opgeheven. De met de negatieve adsorptie-methode verkregen ruwe schattingen van het specifiek oppervlak zijn lager dan het BET-oppervlak, hetgeen op een

zekere porositeit duidt.

Aanwijzingen voor porositeit werden vooral gevonden in N_2-adsorptiemetingen verricht volgens de statische methode. De adsorptie-isotherm vertoont een duidelijke hysterese. Het is een isotherm van het type IV, wat betekent dat er poriën aanwezig zijn met een doorsnee van 20 à 200 Å. De porositeit blijkt ook, hoewel minder duidelijk, uit de '*t*-plot'. Een kwantitatieve schatting van de graad van porositeit is (nog) niet mogelijk wegens gebrek aan standaardgegevens voor niet-poreus hematiet.

Door middel van thermogravimetrische analyses werd indirect aangetoond dat de buitenste lagen van de hematietdeeltjes gehydrateerd of, beter gezegd, gehydroxyleerd zijn.

In hoofdstuk 3. worden metingen en berekeningen beschreven van de oppervlaktelading (gevolg van de adsorptie van potentiaalbepalende ionen) en van de tegenlading (gevolg van de verdeling van indifferente ionen) als functie van de pH en van de zoutconcentratie. De oppervlaktelading (σ_0) werd bepaald met behulp van potentiometrische zuur-base titraties. Oriënterende metingen toonden aan dat de voor de titraties vereiste CO_2-vrije atmosfeer alleen kon worden bereikt met behulp van een gasdichte cel met een gecontroleerde N_2-atmosfeer.

De pH werd gemeten met een glaselektrode en een calomelelektrode waarbij de laatste door middel van een zoutbrug met de oplossing (c.q. het sol) in de meetcel was verbonden. In de zoutbrug bevond zich dezelfde elektrolytoplossing als in de meetcel. Deze constructie gaf minder praktische problemen dan het gebruik van een 'VAN LAAR-brug' of het plaatsen van de calomelelektrode direct in de vloeistof. Het feit, dat men door deze opzet bovendien geen last heeft van het suspensie-effect, was in dit onderzoek van ondergeschikt belang.

De standaardtitratie-procedure, die uiteindelijk werd toegepast, was een snelle zuurtitratie van pH 10 tot 4. Er werd van 'natte' (nooit gedroogde) monsters gebruik gemaakt die vóór elke titratie weer bij pH 10 in evenwicht met de oplossing werden gebracht. De grootte van de langzame adsorptie, die na de aanvankelijke snelle adsorptie nog optrad, bedroeg niet meer dan 20% van de totale adsorptie. De reproduceerbaarheid van de standaardtitraties was ongeveer 3%.

Het ladingsnulpunt werd verkregen uit het snijpunt van de (σ_0–pH)-curven bij verschillende zoutconcentraties. Ter controle van de gevonden ladingsnulpunten werden ook metingen met de 'toevoegmethode' verricht, waarin de pH-verandering ten gevolge van de toevoeging van (gedroogd) hematiet werd geregistreerd. De overeenstemming tussen beide methoden was goed voor de gebruikte (2–1) elektrolyten. Voor de overige elektrolyten werden met de 'toevoegmethode' lagere waarden verkregen, mogelijk als gevolg van het drogen.

Tot slot wordt in hoofdstuk 3. beschreven hoe voor enkele elektrolyten onder

dezelfde omstandigheden zowel de oppervlaktelading als de tegenlading werd gemeten.

De resultaten van de bovenbeschreven metingen worden in hoofdstuk 4. behandeld. De gebruikte elektrolyten zijn de chloriden van Li^+, K^+ en Cs^+, de nitraten van Mg^{2+}, Ca^{2+}, Sr^{2+} en Ba^{2+} en K_2SO_4. De (σ_0–pH) curven vertonen veel overeenkomst met die van andere (ijzer)oxiden. De curven zijn meestal convex ten opzichte van de pH-as en de oppervlaktelading bereikt vaak veel hogere waarden (enkele tientallen $\mu C\ cm^{-2}$) dan bij bijvoorbeeld zilverjodide en kwik. Er werd nagegaan of de hoge oppervlaktelading kon worden toegeschreven aan penetratie van potentiaalbepalende ionen en tegenionen in de vaste fase, zoals door andere onderzoekers is gevonden voor geprecipiteerd silica en glas.

De resultaten voor Li^+ en Mg^{2+} bij hoge zoutconcentratie wijzen inderdaad in deze richting. Beide ionen worden onder deze omstandigheden met grote voorkeur geadsorbeerd. Dit houdt vermoedelijk verband met het feit dat van de onderzochte kationen alleen Li^+ en Mg^{2+} in de octaëderposities van het hematietrooster passen. Tenslotte blijken de (σ_0–pH)-curven voor Li^+ en Mg^{2+} redelijk goed door de poreuze dubbellaag-theorie van LYKLEMA te kunnen worden beschreven. Voor de overige ionen zijn de aanwijzingen voor penetratie minder duidelijk. Het is echter met de huidige dubbellaagtheorieën voor oxiden ook niet mogelijk om te bewijzen dat de (σ_0–pH)-curven volledig *zonder* penetratie kunnen worden verklaard.

Wat verder opviel bij de bestudering van de (σ_0–pH)-curven is dat het ladingsnulpunt door toevoeging van bepaalde elektrolyten verschuift. Dit is een voor oxiden nog niet eerder beschreven verschijnsel. In aanwezigheid van KCl ligt het ladingsnulpunt bij pH 8,5. In aanwezigheid van LiCl en van de aardalkalinitraten blijkt een verschuiving naar lagere pH op te treden, terwijl bij K_2SO_4 juist een verschuiving naar hogere pH plaats vindt. Deze verschuivingen zijn een gevolg van het optreden van (specifieke) adsorptie in het ladingsnulpunt van respectievelijk het kation en het anion van het indifferente elektrolyt. De richting van de verschuiving bleek in overeenstemming met de thermodynamisch afgeleide ESIN-MARKOV coëfficiënt. Voor zover dat kon worden nagegaan (bij hoge oppervlakteladingen) werd ook een goede kwantitatieve overeenstemming gevonden tussen de theoretische en experimentele waarden voor deze coëfficiënt.

De in hetzelfde experiment verrichte meting van de oppervlaktelading en de tegenlading bleek de verwachte resultaten te geven, zowel voor de verdeling van de tegenlading over de kationen en de anionen als voor de balans tussen oppervlaktelading en tegenlading.

In hoofdstuk 5. worden de opzet en de resultaten van de stabiliteitsexperimenten beschreven. Voor de bepaling van de vlokwaarde werd van de klassieke vlokbuizenmethode gebruik gemaakt, waarbij de grens stabiel-instabiel visueel

wordt waargenomen. Met behulp van de DLVO-theorie voor bolvormige deeltjes werd uit de vlokwaarde de diffuse dubbellaag-potentiaal berekend en hieruit de lading in het diffuse deel van de dubbellaag. De lading in de STERN-laag (inclusief die welke eventueel in de vaste fase aanwezig is) werd gevonden als het verschil tussen de oppervlaktelading en de diffuse lading.

De geadsorbeerde éénwaardige kationen en anionen blijken zich voor het grootste deel (onder vlokomstandigheden meer dan 85%) in de STERN-laag en/of de vaste fase te bevinden. Voor de aardalkali-ionen (en vermoedelijk ook voor sulfaat) bedraagt dit percentage praktisch 100%, zoals blijkt uit de instabiliteit van het hematietsol wanneer alleen deze ionen als tegenion aanwezig zijn. Bij de aardalkali-ionen treedt tussen pH 8,5 en pH 6,5 omlading op. De verwachte verschuiving van het iso-elektrisch punt naar een hogere pH werd niet gevonden, mogelijk doordat de stabiliteitsmetingen in dit opzicht niet gevoelig genoeg zijn.

Bij de tot dusver besproken elektrolyten is gebleken dat de ionen zich gedragen als normale, zij het vaak sterk specifiek adsorberende, tegenionen. Voor fosfaat geldt dit echter niet; reden waarom er een apart hoofdstuk aan gewijd werd (hoofdstuk 6.). Allereerst wordt hierin een kort overzicht gegeven van de literatuur welke op het onderzoek betrekking heeft. Daarna wordt een eigen werkhypothese voor het fosfaatadsorptie-mechanisme gegeven. Volgens deze hypothese vindt de adsorptie plaats door middel van omwisseling (volgens in hoofdstuk 6. gegeven reacties) van fosfaationen tegen oppervlaktegroepen (vooral -OH en $-OH_2^+$). Verder wordt verondersteld dat de fosfaatdissociatie-evenwichten niet veranderen door adsorptie. De experimenten die zijn verricht betreffen rechtstreekse metingen van (1) de fosfaatadsorptie, (2) de hoeveelheid zuur die nodig is om de pH constant te houden tijdens deze adsorptie en (3) de kolloïdale stabiliteit van het hematietsol in aanwezigheid van fosfaat.

Met betrekking tot de adsorptie van fosfaat verklaren de voorgestelde omwisselingsreacties de adsorptie aan negatief geladen hematiet en de toename van de adsorptie met afnemende pH en toenemende concentratie van het indifferente elektrolyt. De relatief sterke toename van de adsorptie rond pH = pK kon niet worden verklaard. (Er werd gesuggereerd dat dit verschijnsel misschien aan een onvolledige instelling van het adsorptie-evenwicht moet worden toegeschreven). De hoeveelheid zuur welke werd verbruikt tijdens de adsorptie van fosfaat is eveneens in overeenstemming met de omwisselingsreacties. De invloed van het indifferente elektrolyt was hier echter niet altijd duidelijk. De adsorptie van fosfaat en de stoechiometrie van de omwisselingsreacties kon dus slechts gedeeltelijk met behulp van de voorgestelde reacties worden verklaard. Nader onderzoek is daarom gewenst. Uit de stabiliteitsmetingen bleek onder andere dat alleen de meerwaardige fosfaationen (i.c. de tweewaardige ionen) in staat zijn om, na het hematietsol bij zeer lage concentraties te hebben uitgevlokt,

voor restabilisatie te zorgen. In het licht van de werkhypothese gezien betekent dit, dat deze ionen zich als potentiaalbepalende ionen gedragen. Tenslotte wordt nog opgemerkt dat er geen duidelijke aanwijzingen zijn gevonden voor het optreden van meer dan één adsorptiemechanisme.

Uit dit onderzoek kan in de eerste plaats worden geconcludeerd dat de adsorptie van ionen aan hematiet zich kenmerkt door een grote verscheidenheid in de wijze van wisselwerking met het oppervlak. In volgorde van toenemende wisselwerking kunnen worden onderscheiden:

1. de chloriden van K^+ en Cs^+. Meer dan 85% van de ionen in de STERN-laag en/of de vaste fase. Geen ladingsnulpuntverschuiving ($pH^0 = 8{,}5$)
2. LiCl. Gedrag bij lage zoutconcentratie gelijk aan dat van KCl en CsCl. Bij hoge zoutconcentratie penetratie in de vaste fase en ladingsnulpuntverschuiving ($pH^0 = 7{,}8$ in 1 M)
3. K_2SO_4. Ladingsnulpunt verschuift naar hogere pH ($pH^0 = 9{,}6$). Geen restabilisatie.
4. de nitraten van Ca^{2+}, Sr^{2+} en Ba^{2+}. Adsorptie volledig in de STERN-laag. Ladingsnulpunt verschuift naar lagere pH ($pH^0 = 6{,}5$). Ladingsomkeer tussen pH 8,5 en 6,5.
5. $Mg(NO_3)_2$. Gedrag als bij de overige aardalkali-ionen, maar bij hoge zoutconcentratie penetratie net als bij Li^+.
6. fosfaat. Omwisseling tegen oppervlaktegroepen (voornamelijk -OH en $-OH_2^+$). Ladingsomkeer tussen pH 8,5 en 6,0. Meerwaardige ionen potentiaal bepalend.

In de tweede plaats blijkt uit dit onderzoek dat een beter inzicht in de adsorptie van ionen door ijzeroxiden, en door oxiden in het algemeen, kan worden bereikt door een combinatie van oppervlaktechemische en kolloïdchemische technieken, in het bijzonder metingen van de oppervlaktelading en de stabiliteit.

REFERENCES

ABENDROTH, R. P. (1970) J. Colloid Interface Sci. **34**, 591.
AHMED, S. M. (1966) Can. J. Chem. **44**, 1663.
AHMED, S. M. and D. MAKSIMOV (1968) Can. J. Chem. **46**, 3841.
AHMED, S. M. and D. MAKSIMOV (1969) J. Colloid Interface Sci. **29**, 97.
AREA, M. N. and S. B. WEED (1966) Soil Sci. **101**, 164.
ATKINSON, R. J., A. M. POSNER and J. P. QUIRK (1967) J. Phys. Chem. **71**, 550.
AYLMORE, L. A. G., M. KARIM and J. P. QUIRK (1967) Soil Sci. **103**, 10.
BACHE, B. W. (1964) J. Soil Sci. **15**, 110.
BATES, R. G. (1964) Determination of pH, Wiley, New York.
BÉRUBÉ, Y. G., G. Y. ONODA and P. L. DE BRUYN (1967) Surface Sci. **8**, 448.
BÉRUBÉ, Y. G. and P. L. DE BRUYN (1968a) J. Colloid Interface Sci. **27**, 305.
BÉRUBÉ, Y. G. and P. L. DE BRUYN (1968b) J. Colloid Interface Sci. **28**, 92.
BLOK, L. (1968) Thesis, State University, Utrecht, The Netherlands.
BLOK, L. and P. L. DE BRUYN (1970) J. Colloid Interface Sci. **32**, 518, 527, 533.
BLYHOLDER, G. and E. A. RICHARDSON (1962) J. Phys. Chem. **66**, 2597.
BOER, J. H. DE, B. G. LINSEN, TH. VAN DER PLAS and G. J. ZONDERVAN (1965) J. Catal. **4**, 649.
BOLT, G. H. (1957) J. Phys. Chem. **61**, 1166.
BOLT, G. H. and B. P. WARKENTIN (1958) Kolloid-Z. **156**, 41.
BREEUWSMA, A. and J. LYKLEMA (1971) Discussions Faraday Soc. **52**, 324.
BREEUWSMA, A. and J. LYKLEMA (1973) J. Colloid Interface Sci., to be published.
BRUGGENWERT, M. G. M. (1972) Thesis, Agricultural University, Wageningen, The Netherlands; Centre for Agricultural Publishing and Documentation, Agric. Res. Report 768.
BRUNAUER, S., P. H. EMMETT and E. TELLER (1938) J. Amer. Chem. Soc. **60**, 309.
BRUNAUER, S., L. S. DEMING, W. E. DEMING and E. TELLER (1940) J. Amer. Chem. Soc. **62**, 1723.
BURINGH, P. (1970) Introduction to the Study of Soils in Tropical and Subtropical Regions, Centre for Agricultural Publishing and Documentation, Wageningen.
BIJSTERBOSCH, B. H. (1965) Thesis, State University, Utrecht, The Netherlands; Commun. Agric. Univ., Wageningen 65–4.
BIJSTERBOSCH, B. H. and J. LYKLEMA (1965) J. Colloid Sci. **20**, 665.
BYE, G. C. and K. S. W. SING (1967) Chem. Ind. (London), 1139.
CARRUTHERS, J. D., P. A. CUTTING, R. E. DAY, M. R. HARRIS, S. A. MITCHELL and K. S. W. SING (1968) Chem. Ind. (London), 1772.
CARSTEA, D. D. (1968) Clays and Clay Minerals **16**, 231.
CHAO, T. T., M. E. HARWARD and S. C. FANG (1962) Soil Sci. **94**, 276.
CHARLOT, G. and D. BÉZIER (1957) in: Quantitative Inorganic Analysis, Wiley, New York, 535.
CHATEAU, H. (1954) J. Chim. Phys. **51**, 590.
CHESTERS, G., O. J. ATOE and O. N. ALLEN (1957) Soil Sci. Soc. Amer. Proc. **21**, 272.
CLARK, J. S. (1966) Soil Sci. Soc. Amer. Proc. **30**, 11.
CLARK, J. S. and W. E. NICHOL (1968) J. Soil Sci. **48**, 173.
COLEMAN, N. T., G. W. THOMAS, F. H. DE ROUX and G. BREDELL (1964) Soil Sci. Soc. Amer. Proc. **28**, 35.
DEER, W. A., R. A. HOWIE and J. ZUSSMAN (1962) Rock-forming Minerals, Vol. 3, Longmans, London.
DELAHAY, P. (1965) Double Layer and Electrode Kinetics, Intersci. Publ., New York.
DERYAGIN, B. V. and L. LANDAU (1941) Acta Physicochim. U.R.S.S. **14**, 633.
DUBININ, M. M. (1960) Chem. Rev. **60**, 235.
DUMONT, F. and A. WATILLON (1971) Discussions Faraday Soc. **52**, 352.
EMMETT, P. H. and S. BRUNAUER (1937) J. Amer. Chem. Soc. **59**, 1553.

ESIN, O. and B. MARKOV (1939) Acta Physicochim. U.R.S.S. **10**, 353.
ETTRE, L. S., N. BRENNER and E. W. CIEPLINSKY (1962) Z. Phys. Chem. (Leipzig) **219**, 17.
FOWKES, F. M. (1964) Ind. Eng. Chem. **56**, 41.
FRENS, G. (1968) Thesis, State University, Utrecht, The Netherlands.
FREUNDLICH, H. (1903) Z. Physik. Chem. **44**, 151.
FRIPIAT, J. J. and M. PENNEQUIN (1965) Bull. Soc. Chim. Fr., 1655.
GIESSEN, A. A. VAN DER (1966) Chem. Weekblad **62**, 305.
GRAHAME, D. C. (1947) Chem. Rev. **41**, 441.
GRAHAME, D. C. (1955) Ann. Rev. Phys. Chem. **6**, 352.
GREGG, S. G. and K. S. W. SING (1967) Surface Area and Porosity, Academic Press, London, New York.
HAAN, F. A. M. DE, and G. H. BOLT (1963) Soil Sci. Soc. Amer. Proc. **27**, 636.
HAAN, F. A. M. DE (1964) J. Phys. Chem. **68**, 2970.
HAAN, F. A. M. DE (1965) Thesis, Agricultural University, Wageningen, The Netherlands; Centre for Agricultural Publishing and Documentation, Agric. Res. Report 655.
HAMAKER, H. C. (1937) Physica **4**, 1058.
HASEMAN, J. F., E. H. BROWN and C. D. WHITT (1950) Soil Sci. **70**, 257.
HAZEL, F. and G. H. AYRES (1931) J. Phys. Chem. **35**, 2930.
HEALY, T. W., R. D. JAMES and R. COOPER (1968) Advan. Chem. Ser. **79**, 62.
HEYWOOD, H. (1970) Symposium on Surface Area Determination (Bristol 1969), Butterworths, London.
HINGSTON, F. J., R. J. ATKINSON, A. M. POSNER and J. P. QUIRK (1967) Nature **215**, 1459.
HINGSTON, F. J., R. J. ATKINSON, A. M. POSNER and J. P. QUIRK (1968) Trans. 9th Int. Congr. Soil Sci. (Adelaide), Vol. 1, 669.
HINGSTON, F. J., A. M. POSNER and J. P. QUIRK (1970) Search **1**, 324.
HSU, P. H. (1964) Soil Sci. Soc. Amer. Proc. **28**, 474.
HUANG, C. P. (1971) Thesis, Harvard University, U.S.A.
HUL, H. J. VAN DEN (1966) Thesis, State University, Utrecht, The Netherlands; Commun. Agric. Univ., Wageningen 66–2.
HUL, H. J. VAN DEN and J. LYKLEMA (1967) J. Colloid Interface Sci. **23**, 500.
HUL, H. J. VAN DEN and J. LYKLEMA (1968) J. Amer. Chem. Soc. **90**, 3010.
JACOBS, T. (1968) C.R. Acad. Sci. Ser. C, 341.
JOHANSEN, P. G. and A. S. BUCHANAN (1957a) Austr. J. Chem. **10**, 392.
JOHANSEN, P. G. and A. S. BUCHANAN (1957b) Austr. J. Chem. **10**, 398.
JOY, A. S. and D. WATSON (1964) Bull. Inst. Mining Met. **687**, 323.
JOYNER, L. G., E. B. WEINBERGER and C. W. MONTGOMERY (1945) J. Amer. Chem. Soc. **67**, 2182.
JURINAK, J. J. (1966) Soil Sci. Soc. Amer. Proc. **30**, 559.
KITTRICK, J. A. and M. L. JACKSON (1955) Soil Sci. Soc. Amer. Proc. **19**, 292.
KLOMPÉ, M. A. M. (1941) Thesis, State University, Utrecht, The Netherlands; H. R. KRUYT and M. A. M. KLOMPÉ (1942) Kolloidchem. Beihefte **54**, 484.
K.N.C.V. (1962) Tabellenboekje (Summary of Physical and Chemical Constants) Centen's Uitg. Mij., The Hague.
KOENIGS, F. F. R. (1961) Thesis, Agricultural University, Centre for Agricultural Publishing and Documentation, Wageningen, The Netherlands; Agric. Res. Report 677.
LAAR, J. A. W. VAN (1952) Thesis, State University Utrecht, The Netherlands.
LEVINE, S. and A. L. SMITH (1971) Discussions Faraday Soc. **52**, 290.
LI, H. C. and P. L. DE BRUYN (1966) Surface Sci. **5**, 203.
LIPPENS, B. C. and J. H. DE BOER (1965) J. Catal. **4**, 319.
LOEB, A. L., P. H. WIERSEMA and J. TH. G. OVERBEEK (1961) The Electrical Double Layer around a Spherical Colloid Particle, M.I.T. Press, Cambridge, Mass.
LYKLEMA, J. (1961) Kolloid-Z. **175**, 129.
LYKLEMA, J. and J. TH. G. OVERBEEK (1961) J. Colloid Sci. **16**, 595.
LYKLEMA, J. (1963) Trans. Faraday Soc. **59**, 418.

LYKLEMA, J. (1966a) III Intern. Vortragung über Grenzflächenaktiven Stoffe (Berlin);Abh. Deutschen Akad. Wissenschaften Berlin 6b, 542.
LYKLEMA, J. (1966b) Discussions Faraday Soc. **42**, 81.
LYKLEMA, J. (1968) J. Electroanal. Chem. **18**, 341.
LYKLEMA, J. and H. J. VAN DEN HUL (1970) Symposium on Surface Area Determination (Bristol 1969), Butterworths, London, 341.
LYKLEMA, J. (1970) Croat. Chem. Acta **42**, 151.
LYKLEMA, J. (1971) Croat. Chem. Acta **43**, 249.
LYKLEMA, J. (1972) J. Electroanal. Chem. **37**, 53.
MACKENZIE, R. C. (1957) in: The Differential Thermal Investigation of Clays, R. C. MACKENZIE Ed., (1957) Mineral. Soc. London, Ch. 12.
MAREL, H. W. VAN DER (1966) Contr. Mineral. Petrol. **12**, 96.
MCCAFFERTY, E. M., V. PRAVDIČ and A. C. ZETTLEMOYER (1970) Trans. Faraday Soc. **66**, 1720.
MEHRA, O. P. and M. L. JACKSON (1960) Clays and Clay Minerals, 7th Conf., Pergamon Press, London, 317.
MELLOR, J. W. (1934) A Comprehensive Treatise on Inorganic and Theoretical Chemistry, Vol. 13, part 2, Longmans, London.
MODI, H. J. and D. W. FUERSTENAU (1957) J. Phys. Chem. **61**, 640.
MORIMOTO, T., M. NAGAO and F. TOKUDA (1969) J. Phys. Chem. **73**, 243.
MULJADI, D., A. M. POSNER and J. P. QUIRK (1966) J. Soil Sci. **17**, 212.
MURMANN, R. P. and M. PEECH (1969) Soil Sci. Soc. Amer. Proc. **33**, 205.
NELSON, F. M. and F. T. EGGERTSEN (1958) Anal. Chem. **30**, 1387.
NEN (1967) Receptbladen voor de Statistische Verwerking van Waarnemingen (Instructions for Statistical Treatment of Data) NEN 1047, blad 3.3, Ned. Normalisatie Instituut, Rijswijk, The Netherlands.
NINHAM, B. W. and V. A. PARSEGIAN (1970) J. Chem. Phys. **52**, 4578.
OLSEN, S. R. and F. S. WATANABE (1957) Soil Sci. Soc. Amer. Proc. **21**, 144.
ONODA, G. Y. and P. L. DE BRUYN (1966) Surface Sci. **4**, 48.
OVERBEEK, J. TH. G. (1952) in: Colloid Science, Vol. 1, H. R. KRUYT Ed., Elsevier, Amsterdam.
PARKS, G. A. (1960) Thesis, M.I.T., Cambridge, Mass.
PARKS, G. A. and P. L. DE BRUYN (1962) J. Phys. Chem. **66**, 967.
PARKS, G. A. (1965) Chem. Rev. **65**, 177.
PARSONS, R. (1957) Proc. 2nd Int. Congr. Surf. Act. (London 1956), Vol. 3, 38.
PARSONS, R. (1959) Handbook of Electrochemical Constants, Butterworths, London.
PAYNE, D. A. and K. S. W. SING (1969) Chem. Ind. (London), 918.
PICKNETT, R. G. (1968) Trans. Faraday Soc. **64**, 1059.
PIERCE, C. and B. EWING (1964) J. Phys. Chem. **68**, 2562.
PIERCE, C. (1968) J. Phys. Chem. **72**, 3673.
QUIRK, J. P. (1971) Discussions Faraday Soc. **52**, 343.
REERINK, H. and J. TH. G. OVERBEEK (1954) Discussions Faraday Soc. **18**, 74.
REISENAUER, H. M., A. A. TABIKH and P. R. STOUT (1962) Soil Sci. Soc. Amer. Proc. **26**, 23.
RENNIE, D. A. and R. B. MCKERCHER (1959) Can. J. Soil Sci. **39**, 64.
REYES, E. D. and J. J. JURINAK (1967) Soil Sci. Soc. Amer. Proc. **31**, 637.
RICH, C. I. (1960) Soil Sci. Soc. Amer. Proc. **24**, 26.
RICH, C. I. (1968) Clays and Clay Minerals **16**, 15.
ROOKSBY, H. P. (1961) in: The X-ray Identification and Crystal Structures of Clay Minerals, G. BROWN Ed., Mineral. Soc., London.
SADEK, H., A. K. HELMY, V. M. SABET and TH. F. TADROS (1970) J. Electroanal. Chem. **27**, 257.
SCHAHABI, S. and U. SCHWERTMANN (1970) Z. Pflanzenernaehr. Bodenk. **125**, 193.
SCHEFFER, F. and P. SCHACHTSCHABEL (1966) Lehrbuch der Bodenkunde, Ferdinand Enke Verlag, Stuttgart.
SCHOFIELD, R. K. (1947) Nature **160**, 408.

SCHUYLENBORGH, J. VAN and A. M. H. SÄNGER (1949) Rec. Trav. Chim. Pays-Bas **68**, 999.
SCHUYLENBORGH, J. VAN, D. L. ARENS and J. G. J. KOK (1950) Rec. Trav. Chim. Pays-Bas **69**, 1557.
SCHWERTMANN, U. (1959) Z. Pflanzenernaehr. Düng. Bodenk. **84**, 194
SCHWERTMANN, U. (1965) Z. Pflanzenernaehr. Düng. Bodenk. **108**, 37.
SCHWERTMANN, U., W. R. FISCHER and H. PAPENDORF (1968) Trans. 9th Int. Congr. Soil Sci. (Adelaide) Vol. 1, 645.
SILLÉN, L. G. and A. E. MARTELL (1964) Stability Constants of Metal-ion Complexes, Chem. Soc., London.
SIMS, J. R. and F. T. BINGHAM (1968) Soil Sci. Soc. Amer. Proc. **32**, 364.
SING, K. S. W. (1968) Chem. Ind. (London), 1520.
SING, K. S. W. (1970a) Symposium on Surface Area Determination (Bristol 1969), Butterworths, London, 25.
SING, K. S. W. (1970b) personal communication.
SMITH, F. G. and D. J. KIDD (1949) Amer. Mineral. **34**, 403.
Soil Taxonomy (1970) Unedited text, U.S. Department of Agriculture, Washington D.C.
STERN, O. (1924) Z. Elektrochem. **30**, 508.
STUMM, W., C. P. HUANG and S. R. JENKINS (1970) Croat. Chem. Acta **42**, 223.
SUMNER, M. E. (1963) Clay Mineral Bull. **29**, 218.
SUMNER, M. E. and N. G. REEVE (1966) J. Soil Sci. **17**, 274.
TADROS, TH. F. and J. LYKLEMA (1968) J. Electroanal. Chem. **17**, 267.
TADROS, TH. F. and J. LYKLEMA (1969a) J. Electroanal. Chem. **22**, 1.
TADROS, TH. F. and J. LYKLEMA (1969b) J. Electroanal. Chem. **22**, 9.
TADROS, TH. F. (1971) Discussions Faraday Soc. **52**, 345.
TAMINI, Y. N., Y. KANEHIRO and G. D. SHERMAN (1964) Soil Sci. **98**, 249.
TAMINI, Y. N., Y. KANEHIRO and G. D. SHERMAN (1968) Soil Sci. **105**, 434.
TAYLOR, R. W., E. L. GURNEY and E. C. MORENO (1964) Soil Sci. Soc. Amer. Proc. **28**, 49.
TROELSTRA, S. A. (1941) Thesis, State University Utrecht, The Netherlands; H. R. KRUYT and S. A. TROELSTRA (1943) Kolloidchem. Beihefte **54**, 225.
VERWEY, E. J. W. and J. TH. G. OVERBEEK (1948) Theory of the Stability of Lyophobic Colloids, Elsevier, Amsterdam.
VINCENT, B., B. H. BIJSTERBOSCH and J. LYKLEMA (1971) J. Colloid Interface Sci. **37**, 171.
VOET, A. (1969) J. Colloid Interface Sci. **30**, 264.
WEISER, H. B. (1935) Inorganic Colloid Chemistry, Vol. 2.
WEISER, H. B. and W. D. MILLIGAN (1935) J. Phys. Chem. **39**, 25.
WELLS, A. F. (1945) Structural Inorganic Chemistry, Oxford Univ. Press.
WIESE, G. R., R. O. JAMES and T. W. HEALY (1971) Discussions Faraday Soc. **52**, 302.
ZETTLEMOYER, A. C. and E. MCCAFFERTY (1969) Z. Phys. Chem. (Frankfurt am Main) **64**, 41.

ABREVIATIONS AND SYMBOLS

BET	BRUNAUER – EMMETT – TELLER
BDDT	BRUNAUER – DEMING – DEMING – TELLER
DLVO	DERYAGIN – LANDAU – VERWEY – OVERBEEK
GCSG	GOUY – CHAPMAN – STERN – GRAHAME
i.e.p.	iso-electric point
IHP	Inner HELMHOLTZ Plane
M	molarity
N	normality
OHP	Outer HELMHOLTZ Plane
p.d.	potential-determining
p.z.c.	point of zero charge
a	particle radius
a_{H^+}	activity of the H^+ ion
a_m	molecular area
$a_{p.d.}$	activity of the p.d. ion
a_s	volume of gas adsorbed at a given p/p_0 divided by the volume adsorbed at $p/p_0 = 0.4$
A	HAMAKER constant
B	constant in eqn. (4–25)
c	constant in the BET equation (section 2.5.2.)
c, c_{salt}	electrolyte concentration
Δc	increase in electrolyte concentration
c_c	coagulation concentration
c_{H^+}, c_{OH^-}	concentration of H^+ and OH^- ions, respectively
c_p	concentration of phosphate
C	differential capacity
C_d	differential capacity of the diffuse part of the double layer
C_m	differential capacity of the STERN layer
C_{exp}	experimental differential capacity defined in eqn. (4–17)
d	distance between the OHP's of two interacting particles
d_i	diameter of a circle having the same area as the projected image of particle i
e	elementary charge
E	cell-EMF
E^s	*ibid.* in a standard solution
E_{cal}	potential of the calomel electrode
E^0_{glass}	standard potential of the glass electrode

E_j	liquid junction potential; extra subscripts refer to the type of liquid junction and the type of cell used (section 3.2.3.2.)
$f_\pm$	mean ion activity coefficient
F	the FARADAY
ΔG_{ads}	adsorption free energy per ion
$[H^+]_s$	concentration of H^+ ions in the surface phase in moles l^{-1}
I, I_+, I_-	functions in the diffuse double layer theory for spherical particles (sections 2.5.4.1. and 4.1.1.)
k	BOLTZMANN constant
K	shape factor in eqn. (2–1)
K_1, K_2, K_3	dissociation constants for phosphoric acid
K_a	equilibrium constant for the association equilibrium in eqn. (4–14)
K_d	*ibid.* for the dissociation equilibrium in eqn. (4–14)
K_d^m	'microscopic' acidity constant (section 4.3.3.)
m	amount of adsorbent
n_i	number of particles with diameter d_i
n_+, n_-	added amount of cations and anions, respectively, in equivalents
n_{H^+}, n_{OH^-}	*ibid.* of H^+ ions and OH^- ions, respectively
n_s	total number of surface sites per unit area
$n(x)$	number of surface charges per unit volume in the solid, at a distance x to the surface
$n(0)$	*ibid.* at the surface
n_X	number of uncharged surface sites per unit area
n_{X^+}	number of positive surface sites per unit area
n_{X^-}	number of negative surface sites per unit area
N_{Av}	AVOGADRO's number
p	reciprocal penetration depth in eqn. (4–23)
p/p_0	relative vapour pressure of the adsorbate (Chapter 2.)
pH	negative logarithm of the activity of the H^+ ions
pH^s	ibid. in a standard solution
pH^0	pH of the p.z.c.
pK	negative logarithm of the equilibrium constant K
q_0	reduced radius $\varkappa a/\lambda$
r	crystal ionic radius
R	gas constant (Chapter 3.)
R	distance between the centres of two interacting particles (Chapter 5.)
R	ratio of the amount of acid (required to keep the pH constant during adsorption of phosphate) to the amount of phosphate

	adsorbed (Chapter 6.)
s	R/a (Chapter 5.)
s_{max}	*ibid.* if $V_t = V_t^{max}$
S	specific surface area
S_a	*ibid.* determined using the a_s-plot
S_{BET}	*ibid.* using the BET theory
S_{EM}	*ibid.* using electron micrographs (eqn. 2–1)
S_{NA}	*ibid.* using the negative adsorption method
S_t	*ibid.* using the t-plot
t	average thickness of an adsorbed layer in gas adsorption
T	absolute temperature
u	reduced distance px in eqn. (4–23)
v	volume of gas adsorbed in cm^3 (STP) per gram of solid
v_m	*ibid.* in a monolayer
V	liquid volume
V_A	attractive free energy in ergs
V_R	repulsive free energy in ergs
V_A^{max}	value of V_A if $V_t = V_t^{max}$
V_R^{max}	value of V_R if $V_t = V_t^{max}$
V_t	total interaction free energy in ergs (Chapter 5.)
V_t^{max}	value of V_t in its maximum
x	distance to the surface, measured inside the solid phase
X	uncharged surface site
X^+	positive surface site
X^-	negative surface site
$[X^-]$	concentration of negative surface sites in moles 1^{-1}
$[X_T]$	concentration of dissociable surface sites in moles 1^{-1}
y_d	reduced potential $e\psi_d/kT$ (Chapter 2.)
$y(x)$	reduced potential $\pm ze\psi(x)/kT$ in the porous double layer theory (Chapter 4.)
$y(0)$	*ibid.* at the surface
z, z_i	valency (of ion i), sign not included
z_+, z_-	*ibid.* of the cations and anions, respectively
z_{co}, z_{ct}	*ibid.* of the co-ions and counterions, respectively
α	parameter in the porous double layer theory (eqn. 4–27)
α_1, α_2	fraction of total phosphate present in the monovalent and bivalent form, respectively
β	ESIN-MARKOV coefficient
γ	$\tanh(ze\psi_d/4kT)$
Γ_{H^+}, Γ_{OH^-}	adsorption per cm^2 of H^+ and OH^- ions, respectively
Γ_+, Γ_-	*ibid.* of cations and anions, respectively

$\Delta\Gamma$	change in adsorption per cm^2
Δ	thickness of the STERN layer (from OHP to surface)
ε	dielectric constant
ζ	electrokinetic potential
θ	fraction of the surface charge that is compensated for by counterions
θ_0	fraction of surface sites charges at the p.z.c.
θ_m	degree of charge compensation in the STERN layer
θ_{X+}, θ_{X-}	fraction of surface sites carrying a positive and negative charge, respectively
$\varkappa$	reciprocal double layer thickness defined in eqn. (4–3)
λ	$(z_{co}+z_{ct})/2z_{ct}$
μ^s_{H+}	chemical potential of the H^+ ions in the surface
$\mu^{0,s}_{H+}$	standard chemical potential of the adsorbed H^+ ions
$\mu^{0,s}_{X}$	standard chemical potential of the uncharged surface sites
$\mu^{0,s}_{X+}$, $\mu^{0,s}_{X-}$	*ibid.* of the positive and negative surface sites, respectively
ρ	density of the solid
σ_0	surface charge density in $\mu C\ cm^{-2}$
σ_d	diffuse layer charge density in $\mu C\ cm^{-2}$
σ_m	STERN layer charge density in $\mu C\ cm^{-2}$
σ_m^{max}	maximum STERN layer charge density in $\mu C\ cm^{-2}$
σ_m^s	counter charge density in the solid phase in $\mu C\ cm^{-2}$
σ^+, σ^-	counter charge density due to cations and anions, respectively, in $\mu C\ cm^{-2}$
$\Delta\varphi$	difference in GALVANI potential between the solid and liquid phase
ϕ	specific adsorption potential
ψ_0	surface potential defined as $\Delta\phi-\Delta\varphi_{p.z.c.}$
ψ_d	diffuse double layer potential
ψ_m	potential at the IHP
ψ_s	difference in potential between surface and solution in the picture of STUMM et al. (eqn. 4–31)

PERSOONLIJKE GEGEVENS

Na het behalen van het diploma HBS-B aan het Chr. Lyceum te Sneek begon de auteur in 1956 zijn studie aan de Landbouwhogeschool te Wageningen. In juni 1964 werd het Ingenieursexamen afgelegd in de richting Bodemkunde en Bemestingsleer (hoofdvak Bodemscheikunde en -natuurkunde). Tot eind 1969 was hij vervolgens medewerker bij de afdeling Fysische en Kolloïdchemie van de Landbouwhogeschool. Sedert 1 januari 1970 is hij werkzaam bij de afdeling Bodemchemie en Kleimineralogie van de Stichting voor Bodemkartering te Wageningen.